

Digital radiography: Image Acquisition and Scattering Reduction in X-ray Imaging.

EngD Transfer Document

Elena Marimón Muñoz

Supervisory Team:

Dr. Hammadi Nait-Charif

Dr. Philip Marsden

ABSTRACT

The main advantage that has enabled digital radiography to take over the radiography market is the possibility of separating the image acquisition and image processing processes, allowing their individual optimization. The current report looks into both areas, seeking first to improve the design of the new family of CMOS X-ray detectors that PerkinElmer is planning to introduce into the market and second to develop a method to reduce the scattering contribution in mammography examinations using post-processing techniques.

During the CMOS X-ray detector product design phase it is crucial to detect any issue that the sensor or the detector might present. Image characterization techniques have proven to be very efficient in finding these issues. The main challenge is to take these well-known test methods and adapt them so they can act as a red flag, indicating that there is an issue that needs to be studied. The methods chosen have proven effective in finding sensor and detector shortcomings and the design has been optimised in accordance with the findings. The new prototypes will be ready for further characterization by December 2015.

Scattering is one of the main issues left in mammography examinations, as it degrades the quality of the image and makes the diagnosis process even more complicated. The scattering reduction technique currently used in mammography makes use of anti-scatter grids. This method has been found to be inefficient, as it increases the dose delivered to the patient and the price of the equipment and, at the same time, does not get rid of all the scattered radiation and reduces the resolution of the image. This study proposes to reduce the scattering contribution by using an image post-processing technique that convolves the output image using simplified Monte Carlo simulation kernels. A preliminary study of this method has been finished and the set-up is being designed, aiming to start obtaining results in early 2016.

TABLE OF CONTENTS

ABSTRACT.....	ii
LIST OF FIGURES.....	v
LIST OF TABLES.....	vi
1 OVERVIEW.....	1
1.1 DOCUMENT STRUCTURE.....	1
1.2 PROJECT	1
1.3 INTRODUCTION TO THE FIELD	2
1.3.1 Sensor and detector characterization.....	2
1.3.2 Scattering reduction.....	3
1.4 INDUSTRIAL PARTNER: Dexela Ltd – PerkinElmer medical imaging London	4
2 CRITICAL EVALUATION OF DIGITAL X-RAY DETECTORS	5
2.1 REVIEW OF THE STATE OF THE ART	5
2.1.1 Introduction	5
2.1.2 Complementary Metal Oxide Semiconductor (CMOS).....	6
2.1.3 Scintillator technology	8
2.1.4 General design requirements for the next generation of detectors	9
2.2 PROJECT MOTIVATION AND IMPACT ON DESIGN CYCLE.....	16
2.3 PERFORMANCE METRICS AND IMPLICATIONS	17
2.3.1 Methodology.....	17
2.3.2 Implementation	19
2.3.3 Validation	21
2.3.4 Deliverables.....	22
2.4 ISSUES TACKLED TO DATE BY THE EVALUATION PROCESS	22
3 SCATTERING REDUCTION IN X-RAY IMAGING.....	26
3.1 REVIEW OF THE STATE OF THE ART	26
3.1.1 Introduction	26
3.1.2 Physical methods	28
3.1.3 Simulations.....	30
3.1.4 Scattering dependencies.....	32
3.1.5 Typical general mammography parameters for MC simulations:	35
3.1.6 Monte Carlo PSF simulation – GEANT4 simulation toolkit	36

3.2	PROJECT GOALS	37
3.3	PSF EVALUATION USING MC SIMULATIONS	38
3.3.1	Methodology.....	38
3.3.2	Technique validation.....	38
3.4	BREAST THICKNESS ESTIMATION	38
3.4.1	Methodology.....	38
3.4.2	Technique validation.....	38
3.5	SCATTER REMOVAL USING THE PSF POST-PROCESSING TECHNIQUE	39
3.5.1	Methodology.....	39
3.5.2	Technique validation.....	39
4	CONCLUSIONS AND FUTURE WORK	40
4.1	STRUCTURE OF THE FIRST TWO YEARS.....	40
4.2	ENGD PROJECT PLAN	41
4.2.1	Project structure	41
4.2.2	Project timeline - Gantt chart	41
5	Bibliography	43
	APPENDIX A.....	48
A.1	X-ray detector technologies	48
	Screen-Film and CR technology	48
	Solid State X-ray Detectors	50
A.2	Modulation Transfer Function.....	52
A.3	Noise Power Spectrum	54
	APPENDIX B	55
	APPENDIX C	110

LIST OF FIGURES

Figure 1: Overall CMOS architecture.	7
Figure 2: 3T Pixel schematic.....	7
Figure 3: CMOS APS X-ray detector schematic.	8
Figure 4: Signal to noise ratio(SNR) calculation example	15
Figure 5: The top-left graph in the figure shows an example of 7 samples of the ESF. The top-right plot shows the 7 samples superimposed and the bottom figure shows the averaged ESF.....	20
Figure 6: Summary of the ESF method to calculate the MTF.	20
Figure 7: The figure shows an example of a row noise with variable frequency that was seen in a static noise image.	23
Figure 8: On the left there is an example of high frequency noise and clipping affecting some parts of the noise image. The figure on the right shows how the 2D NNPS was affected by the clipping.	23
Figure 9: This figure shows a temporal noise image.....	23
Figure 10: The graph shows an intensity profile of seven consecutive columns plotted across a sharp edge (ESF).....	24
Figure 11: The graph shows the detector response as a function of the frame count for two different exposure levels.	24
Figure 12: This image shows three phantom images acquired in a sequence.	25
Figure 13: The image shows the geometry of the edge spread method.....	28
Figure 14: The image shows the geometry of the beam stop method and the disk region of interest (ROI) that is usually selected.....	28
Figure 15: The image shows the geometry of the scatter medium reposition method.....	29
Figure 16: The image shows the geometry of the slat method.....	29
Figure 17: Schematic of the Electromagnetic (EM) spectrum.....	48
Figure 18: Diagrams comparing configurations for two screen-film combinations.	49
Figure 19: The figure shows the schematic of both the direct conversion a-Se TFT (right) and the indirect conversion a-Si TFT (left) detectors.	51
Figure 20: From left to right: Typical 3 electrodes pixel structure, CCD chip layout and typical Full Frame Readout schematics.....	52
Figure 21: Description of the effect that the imaging system has over pure sinusoidal waves (left) and visual explanation of how the MTF is obtained (right).	53
Figure 22: Distribution of region of interest (ROIs) in a flat image-one frame.....	54

LIST OF TABLES

Table 1: The table shows the expected performance of the three main digital radiography technologies in comparison with the response of an ideal detector.	10
Table 2: The table shows the general geometry parameters used in mammography medical examinations.....	36

1 OVERVIEW

1.1 DOCUMENT STRUCTURE

This document is divided in four chapters. The first chapter provides a general background context of the field and introduces the company I am working with. Chapters 2 and 3 explain the two subprojects of my EngD, image characterization and scattering reduction. Each chapter has a literature review, and a methodology section, including an explanation of why it has been chosen. In addition, chapter two also offers a section introducing the methods, their implementation and validation, finishing with a summary of the results obtained. The final chapter gives an overview of the advances in the project, giving information about the first two years and the plan for the final two years, shown in a Gantt chart. In addition, appendices A, B and C give additional information of the image characterization subproject. Appendix A gives further theory background information while appendices B and C introduce measurement instructions and more information about the methods and results obtained.

1.2 PROJECT

This document presents my work undertaken in collaboration with Dexela Ltd (PerkinElmer Medical Imaging London), the Centre for Digital Entertainment (CDE), and Bournemouth and Bath universities. This report aims to give an overview of the work performed in the first two years of the EngD studies, and to define the structure to be followed over the final two years. The project is based in digital radiography using CMOS sensor technology, focusing on the detector characterization and image post-processing.

PerkinElmer Medical Imaging London is in the process of developing new products to include in their family of CMOS digital X-ray detectors. This new engineering programme includes the on-site development of the CMOS sensors themselves, technology that was previously acquired from third-party companies.

Integral to this development process is a tight regime of testing and performance verification and evaluation. New testing procedures had to be defined for the purposes of design optimisation and product qualification. Most of my research in image characterization has focused on this task, which is a critical input into the design cycle. Although radiographic image quality testing is a well-known subject, it is usually focused in final product characterization and there is very little information about image characterization during the product design phase, as it is not in the private companies' interest to share this kind of information. The main challenge has been to adapt well-known test methods to try to identify detector or sensor issues and map those issues to their root cause. This last step was achieved by working closely with the sensor design and engineering teams. Each detector prototype must be challenged in terms of image quality in order to be able to obtain a final product that is suitable for medical applications and competitive in the market. This characterization process closes the design loop.

The final step of the image characterization project will be to perform a full detector characterization and performance qualification, just prior to product release. The basic imaging performance of X-ray detector systems can be characterized by the study of the resolution, efficiency, noise and contrast. A series of parameters can be measured in order to assess the characteristics of the detector and, therefore, can be used to compare between technologies and industries and/or to find design problems: the response curve,

exposure dynamic range, signal to noise ratio (SNR), grey scale resolution, photon transfer curve (PTC), the modulation transfer function (MTF), noise power spectrum (NPS) and detective quantum efficiency (DQE).

The final image, however, is always delivered to the user after a certain amount of image processing on the raw image. Image processing algorithms manipulate raw radiographs in order to adapt them to the radiologist's requirements. These algorithms are designed to optimize the quality of the output, minimizing the degradation of the image and avoiding the introduction of artefacts that might lead to misdiagnosis. There are many different types of algorithms, indeed each manufacturer or system typically has their own, and they are focused on solving some of the issues that these raw radiographs have.

The second half of my project is based on image enhancement and is focused on scattering reduction in mammography. X-ray scattering is produced when the trajectory of the particles is deviated as a consequence of the photon interaction. This process causes an increase of noise in the acquired image thus it is important to be minimised. The idea behind this sub-project is to post-process an acquired mammogram and reduce the scattering component of the image in order to obtain equal or better image quality to the one obtained with the use of anti-scatter grids, method that is currently broadly used in mammography applications. The aim is therefore to make the anti-scatter grids redundant in mammography examinations.

The motivation behind getting rid of the anti-scatter grids is multiple. The main advantage of removing it is in the possibility of reducing the dose delivered to the patient. As the grid absorbs around 20% of the primary (non-scattered) beam, the dose has to be increased to maintain good contrast information. Moreover, these grids are an expensive addition to the mammography system and either the image has to be post-processed to remove the grid, or the grid needs to have an additional mechanism to move it around its centre position in order for it not to be visible in the image. Finally, the grids do not absorb all the scattered radiation, 30-60% is still transmitted onto the detector. [1] [2] [3] [4]

The work done during the first year and a half of the EngD was mainly focused in defining the image characterization methods, that are needed to test the quality of CMOS X-ray detector prototypes against their design specification, and performing tests and analysis against the definitions in order to prove their effectiveness. A technique was defined and a number of sensors and detectors were successfully characterized and the findings were passed back to the design engineers in order to optimize the design. The scattering reduction sub-project was properly defined towards the second half of the second year; the literature review has been done.

1.3 INTRODUCTION TO THE FIELD

1.3.1 Sensor and detector characterization

The use of X-rays in medicine started right after their discovery in 1895. The first medical radiographic system was a simple single-emulsion glass plate. By the 1920s, the system had evolved into screen-film radiography, where a detector was formed by a cassette containing one or two screens and a film: the X-ray beam interacts with the screen and is converted into light photons. The light is then detected by the film forming a latent image. Finally, the film is chemically processed and the final image is obtained.

Screen-film, or conventional radiography, became the predominant radiographic method for most part of the 20th century, it was not until the late 1990s that digital technology started to take over in the radiography and mammography market [5] [6].

Digital radiography uses digital image capture devices. It allows the user to preview the image and avoids the costly processing steps of conventional radiography. The most important feature, however, is the possibility of dividing the process into three steps: image acquisition, image processing and image display. The physical separation of the acquisition process and the processing of the raw image allows their individual optimization, leading to improvements in image quality.

As a result of the very positive response to the advent of digital radiography, different technologies have been developed and are available for use in hospitals and industry. The wide range of choice in digital radiography has led to more specialised devices, allowing the possibility of defining different imaging requirements for different medical procedures (which organ to be imaged, which details needed, the possibility of body motion, etc.). For example, chest radiography requires a large detector size (43cmx43cm is the standard size) and relatively high energies. Mammography, however, needs high spatial resolution in order to detect microcalcifications, a lower energy range (25-30 keV) and the pixel size of the detector is preferred to be between 25 and 70 μm . While cardiology has the requirement that the system must follow the motion of the heart and so it needs high frame rates [7]. Optimization either allows better image quality or, more importantly, gives the possibility of minimizing the radiation dose. X-ray doses, as for all forms of ionizing radiation, have to be as low as reasonable practicable (ALARP principle, [6]). Due to the damaging effects that radiation has on the human body, a trade-off between image quality and delivered dose has always to be found and dedicated X-ray equipment and imaging technologies can help to find the best outcome possible.

The main digital radiography technologies currently available are Thin-Film Transistor (TFT) based detectors, Charge Couple Devices (CCD) and Complementary Metal Oxide Semiconductors with Active Pixel Sensors (CMOS APS). As these technologies might target different applications, a critical performance study will be necessary in order to allow the client or future user to make an objective decision when choosing the device.

1.3.2 Scattering reduction

Cancer is the term used to describe a group of diseases whose common characteristic is the transformation of a normal cell into one that behaves dangerously for the human body. Breast cancer is one of the most common types of cancer in women; each year around 570 000 new cases of breast cancer appear in the world and there are nearly 15 000 deaths. This high index of mortality makes it one of the leading causes of death in western women as a result of malignant diseases [8] [9]. In fact, one in nine women will develop cancer during their lifetime [9].

Breast lesions can be benign or malignant. Around 90% of them are benign, being fibro-adenomas the most common type. Although they can appear any time after puberty, nearing the menopause is when more incidences are given. Benign and malignant tumours can be differentiated from their shape; in general, benign masses have well-defined contours and are round or oval in shape whereas malignant masses have an irregular outline. Calcifications may also indicate the presence of cancer. [10]

Breast cancer has been proved to be a suitable disease for screening programmes, mainly due to its high incidence in the female population, the simplicity of the exam and the fact that there are high risk groups

that can be targeted, such as women who have had a first-degree relative with breast cancer or who are aged 50 or over. There is a clear improvement in the reduction of the morbidity rate in patients over 50 years old when a mammography scan is performed, i.e. around 20% of relative reduction in mortality [9].

A mammography test requires good contrast, good resolution, low dose and large dynamic range [11]. The breast is composed of soft tissue, fat, blood vessels and it may have calcifications or tumours. These tissues all have very similar composition, therefore a X-ray scan must be sensitive to small differences in order to obtain enough contrast to distinguish the different types of tissue. For this reason, it is preferred to have photoelectrical events as the dominant photon interaction so low energy X-ray beams are employed, typical range 25-30keV [12].

Scattered radiation remains one of the main challenges in digital mammography [1], limiting the quantitative usefulness of radiographic images. It reduces the quality of the image, degrades the contrast and the “signal to noise” ratio, reduces the dynamic range and therefore affects the diagnosis of low contrast lesions [13] [14] [15] [2].

In addition to the risk of misdiagnosis, X-ray scatter also causes underestimation in attenuation measurement and the thickness estimation. From the different mammography techniques, dual-energy mammography is especially affected, as it suffers from the scatter contribution from low and high energies, introducing independent errors into the images and affecting the separation of soft and dense tissue, one of the main advantages of dual-energy radiography test. [14] [2]

To reduce the scattered radiation in mammography the most widespread technique, at the moment, is the use of anti-scatter grids. Anti-scatter grids are, however, an incomplete solution that ends up adding complexity and cost to the mammography process. Although they help to improve the quality of the image they also attenuate primary radiation, leading to an increase in the delivered dose (up to a factor of 3) to maintain a constant detector air kerma (DAK) [1] [3] [4].

The limitations of the anti-scatter grids combined with the introduction of new mammography screening techniques that do not allow the use of grids, such as digital breast tomosynthesis, have contributed to the emergence of new scatter reduction techniques based on image post-processing.

1.4 INDUSTRIAL PARTNER: DEXELA LTD – PERKINELMER MEDICAL IMAGING LONDON

PerkinElmer, Inc. (PKI) is an American multinational blue chip technology corporation, focused on the business areas of human and environmental health. The company produces analytical instruments, genetic testing and diagnostic tools, medical imaging components, software, instruments, and consumables for multiple end markets.

In June 2011, Dexela Ltd, a software and X-ray detector Medical Imaging Company, founded in 2005, was acquired by PerkinElmer adding CMOS technology to the company's medical and industrial imaging portfolio.

2 CRITICAL EVALUATION OF DIGITAL X-RAY DETECTORS

2.1 REVIEW OF THE STATE OF THE ART

The X-ray detector literature review focuses on the key areas of digital radiography image characterization, giving an introduction of the main theoretical points and presenting some of the ideas and results previously published in the literature that can affect the development of part of my project.

This section gives a general overview of Analogue and Digital radiography, explaining the main radiographic technologies and their components with a special emphasis on CMOS APS X-ray detector technology, highlighting its main advantages, which are allowing it to take over from the CCD sensor technology market.

The section finishes with a discussion of the main parameters and characteristics that a digital detector must have nowadays, and will be required to have in the future, in order to be successful in the medical imaging area.

2.1.1 Introduction

The performance of radiography scanners has improved in the last decades, with the development of X-ray equipment and recording systems. In the earlier stages, non-dedicated detectors and industrial film detectors were used. Consequently, the contrast in the images was low and the radiation dose delivered to the patient was high, between 50-100 times larger than the average doses currently delivered in mammography, for example [16].

Nowadays, more dedicated equipment is used and two main recording systems are available: Film-screen and digital radiography detectors. In this section, both methods are explained and their main characteristics compared. In order to address this comparison, a series of parameters have to be defined:

- *Signal-to-Noise Ratio (SNR)*: It is the ratio between the intensity of the signal and the noise. The higher the SNR, the better the image quality obtained. [17]
- *Dynamic Range (DR)*: Is the ratio between the maximum signal that the detector can read and the signal equivalent to the noise of the detector. [18]
- *Spatial Resolution*: Is the parameter that determines the dimensions of the smallest object that can be resolved in the image.
- *Modulation Transfer Function (MTF)*: Is the measurement of the spatial resolution in the spatial frequency domain.
- *Detective Quantum Efficiency (DQE)*: Is the quantity that measures the efficiency with which the information is transferred from the imaging system to the final displayed image, allowing quantification how good the imaging system is. [17]

The terms described above are some of the parameters needed to assess the quality of the images. They will be defined further in the next section.

Digital radiography was introduced in the mid-1980s and, with increasing popularity, is now competing with conventional Screen-film radiography in all radiographic applications [19].

The main characteristic and advantage of digital radiography is the separation of image acquisition, image processing and image display. This allows the individual optimization of these three steps, avoiding the need for compromise [18] [20].

Other advantages are a wider dynamic range, higher contrast resolution and higher Detective Quantum Efficiency. This allows either to reduce the delivered dose to the patient without increasing the SNR or to improve the image quality, compensating for the lower spatial resolution that digital systems typically have [18] [17]. All these improvements, together with easier processing and data management, and the possibility of increasing the scope of medical applications, such as in computer-aided diagnosis (CAD) or three-dimensional mammography, makes digital radiography the best system for radiographic screening [18] [17].

There are also drawbacks to a digital radiography system. In addition, to the lower image resolution, there is a possibility of introducing image artefacts, increasing the number of false positive diagnosis. Although some of the artefacts can be corrected, like the non-uniformity in the response of individual detection elements, there are others which are difficult to avoid; for example, dead areas in the images caused by the gap when two image sensors are joined together to make a large area detector. The detector itself can also lead to problems, if the detector field of view is not big enough, for example. Finally, there are also some minor drawbacks; for example the need of multiple monitors of large dimensions, with large contrast resolution and high luminescence, to allow radiologists to review mammograms in an easy way and to allow the comparison between different images at the same time and with high speed [18].

Despite the main advantages that digital radiography has over the conventional screen-film technology, investing in a change of technology has to be justified. There are several, essential properties that a digital system has to provide. The most important being: an acquired image of diagnostic quality, a radiation dose equal or less compared to film, compatibility with existing X-ray generators and image acquisition and processing time comparable to film. Although it is not necessary for a digital detector to give the same response for all parameters, it has to give a comparable image quality, i.e. if the spatial resolution is lower, it must be compensated with other features, such as higher image contrast or sensitivity [21].

As mentioned above, different manufacturers have adopted different approaches and introduced different detector technologies into the market, each of them capable of producing high-quality performance. The main technologies that are currently available are screen film, photostimulable storage phosphor computed radiography (PSP CR) and solid state detectors, including thin film transistor (TFT: Amorphous silicon, a-Si, or amorphous selenium, a-Se), CCD and CMOS detectors. More information about these different technologies can be found in Appendix A, with the exception of CMOS technology that will be explained in the section below.

2.1.2 Complementary Metal Oxide Semiconductor (CMOS)

CMOS detectors are another type of indirect solid-state detectors. CMOS technology used as image sensors was introduced around the 1960s, but it did not become competitive until the 1990s, and in early 2000s for medical applications. The first generation of CMOS sensors were based on passive pixel arrays (PPS), but the results obtained were not comparable to the image quality of the CCD technology. The second generation, named CMOS Active Pixel Sensors (APS), presented lower readout noise and higher speed, improving stability. Due to the good response of this new generation, the ongoing research has been focused on the APS technology [22].

2.1.2.1 CMOS sensor:

The general architecture of a CMOS sensor consists of a pixel matrix array selected a row at a time by row select logic. A pixel is addressed when the column and row decoder is active. The pixel is read out when the signal is buffered by an amplifier and the value is sent to vertical column busses that connect the selected row of pixels to a group of Analogue Signal Processors (ASP). The sampled signal is held in a Sample-and-Hold (S/H) capacitor that is connected to each column bus and then is exported from the chip by an output amplifier, see Figure 1 [22] [23] [24].

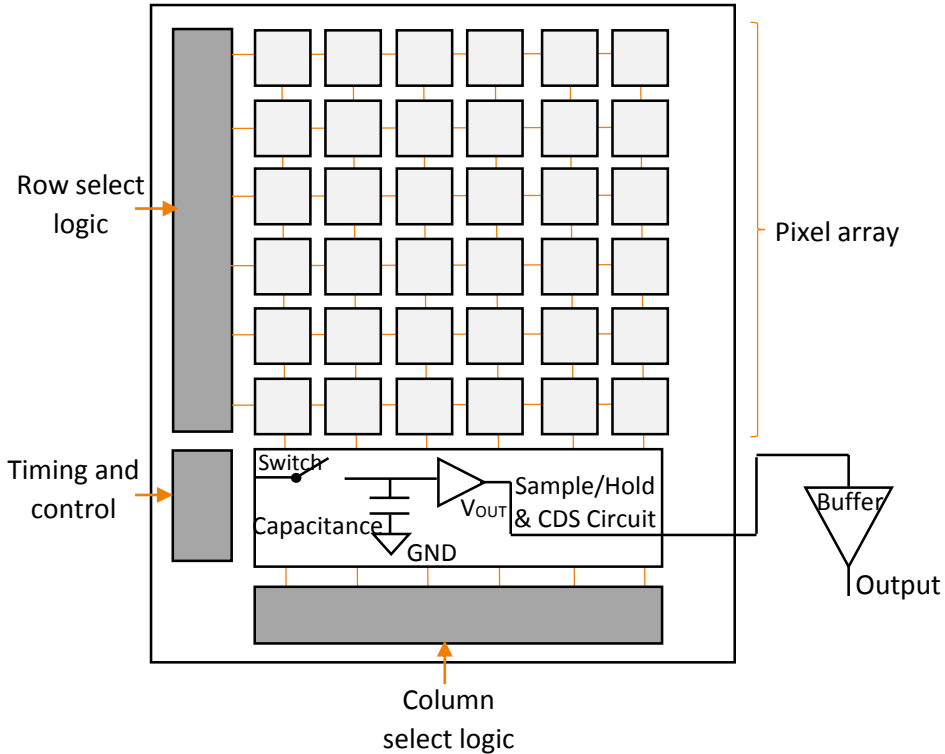


Figure 1: Overall CMOS architecture showing the pixel array, the row and column decoders, the analogue signal processors (S/H, CDS Capacitors and Amplifiers). This image has is a modified version of the CMOS architecture schematic from [23] and [24].

The PPS pixel structure consists of a photodiode and a pass (access) transistor. During readout, a large capacitive load is connected to each pixel, generating high pixel readout noise and reducing the readout speed. The APS approach introduces an active amplifier (source follower) within the pixel structure, leading to a reduction in the capacitance and, therefore, reduction in the readout noise and increase of the Dynamic Range and the SNR.

The most common pixel type in radiography is the 3T (three transistor) pixel, formed by a photodiode, which is composed of a reverse-biased p-n junction, and three transistors: a reset transistor (RST), a source follower transistor (SF) and a row selector transistor (RS). The schematic of a 3T pixel can be seen in Figure 2.

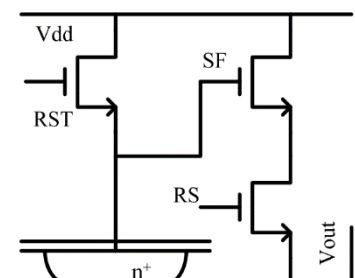


Figure 2: 3T Pixel schematic. Image obtained from [24].

Before the exposure, the photodiode capacitor is charged to a reset voltage through the RST. During the exposure, the RST is turned off and the capacitor gets discharged as the photon-generated electrons are integrated. Therefore, a bright pixel will have lower analogue signal voltage than a dark pixel.

After the exposure, the voltage signal level is read out, the pixel is reset, a new exposure is started and the reset voltage of the second frame is read out. Both voltages are sequentially transferred to the S/H capacitance in a CDS circuit. The signal level is subtracted from the voltage level in order to reduce the fixed pattern noise (FPN), the kTC noise of the photodiode capacitance and the 1/f noise. However, as the sampling process, called delta double sampling (DDS), uses voltages from two different frames the kTC noise is not eliminated and it becomes the main limiting factor in the 3T performance. [24]

The CMOS APS technology presents a cost-effective radiographic detector with low power consumption and very fast image acquisition due to the random pixel addressing capability. It is possible to achieve large active pixel areas using stitching and tiling technologies and medium size pixel pitch, around 50 to 100 μm . The performance at high frame rates is good, as the column parallel read out reduces the read noise. The low read noise leads to high DQE values at low exposures and it is possible to avoid blooming and smearing effects, features that appear with CCDs.

The main drawbacks compared with CCDs, are a reduced sensitivity to incident light (due to low fill factor and quantum efficiency), lower dynamic range, which is limited by the photosensitive-area size, the integration time, stochastic noise and high fix pattern noise. [25] [22]

2.1.2.2 CMOS APS X-ray detector:

Since CMOS detectors are indirect solid-state detectors, a scintillator plate is required to convert the incident X-rays into light. Despite the relatively high radiation tolerance of CMOS sensors, a Fibre Optic Plate (FOP) is typically placed between the scintillator and the sensor with the objective of absorbing the X-ray photons that are not absorbed in the scintillator. See schematic below, Figure 3.

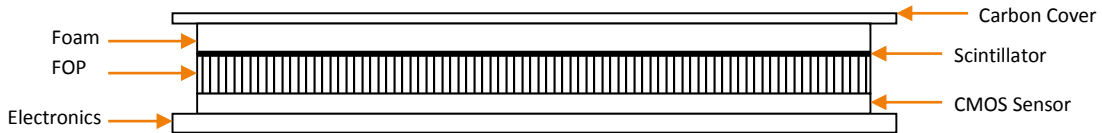


Figure 3: CMOS APS X-ray detector schematic. The X-rays pass through the Carbon Cover and are converted into light photons by the scintillator, which is pressed firmly against the Fibre Optic Plate (FOP) in order to eliminate air gaps. The FOP, bonded to the CMOS sensor, absorbs the remaining X-rays while also guiding the light photons that are finally detected by the sensor. Finally, the output signal is processed and digitalized in ancillary electronics.

2.1.3 Scintillator technology

Scintillator screens are materials that, when traversed by an X-ray beam, emit light photons of a specific wavelength. When radiation passes through a material, the atoms become excited and light is emitted when electrons return to their ground state. If the emission is close in time to the absorption, the scintillation process is called fluorescence. If the emission is delayed, due to the presence of metastable states, the process is called phosphorescence. Phosphorescence can occur after some microseconds up to hours. It is important to minimize this effect as it contributes to an increase in noise in the image reducing the quality of the acquired image. [26] [27]

The main characteristics that an ideal scintillator material would have are [28] [29]:

- Linear light output with the deposited energy.
- High density and atomic number. This leads to high X-ray absorption, improving the spatial resolution and protecting the sensor from radiation damages
- High light output
- Transparency to its own fluorescent radiation
- Appropriate wavelength matching the sensor quantum efficiency curve
- Short decay time without phosphorescence
- Low cost
- Mechanical and chemical ruggedness

Unfortunately, a material with all the above properties does not exist. The most common materials used in X-ray detectors are Thallium-activated structured Caesium Iodide crystals (CsI:TI) and Gadolinium Oxysulfide (GOS or Gadox) ceramic screens.

CsI:TI scintillators are grown in a needle-like columnar structure, perpendicular to a substrate (usually carbon or aluminium). The light is channelled to the sensor when the scintillation fluorescence direction is within the acceptance cone of the CsI light guide. If the angle is bigger, the light is scattered to neighbour needles until the incident angle is acceptable to be channelled [30]. A general restriction of scintillator materials is their thickness: a thick material leads to a higher X-ray absorption but, at the same time, substantially increases the light scattering and image blur. The needle structure of CsI scintillators reduces the light scattering, allowing an increase of the thickness of the screen without losing spatial resolution quality. This material emits green light and has a response time in the region of 1 to 3ms [28]. It has one of the highest scintillation yields and, for the energies used in diagnostic imaging, the number of optical photons emitted per absorbed X-ray is large (>1000) [31]. It also has high detectability, due to the K-absorption edge of the Iodine and Caesium, 33.2keV and 36.0keV respectively [25]. For all these reasons, this material is widely used in X-ray diagnostic imaging.

Gadox screens, $\text{Gd}_2\text{O}_2\text{S:Tb}$, present high efficiency (a response time between 1 and 3ms) green light emission (peak around 545nm) and a main absorption edge at 50keV. It is a very stable and easily handled material [28]. Its main drawbacks are the thickness limitation, as it is unstructured the light scattering increases considerably with the thickness, and the deep notch in sensitivity right at the peak of the X-ray beam spectrum for radiography diagnosis applications [29]. Although CsI:TI screens are a better option, the low cost of Gadox screens makes them a good alternative for some applications.

2.1.4 General design requirements for the next generation of detectors

The objective of acquiring images for medical use is to achieve accurate diagnosis. The last word about the quality of the image is given by the radiologists, who are the subjective receptors. However, there are a series of parameters that define the performance of the X-ray detector and have to be optimized before the product is released.

Any ideal detector would have:

- No dark current, i.e. no electrons generated and collected without light input.
- Infinite dynamic range
- 100% of quantum efficiency, i.e. ratio of incident photons to converted electrons equal to 1.

- 100% of fill factor
- No fixed pattern noise, i.e., no non-uniformities on dark current generation or pixel response, threshold variations or gain and offset differences.
- No sensor noise
- High frame rate
- High resolution
- High signal to noise ratio
- High sensitivity
- No power consumption
- Linear response
- Radiation hardness
- Choice of active area (length)
- Choice of pixel size
- Absence of image lag or ghosting

The limitations present in every sensor technology make impossible to achieve this ideal case. But in order to develop a product that can be sold in the medical market, the manufacturers will have to optimize these parameters, i.e. low dark current, noise and power consumption and high dynamic range, quantum efficiency, frame rate, resolution and sensitivity, for example.

Each digital detector technology has a series of strengths and weaknesses that can be referred to the parameters above. The choice of technology will be decided depending on the desired medical application and, therefore, the performance optimization will be affected by the requirements of this targeted application.

The most restrictive parameters that are decisive when choosing between technologies are shown in the table below. Some parameters like the fixed pattern noise or the linearity can be corrected in firmware or software and others, like the spatial resolution, can be improved with the choice of scintillator, so they were not taken into account in the table.

Table 1: The table shows the expected performance of the three main digital radiography technologies in comparison with the response of an ideal detector. A colour legend explains the main requirements for different medical applications and highlighted in red are the main restrictions the technologies have.

Parameters	Ideal	a-Si	CCD	CMOS-APS
DR	Infinite	Wide	Wide	Restricted
Fill Factor	100%	Restricted	100%	Restricted
Read Noise	None	High	Variable with mode	Low
Frame rate	Infinite	Low	Low	High
Power cons.	None	High	High	Low
Rad. Hardness	Yes	Yes	No	Yes (FOP use)
Length	Large	Large	Small	Medium
Pixel size	Small/Medium	Large	Small	Medium
	CT, tomography or fluoroscopy applications require high frame rate and low read noise			
	General radiography applications require a large/medium detector active area			
	Mammography applications require a small or medium pixel size and low read noise			

From Table 1 it can be seen how the CCD technology is non-acceptable for CT, tomography or fluoroscopy applications due to the reduction in the frame rate needed to keep a low read noise. The most spread technologies for this application are the a-Si and a-Se sensors; however, the possibility of bonding several sensors together, increasing the active area, and the low read noise of the CMOS sensors is helping this technology to take over the market.

The large active area of a-Si and a-Se X-ray detectors makes them the leading technology for general radiography. CMOS sensors on the other hand have taken over CCD sensors in mammography applications.

When a sensor is being developed, after the technology and application have been decided, its response has to be optimised and its limitations minimised. Due to the complicate structure of the sensor, it is very difficult to simulate the performance of the detector with high accuracy. This leads to a series of sensor versions that have to be tested against the product specifications. The quality of the image characterization tests will define the quality of the final product, so it is critical for the manufacturer to cover all the possible errors that the sensor might have before freezing the design.

The following parameters define the performance of the system.

2.1.4.1 Electro-optical performance: Sensor evaluation.

Noise

Noise is a variation in the pixel value of an acquired image that was not present in the original object. There are many factors that contribute to the final noise observed in an image and they have to be minimized in order to improve the image quality.

The main noise sources in a digital detectors are:

TEMPORAL NOISE:

In electronic detectors, it is the flow of electrons that conveys the output signal. These electrons can be produced by the input signal or be artificially introduced, causing the electronic noise. [7]

The temporal noise is composed of [32]:

- Read noise: It is mainly comprised of pixel source follower noise and it is not function of the signal.
- Reset or kTC noise: It appears due to the uncertainty of the capacitor's amount of charge after it has been charged through a resistor.
- Thermal noise: It is generated in resistors and MOS transistors.
- 1/f noise or flicker noise: It is a low frequency noise that appears in MOS transistors.
- Dark current shot noise: It is the statistical variation on the amount of electrons generated in dark (without light input).
- ADC quantization noise: Analogue to Digital convertors produce discrete output levels. Therefore, some analogue inputs give the same output value.
- Phase noise: It comes from external sources rather than being caused in the sensor, i.e. power supply.

Temporal noise is especially problematic at low signal levels, in particular when the noise-electrons are added to the system before the amplification circuits. [6]

INPUT SIGNAL NOISE: Photon shot noise

Photon shot noise, or quantum noise, is the variation of the number of X-ray photons detected. These counting statistics follow the Poisson distribution (and it can be approximated to the normal or Gaussian distribution if the variance, σ^2 , is assumed to be equal to the mean number of photons detected, N). The relative noise of the image is therefore equal to the square root of N , meaning that the noise decreases when the number of detected photons increases. [6]

FIXED PATTERN NOISE (FPN):

FPN, also called structured noise, refers to two parameters: the dark signal non uniformity (DSNU) and the photo response non uniformity (PRNU). The DSNU noise is the offset between pixels in a dark image, i.e. no illumination level, at a specific temperature and exposure time. The PRNU is the response variation between pixels under illumination.

The FPN is usually caused by the read out channels of pixelated detectors, although dust or imperfections in the sensor contribute to it as well. CMOS detectors, for example, have parallel read out channels with their own amplification circuits, so they cannot be perfectly matched with respect each other, creating a different offset and gain response between pixels. [6]

The main advantage of the FPN is that it is a correlated, non-stochastic noise, i.e. relatively constant in time, so the gain and offset factors of each pixel can be characterized and the image corrected.

The gain and offset correction algorithm is described in Equation 1:

$$I_{\text{corr}} = g \frac{I_{\text{raw}} - I_{\text{offset}}}{I_{\text{gain}} - I_{\text{offset}}} \quad \text{Equation 1}$$

Where,

g = Mean Pixel Value of the Offset corrected gain image ($I_{\text{gain}} - I_{\text{offset}}$)

I_{raw} = Raw image to correct

I_{offset} = Offset or Dark image, acquired with no illumination. Usually 10 to 20 dark images are averaged.

I_{gain} = Gain or Flat image, acquired at a similar illumination level that the image to correct. Usually 10 to 20 flat images are averaged.

All the images have to be taken at the same exposure time.

The I_{offset} and I_{gain} images need to be collected at regular intervals to account for temperature or position variations. [6] [32]

Conversion Gain

The Conversion Gain gives the conversion factor to transform the digital numbers (DN), i.e. count unit (ADC) given by the detector which is meaningless by itself, to electrons.

A way of calculating K is following the mean-variance (MV) analysis, described in [32]:

$$\sigma_S^2 = G\bar{S} + \sigma_R^2 \quad \text{Equation 2}$$

Where,

σ_S^2 [DN²] is the total measured temporal noise (signal independent and dependent). The way of calculating this variable is acquiring a number (N) of images at a constant signal level and quantifying the temporal variation of each pixel around its averaged value. The mean of the resulting 2D matrix gives the total measured temporal noise.

σ_R^2 [DN²] is the signal independent read noise.

\bar{S} [DN] is the signal level.

G is the conversion gain in [DN/e⁻].

Plotting the total measured temporal noise versus the signal level and fitting the straight area of the curve will lead to the Conversion Gain (slope of the curve) and the signal independent read noise (y-intercept).

Full Well Capacity (FWC)

The FWC is the maximum electronic charge that the photodiode's sense node in each pixel can accommodate before the pixel is saturated.

It can be calculated by multiplying the Conversion Gain and the mean signal level corresponding to the higher variance without previous subtraction of the dark level, value obtained from the mean-variance analysis in the conversion gain calculation (see above). [32]

Dynamic Range (DR)

The dynamic range is the ratio between the largest and smallest value of the signal. It is given by the ratio of the output saturation signal to the r.m.s. output detector noise or, in other words, the ratio between the FWC and the read noise. It is described by the equation below. [33] [32]

$$DR \text{ (dB)} = 20 \log \frac{FWC \text{ (e⁻)}}{\sigma_R \text{ (e⁻)}} \quad \text{Equation 3}$$

2.1.4.2 X-ray evaluation.

Spatial Resolution. Modulation Transfer Function

The spatial resolution is a measure of the smallest object that can be resolved in an imaging system, describing the level of detail that can be appreciated in an acquired image [6]. For digital systems, the lower limit to the size that can be resolved is equal to the pixel size. However, smaller objects can be detected if the signal amplitude is enough to affect the grey scale value of that pixel, i.e. high-contrast objects. Although the pixel size is the lowest limit achievable there are other factors that can limit more the spatial resolution, restricting it further.

The modulation transfer function (MTF) is a metric that describes the spatial resolution in the spatial frequency domain. It gives more accurate and objective results than the ones obtained with resolution phantoms or line pair phantoms.

The MTF evaluation is very sensitive to the method followed, the analysis process and the measurement settings. The International Standard created the documents IEC 62220-1: Medical Electrical Equipment - Characteristics of Digital X-ray Imaging Devices - Part 1: Determination of the Detective Quantum Efficiency, [34], and IEC 62220-1-2: Medical Electrical Equipment - Characteristics of Digital X-ray Imaging Devices - Part 1-2: Determination of the Detective Quantum Efficiency – Detectors used in mammography, [35], in order to regulate the MTF measurement method, reducing the number of variables that complicate the comparison between systems. More information about the concept of MTF can be found in Appendix A, section A.2. For more details about MTF evaluation methods refer to section 2.3.2.1 of this chapter and to Appendix C.

E. Samei, J.T. Dobbins and N. T. Ranger, [36], made a study of the relationship between two different methods, developed before the international standard, and the IEC 62220-1 document, aiming to find the relationships between the three methods that would allow the comparison of results in the literature. In their study, they also included an analysis of the impact of different measurement settings in the MTF results. They found that there is very little difference between the MTF measurement in the horizontal and vertical directions. That the presence of external collimators affect the final measurement of the MTF between a $4.0\% \pm 0.9\%$ and $7.0\% \pm 0.9\%$, for external apertures and internal beam collimators respectively, and that a misalignment between the edge and the axis of the X-ray beam does not introduce significant changes in the MTF estimates. Their evaluation concluded that the method introduced by the IEC standard, using an opaque edge test device for measuring the ESF, gives lower MTF measurements. The averaged relative differences up to the Nyquist frequency was found to be $5.2\% \pm 0.2\%$ when compared with a method using a slit test device for calculating directly the LSF, method that was introduced by Dobbins et al. [37], and $2.0\% \pm 0.2\%$ when compared to a method using a translucent edge test device, introduced by Samei et al. [38].

Noise Power Spectrum.

The NPS is a parameter that quantifies the spectral decomposition of the noise variance of an image as a function of the spatial frequency [39] [40]. It is a way of quantifying the noise “texture”. Two images can have the same variance but look different; the NPS gives a more accurate description of the noise by measuring the effect that the image system has on the noise input [41]. Refer to Appendix A, section A.3, Appendix C and section 2.3.2.1 of this chapter for more information about the evaluation of the NPS.

The 2D NPS is described by Equation 4:

$$\text{NPS}(u, v) = \frac{\Delta x \cdot \Delta y}{M \cdot N_x \cdot N_y} \sum_{i=1}^M |\text{FFT}\{I(x_i, y_i) - S(x_i, y_i)\}|^2 \quad \text{Equation 4}$$

Equation obtained from IEC 62220-1 [34].

Where,

(u, v) are the spatial frequencies in the horizontal (x-axis) and vertical (y-axis) respectively.

Δx and Δy are the pixel sizes in the x-axis and y-axis respectively. Note that $\Delta x = \Delta y$ for square pixels.

$(N_x \times N_y)$ is the Region of Interest (ROI) size, 256×256 pixels² if the analysis method followed is the IEC 62220-1 [34].

M is the number of ROIs per frame selected.

Contrast Resolution.

Contrast resolution is a measurement of the imaging system's ability to detect subtle changes in the grey scale, i.e. structures that cause small changes in the signal intensity that are difficult to be distinguished from the background.

SIGNAL TO NOISE RATIO (SNR)

The SNR is a measurement of the signal level in the presence of a noisy background, i.e. it describes the signal amplitude relative to the ambient noise. This metric takes into account the shape and size of the object, making it a useful parameter to evaluate contrast when the bright object is not homogeneous. [6]

The SNR measures the signal amplitude on a pixel basis of a ROI compared to the noise background (σ_{bg}). The signal amplitude of each pixel is the difference between the signal level of that pixel and the background mean pixel value ($x_i - \bar{x}_{bg}$). Therefore, the SNR can be described as:

$$SNR = \frac{\sum_i (x_i - \bar{x}_{bg})}{\sigma_{bg}} \quad \text{Equation 5}$$

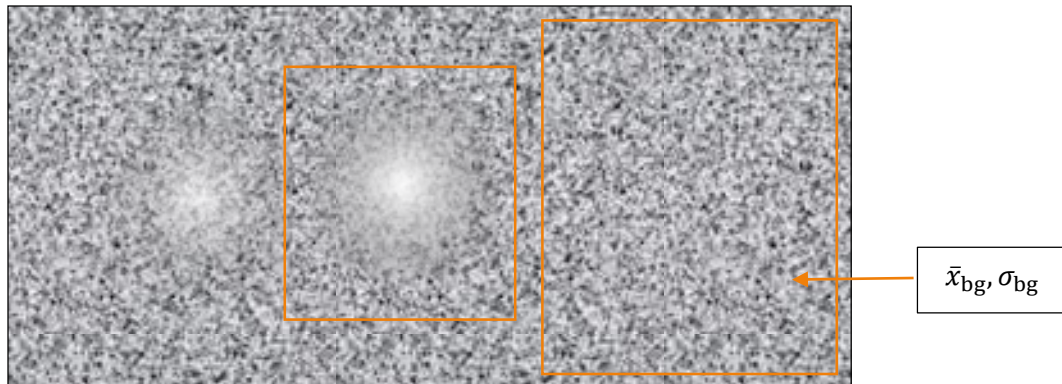


Figure 4: Example of a non-homogeneous bright objects and the parameters needed for the calculation of the Signal to Noise Ratio (SNR). The idea of the image was obtained from [6].

Detective Quantum Efficiency (DQE)

The DQE metric describes the ability that an imaging system has to capture information over a range of spatial frequencies. It expresses the efficiency with which the detector uses the input signal (incident X-ray photons) to form the image, i.e. how effectively the system uses the available input quanta [40] [39].

The DQE depends on the noise generated by the detector and on the spatial resolution, so it gives a measure of the SNR, the contrast resolution and the dose efficiency [20] [42]. An ideal detector would have a DQE equal to 1 for all spatial frequencies while a real detector has values between 0 and 1 which typically decreases as spatial frequency increases, as a consequence of the degradation of the SNR between the output and the input [20] [42] [40]. Therefore, better DQE results in image quality improvement while keeping the dose received by the patient constant or even decreasing it.

The DQE is given by

$$DQE = \frac{SNR_{out}^2}{SNR_{in}^2} = \frac{MTF(f)^2}{\frac{\phi}{k_a} k_a NNPS(f)} \quad Equation \ 6$$

Where,

$SNR_{out}^2 = QE = \frac{MTF(f)^2}{NNPS(f)}$ The NNPS, Normalized Noise Power Spectrum, is already a measure of the variance so it does not need to be squared.

$SNR_{in}^2 = \frac{\phi}{k_a}$ is the fluence per exposure ratio ($\frac{\phi}{k_a}$) multiplied by the exposure karma (in μGy).

There are different ways of calculating the fluence per exposure ratio. The International Standard IEC 62220-1 gives a photon-counting approximation, assuming that an ideal detector behaves like an ideal photon counter. It can be calculated following the equation [32].

$$\frac{\phi}{k_a} = \int_0^{KV} \phi_{norm}(E) \frac{WQ}{\left(\frac{\mu_{en}(E)}{\rho}\right)_{air} E e 10^8} dE \quad Equation \ 7$$

Where,

$\phi_{norm}(E)$ is the normalized spectrum.

W [eV/ion pair] = 33.97 eV/i.p. is an accurate value for X-rays in dry air, [32].

$Q = 2.58 \times 10^{-4}$ C/Kg/R is the charge liberated in air by one R.

$e = 1.6022 \times 10^{-19}$ C is the electronic charge.

As mentioned, the standard gives a photon-counting approximation, but the detectors built at PerkinElmer are energy-integrating detectors. It is possible to perform an energy-weighted calculation of the fluence per exposure ratio, but previous studies, mentioned in Konstantinidis, et al. paper [32], proved that the difference at radiation quality RQA-5 (explained below) is less than 3%, decreasing further for lower voltage spectra.

The International Standard dictates the DQE assessment at different radiation qualities, which corresponds to different radiographic applications. The measurement settings and the photon-counting approximation vary with each radiation quality. For example, the IEC 62220-1-2 gives radiation qualities for mammography (RQA-M), IEC 62220-1 gives radiation qualities RQA3 (paediatrics), RQA5 (general radiography) and RQA7 (higher energy applications).

2.2 PROJECT MOTIVATION AND IMPACT ON DESIGN CYCLE

This project was defined to assist in the development of the new family of CMOS X-ray detectors that PerkinElmer is planning to introduce onto the market on 2016. The main objective was to make use of detector image characterization methods to detect possible issues in detector or sensor design that had to be addressed in order to ensure that the final product will meet the customers' expectations.

There are a series of well-established methods that are needed to make a full image characterization of digital X-ray detectors. Most of the information is, however, not published by private companies and so there is very little information in how to use the methods to optimize the detector design during the

product design cycle. As PerkinElmer has just introduced the on-site development of the CMOS sensor technology, this process needed to be defined and implemented.

The evaluation of the CMOS X-ray detector prototypes has played an important role in the final design of the products. The sensor issues that were found during this process have been addressed and the new version of the sensors will be available for testing from December 2015.

2.3 PERFORMANCE METRICS AND IMPLICATIONS

2.3.1 Methodology

Section 2.1 introduces all of the parameters that need to be considered to design an ideal X-ray detector for medical imaging. Building on these requirements and well-defined test methods, then combining these with prior knowledge of common failure modes and optimisation techniques used by CMOS sensor and electronics design engineers, it is possible to generate a set of tests which both quantify the performance of prototype devices and also acquire very specific metrics for their optimisation. In this section tests are defined and justified.

The theory behind the chosen methods has been introduced in section 2.1.4 while a more detailed description of the measurement and analysis process is explained in Appendix B, a document, created by the author, that presents the work instructions that have been adopted by the R&D department of PerkinElmer - London to characterize the engineering detectors or prototypes, and in Appendix C, a document that shows the measurement and analysis method followed for MTF, NPS and DQE measurements.

The second part will look into the characterization of a fully functioning detector. The idea is to compare its performance, with other technologies or the same technology used by competitor manufacturers, either by performing direct measurements or by comparing the results that have been published previously. This section will be completed once PerkinElmer releases their new family of products. See Chapter 4 of this document for more details of the project plan.

From prior engineering experience and lessons learned during the development cycle, a number of test methods were created by the author to perform the sensor and detector characterization. The motivation for each test is summarised below.

2.3.1.1 *Offset variation with temperature*

When a detector is turned on there is an increase in temperature until stability is reached. Changes in temperature produce changes in the image offset level and the noise values. Plotting the dark level versus the temperature should give a smooth variation. Any abrupt changes or discontinuities might indicate a sensor problem.

2.3.1.2 *Offset variation with exposure time*

The offset and noise levels increase with exposure time until the sensor pixels saturate, usually at times longer than 10 seconds. Increments of time that double the offset should make the noise to increase by the square root of two.

Any non-linear increase of the offset value or non-uniformities in the offset vs. exposure time graph might indicate a sensor problem.

2.3.1.3 *Noise: static and temporal*

The static noise image allows the identification, by visually inspecting the images, of any additional patterned noise introduced by the sensor or the electronics.

A sequence of temporal noise images allows visualisation of frame to frame variations that might be indicative of electronic noise injection.

2.3.1.4 *Sensor response time*

The time that the sensor takes to react to light input, passing from dark to bright, should be negligible or very low and should not depend on the light intensity. A slow rise time of the sensor or variable responses with the intensity level might indicate a sensor problem.

2.3.1.5 *Image lag*

Similar to the sensor response time, this is the amount of time, or number of frames, that the detector takes to react to an input signal when the detector is irradiated with X-rays. Image lag might be indicative of a performance problem with the scintillator.

2.3.1.6 *Image afterglow*

The amount of time that the detector takes to recover from an exposure. The afterglow is visible in the dark images after an object has been illuminated and it varies with the amount of exposure received. Analysis of this effect is usually correlated with scintillator performance.

2.3.1.7 *Pixel crosstalk*

The amount of the signal of one pixel that is transferred to neighbouring pixels. Pixel crosstalk might indicate an issue with the sensor design or electronic system design.

2.3.1.8 *Linearity*

The detector response should be linear with the signal input. Even a small non-linearity can cause problems with the gain-corrections that are applied in hospitals, manifesting itself as an image artefact.

Multiple parts of the system can impact upon the linearity, but common culprits are the sensor design and electronic design.

2.3.1.9 *Modulation transfer function and uniformity*

The modulation transfer function is a measurement of the spatial resolution of the detector. This measurement is particularly useful when compared with previous or predicted results, as lower values might indicate sensor or scintillator problems.

Different MTF results across the detector area might indicate uniformity issues.

Different MTF values when measuring vertical and horizontal directions might indicate either a uniformity problem or non-symmetry in the pixel design.

2.3.1.10 *Detective quantum efficiency*

The detective quantum efficiency measurement is very sensitive to small detector variations. This makes it a very useful measurement to be used as a red flag, indicating that overall detector performance has been compromised.

Large variations between DQE curves calculated at different exposure levels indicate linearity problems.

DQE values that are too high (higher than 0.8 at 0.5lp/mm) can show image lag issues or incorrect calibration of exposure times.

2.3.2 Implementation

The set of methods introduced in the methodology section were used for testing a sequence of engineering prototypes of the new family of CMOS sensors. The result is presented in the “work instructions” document of Appendix B. As mentioned in the methodology, this document explains the measurements and analysis method for performing a detector characterization. In addition, it also provides information with regards the expected result of the measurement and how to analyse the images in order to verify that issues previously identified remain eliminated from the project (regression analysis).

The procedure followed to carry out most of the tests is well known and there is no ambiguity in the measurement or analysis method. However, other tests have been defined to catch some very specific problems that were identified in the sensor development process. This section will focus on these problem-specific tests and on the methods followed in the MTF and DQE calculation, due to the wide ambiguity found in the literature for producing these two metrics.

2.3.2.1 MTF and NPS methods

The three main metrics that have been broadly accepted in the literature to be fundamental in defining detector performance are MTF, NPS and DQE. These parameters can be difficult to measure and variation in the methodology followed can lead to significant differences in the results. The final methods that were chosen followed the International Standards IEC 62220-1 [34] and IEC 62220-1-2 [35]. Although the MTF values obtained following these standards have been proven in the literature to give lower values than alternative measuring methods, see section 2.1.4.2, it is generally a customer’s requirement to follow the standard. Moreover, it allows comparison of the results with other technologies or published data.

The analysis of the MTF and NPS has been performed with a MATLAB analysis tool obtained from Anastasios C. Konstantinidis, used in his graduate studies and explained in UCL thesis “*Evaluation of digital x-ray detectors for medical imaging applications*” [40]. The DQE is obtained from the MTF and the NPS values, see Equation 6.

MTF

In the MTF measurement the standard specifies that the MTF has to be calculated using the ESF method, but it leaves the analysis method open to interpretation. The measurements are made using a straight tungsten edge placed directly in front of the detector, aligned with the central axis of the X-ray beam. The edge has to be tilted between 1.5 and 3 degrees with respect to the detector pixel row or column. This is done to reduce aliasing to between 0 line pairs per mm (lp/mm) and the Nyquist Frequency (f_N), defined as the highest frequency that allows for full reconstruction of the signal; for MTF measurements, it is the inverse of double the pixel size.

The analysis method introduced by Konstantinidis obtains the ESFs directly from the edge image, after it has been properly gain and offset corrected. A series of consecutive lines across the edge (vertical direction when the edge is placed vertical) are chosen and the intensity profile obtained. The averaged ESF, calculated from the consecutive lines after they have been properly shifted (this is done to reduce statistical noise and aliasing), is then calculated. The LSF can be obtained by differentiating the ESF. Finally,

the pre-sampled MTF is calculated applying the Fast Fourier Transform (FFT) to the LSF, see Figure 5 and Figure 6.

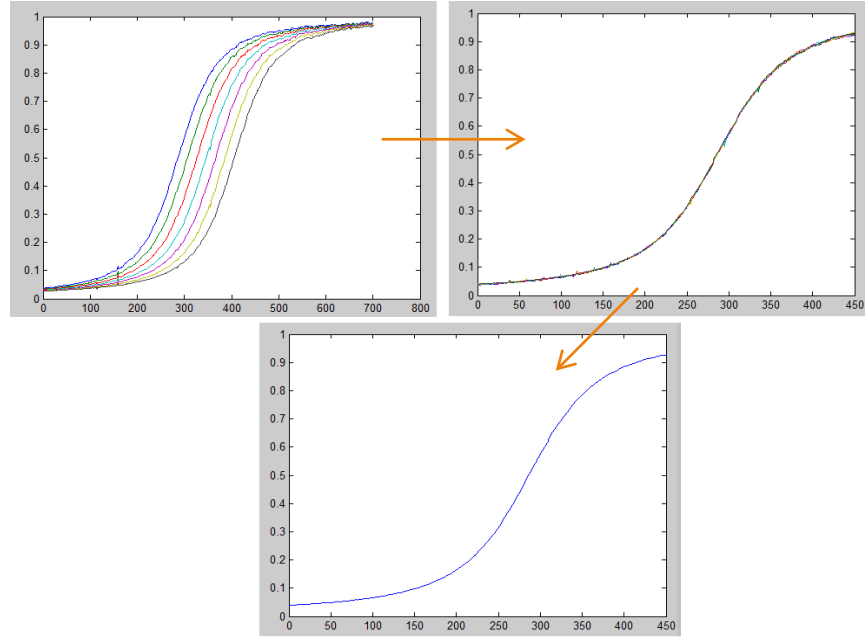


Figure 5: The top-left graph in the figure shows an example of 7 samples of the ESF. The top-right plot shows the 7 samples superimposed and the bottom figure shows the averaged ESF.

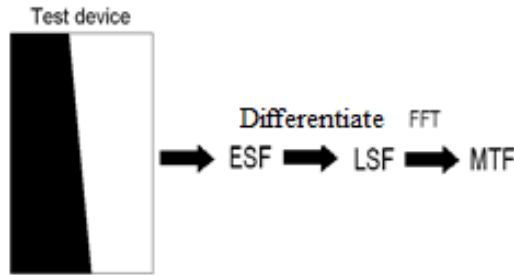


Figure 6: Summary of the ESF method to calculate the MTF.

This method must make use of the whole area of the edge to gain statistics in the analysis. This particular characteristic can lead to erroneous MTF values if the edge used for testing is small or if the usable area is reduced.

NPS

The ambiguity in the NPS calculation when the standard is followed is extremely small. See Appendix C and section 2.1.4.2 for more information about the method. However, it is very important to correct the images for possible non-linearity of the detector. A non-linearity as low as 2% already causes variation in the DQE values obtained at different exposures.

If the images used for the NPS calculations are gain-corrected using an average image obtained with the images themselves, a statistical correction will have to be applied to the values, of the form of [31]:

$$NPS_{corr} = NPS_{measured} \frac{n}{n-1}$$

Equation 8

Where,

n = number of frames used to obtain the average image.

2.3.2.2 *Glowing effect test*

The glowing effect was an issue found in one of the prototypes. It was a combination of pixel crosstalk and variations in the sensor rise time. The effect showed a difference in the response of those columns (row) that were next to a dead column (row). It was named “glowing” because the difference disappeared as soon as the sensor response was stable.

The glowing effect can be tested at the same time as the detector lag and afterglow.

2.3.2.3 *Edge Spread Function (ESF)*

The edge spread function used for MTF calculation proved to be very useful in order to detect pixel crosstalk. It is easily spotted studying the pairing of consecutive intensity profiles, i.e. edge spread functions of consecutive columns.

2.3.3 Validation

The detector issues identified during the first part of the design cycle through the characterization process outlined above helped to further improve this process through iteration, discussion with design engineers and optimization. Since many of the tests were designed to catch a specific failure mode or shortcoming, the positive identification of this shortcoming or exhaustive proof of its absence is seen as a form of self-validation of the technique. This self-validation, combined with the assistance I got from the engineering team of the company by helping me to find the root cause of the problems uncovered, has been accepted as valid proof of the usefulness of the tests by the wider team.

In the case of the MTF, NPS and DQE methods, however, a deeper validation was made, due to the potential ambiguity of the measurements and the standard itself. The methods were first tested with the existing product family of CMOS X-ray detectors, that have been on the medical imaging market for some years and have been tested using different methods by other people.

The first step in the validation was to obtain similar values to those published by Anastasios C. Konstantinidis, as he had developed the MATLAB analysis tool that we were using. The results obtained were compatible with the results published in his thesis, [40], and publications, [32] [25]. Although his work had been previously validated, [40], an additional comparison was made in order to confirm the accuracy of the methods.

The second comparison was made with a PerkinElmer toolkit that is used at the Santa Clara (SC) site for the MTF and DQE measurements of their amorphous silicon detectors. This toolkit follows the method introduced by Granfors and Aufrichtig, [31], also compatible with the IEC 62220-1 and IEC 62220-1-2 standards, [34] [35]. The measurement analysis was performed using both analysis tools and the result was again comparable. However, the DQE values obtained with the PerkinElmer - SC tool were slightly

lower. The reason was found in the NPS correction mentioned above, see Equation 8, as Konstantinidis' method did not apply such correction.

2.3.4 Deliverables

- Conversion Function, Modulation Transfer Function and Detective Quantum Efficiency Measurement and Analysis document, see Appendix C. This document gives the instructions to perform the measurement and the analysis of the MTF and DQE metrics according to the standards IEC 62220-1 and IEC 62220-1-2 standards, [34] [35].
- Detector Imaging Testing – Work Instructions document, see Appendix B. This document specifies the instructions to be followed to perform a full detector characterization.
- Test analysis reports: produced for the prototypes of the new family of CMOS X-ray detectors and used to give feedback to the designers and the engineers whenever an issue was found. Detailed examples are not given since this is regarded as confidential design information by PKI.

2.4 ISSUES TACKLED TO DATE BY THE EVALUATION PROCESS

In the design cycle, there have been various image artefacts and performance issues that required investigation. Each investigation was performed in close collaboration with various parts of the engineering team, as various possible sources of the issue were investigated. Typically, this would cycle through (in no particular order) electronic design, electronic system tuning, FPGA (field-programmable array) logic and design (firmware), X-ray component performance and sensor design. When there was a finding, there was a root cause investigation and, once it was found, the problem was reported to the corresponding engineer and the issue fixed. Issues encountered with the electronics or the firmware have, for example, been high and low frequency noise, noise flickering, bit errors and image clipping. Some examples can be seen in Figure 7 to Figure 9.

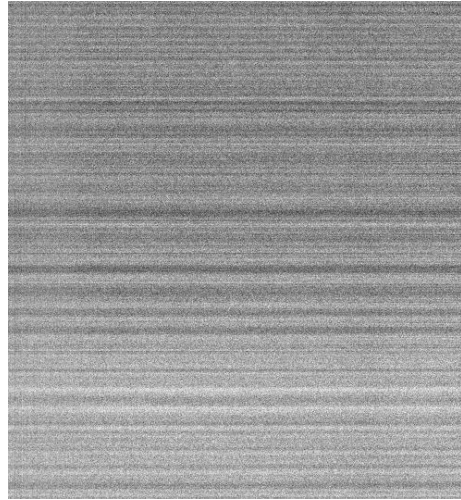


Figure 7: The figure shows an example of a row noise with variable frequency that was seen in a static noise image.

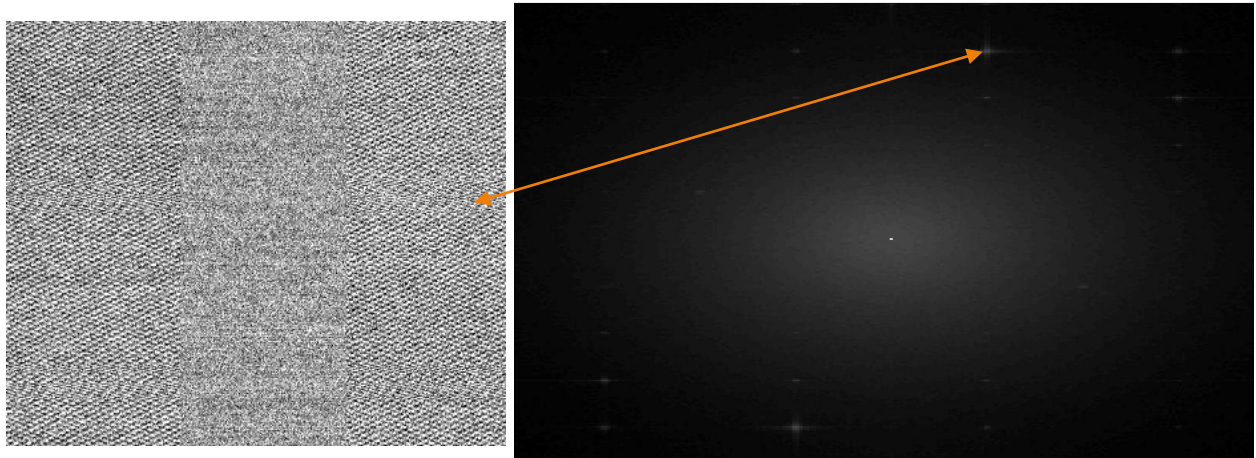


Figure 8: On the left there is an example of high frequency noise and clipping affecting some parts of the noise image. The figure on the right shows how the 2D NNPS was affected by the clipping.

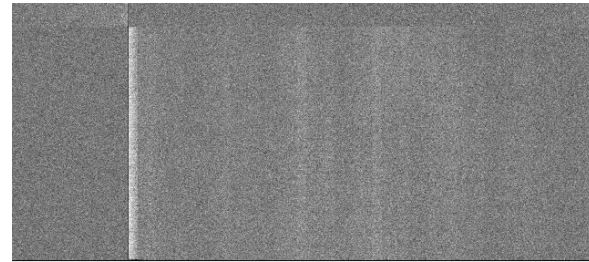


Figure 9: This figure shows a temporal noise image. The non-uniformities indicate that there is a frame to frame variation and that the image flickers.

Some minor shortcomings found in the sensor design were pixel crosstalk, non-linearity, linearity variations throughout the sensor, image lag variations, etc. Some examples can be seen in Figure 10 to Figure 12.

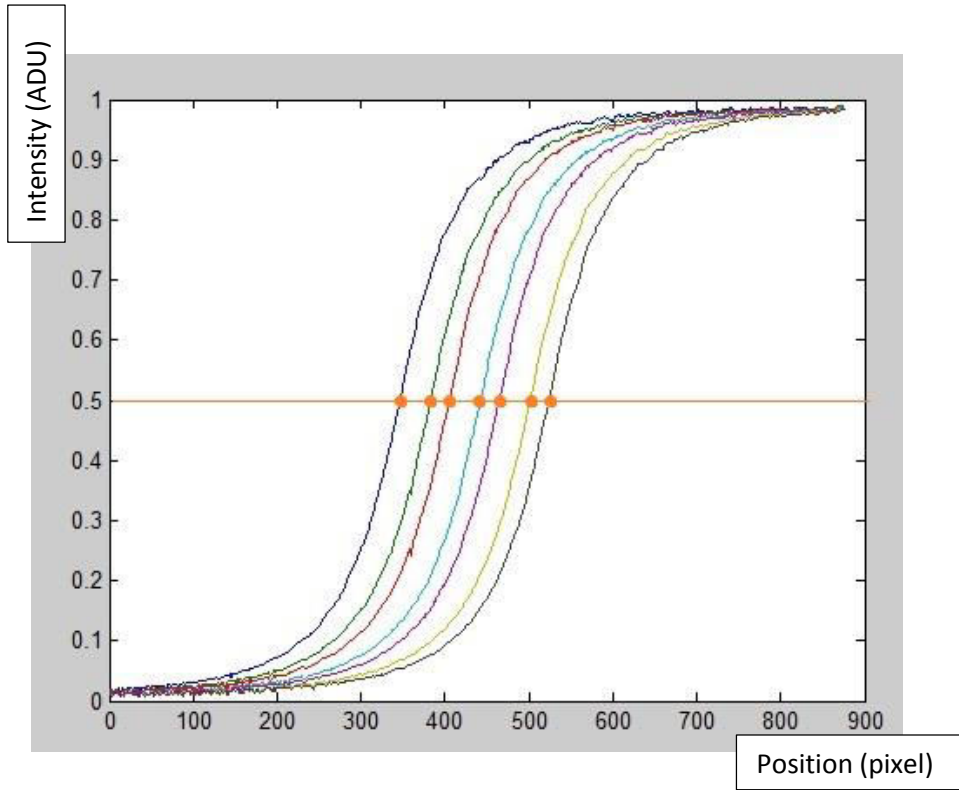


Figure 10: The graph shows an intensity profile of seven consecutive columns plotted across a sharp edge (ESF). The orange dots should be at a constant distance from each other. However, the distances are paired, i.e. the distance changes every second column from D1 to D2. This is an indication of pixel crosstalk between columns.

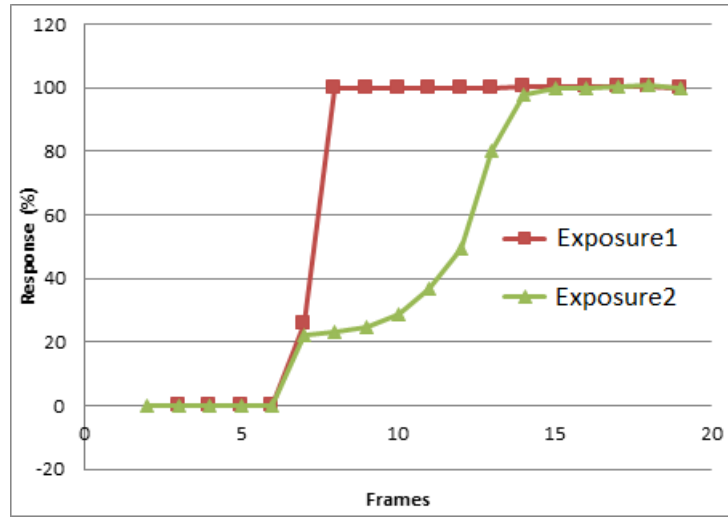


Figure 11: The graph shows the detector response as a function of the frame count for two different exposure levels (Exposure1>Exposure2). The detector was initially obtaining dark frames (response 0) and then it was irradiated from frame 6 onwards until reaching the 100% of response. The red curve shows the typical response of a detector, where in a matter of one or two frames the response level is constant at constant illumination. The green curve shows a lag problem, the detector takes 9 frames to return a constant response.



Figure 12: This image shows three phantom images acquired in a sequence. The middle line disappears after 14 frames have been acquired, showing that this line has a different lag response than the rest of the sensor.

For more information see Appendix B.

3 SCATTERING REDUCTION IN X-RAY IMAGING

3.1 REVIEW OF THE STATE OF THE ART

The scattering reduction literature review offers an overview of scattering reduction methods introduced as an alternative to anti-scatter grids. It gives an overview of the main techniques, paying special attention to the convolution-based scattering corrections, where it explains the different methods that have been presented in the literature and the results obtained to date. The dependencies between the acquisition geometries and the scattering are then investigated and the typical mammography geometry set up is presented. Finally, a Monte Carlo simulation toolkit is described and its use in prior work explained.

3.1.1 Introduction

A digital X-ray detector produces an image from the accumulation of events that hit individual pixels. Each of these events can be attributed either to the primary X-ray beam, that has passed through the body with no directional change, or to scattered radiation. Therefore, a radiographic image, $I(x,y)$, can be described as the sum of a primary image, $P(x,y)$, and a scatter image, $S(x,y)$:

$$I(x,y) = P(x,y) + S(x,y) \quad \text{Equation 9}$$

The two dimensional description of the scatter can be seen as a low-pass filtered primary image [14] [43]:

$$S(x,y) = P(x,y) * f(x,y) \quad \text{Equation 10}$$

Where, $f(x,y)$ is an unknown filtering kernel.

However, as $P(x,y)$ is unknown, and the determination of which is the principal objective of this study, it is not possible to use it to calculate $S(x,y)$. To address this problem, different authors use different methods:

- Love and Kruger, [43], obtain $P(x,y)$ by approximating $S(x,y)$ to:

$$S(x,y) \approx I(x,y) * h(x,y) \quad \text{Equation 11}$$

Where, $h(x,y)$ is a different low-pass filter kernel that has also to be determined.

From that equation, $P(x,y)$ can be estimated subtracting the scatter image to the output image:

$$P(x,y) = I(x,y) - S(x,y)$$

$$P(x,y) = I(x,y) - I(x,y) * h(x,y) \quad \text{Equation 12}$$

- Ducote and Mollo, [14], propose to work in the frequency domain to avoid the approximation step introduced in the method above. Their technique uses image deconvolution in order to decouple the convolution of the scatter component with the primary component:

$$P(x, y) + S(x, y) = P(x, y) * g_{p+s}(x, y) \quad \text{Equation 13}$$

$$I(x, y) = P(x, y) * g_{p+s}(x, y) \quad \text{Equation 14}$$

Where g_{p+s} is the redefined convolution kernel that maps both the scatter and the primary components.

The primary component can then be isolated if the Fourier transform is applied:

$$\text{FFT}(I(x, y)) = \text{FFT}(P(x, y) * g_s(x, y)) \quad \text{Equation 15}$$

$$\text{FFT}(I(x, y)) = \text{FFT}(P(x, y)) \times \text{FFT}(g_s(x, y)) \quad \text{Equation 16}$$

$$\text{FFT}(P(x, y)) = \frac{\text{FFT}(I(x, y))}{\text{FFT}(g_s(x, y))} \quad \text{Equation 17}$$

$$P(x, y) = \text{FFT}^{-1} \left(\frac{\text{FFT}(I(x, y))}{\text{FFT}(g_s(x, y))} \right) \quad \text{Equation 18}$$

Instead of Cartesian coordinates, it might be of interest to use polar coordinates. If that is the case, it would be possible to drop the angular dependence if circular symmetry is assumed: $(r, \theta) \rightarrow (r)$ [13] [44].

There are various ways of quantifying the scattered radiation, a couple of them are the scatter to primary ratio (SPR) and the scatter fraction (SF), defined in Equation 19 and Equation 20:

$$\text{SPR} = \frac{S}{P} \quad \text{Equation 19}$$

$$\text{SF} = \frac{S}{S+P} \quad \text{Equation 20}$$

Where S and P are, respectively, the integrated energy of scattered radiation and the integrated energy of the primary radiation that strikes the region of interest [13]. Another unit is the mean radial extent (MRE) that helps to characterize the spreading of the pencil beam, when the X-ray beam is simplified to a normally incident delta function [45].

The main objective is to find a primary image $P(x, y)$ that is similar or better to the image that would have been obtained with the anti-scatter grid. If that is achieved, the possibilities of introducing artefacts with the grid removal post-processing methods would disappear, the dose delivered to the patient could be potentially reduced and some of the image contrast recovered [1].

The accuracy of the post-processing scatter correction depends strongly in the model chosen for the scatter. An inaccurate simulation will lead to inaccurate corrections, obtaining suboptimal improvements or even artefacts in the image [45]. The methods considered in this literature review can be divided between physical and simulated methodologies. Within the physical techniques it is possible to find the edge spread methodology, the beam stop methodology, the scatter medium reposition methodology and the slat methodology. The simulated techniques are divided here into Monte Carlo (MC) simulations and scatter convolution methods. The differences between the above methods can be found in the next sections.

3.1.2 Physical methods

3.1.2.1 Edge Spread methodology [15]:

This method uses a lead edge device placed on top of a scatter medium which is on top of the detector surface and facing the X-ray beam. One image is acquired with the entire set up, including the scatter material and the lead area (S+P image) and another image keeping the same geometry, see Figure 13-left, but without the scatter material (P image).

From the acquired images it is possible to plot an intensity profile across the edge, Figure 13-right. In the plot, the plateau (A in the figure) is composed by primary and scattered radiation (P+S), while the points B and C are P+S/2 and S/2 respectively. Point C is not 0 due to the scattered radiation signal “leaking” across the edge.

If the P image is subtracted from the S+P image, after normalization, the difference results in separate measurements of the scatter and primary radiation. The final plots can be then differentiated to obtain the scatter line spread function (LSF), that gives the scatter profile.

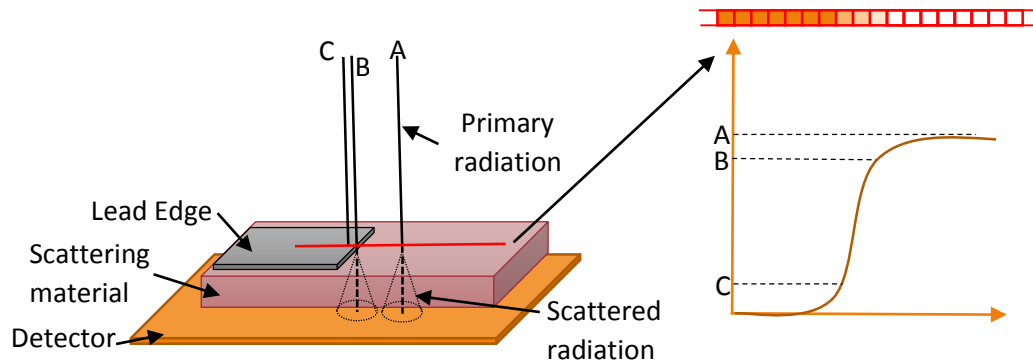


Figure 13: On the left the figure shows the geometry of the edge spread method, a lead edge is placed on top of the scatter material and an image is acquired. The right image shows an example of the intensity profile across the edge needed to calculate the scattering contribution.

3.1.2.2 Beam stop methodology:

A series of different diameter disks are placed between the beam and a phantom + detector. The signal under the disk is measured as close as possible to the centre of the disk and the signal vs. diameter is then plotted. The scatter signal can be calculated by extrapolating to a 0mm diameter. The SPR is obtained by comparing the scatter signal and an open field measurement, i.e. measurement without the disk. [13].

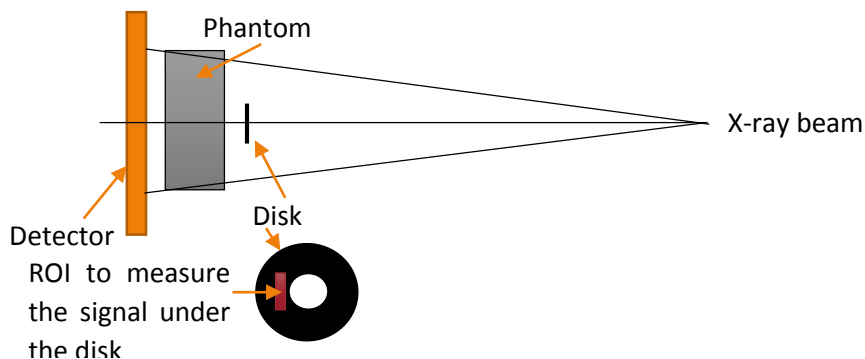


Figure 14: The image shows the geometry of the beam stop method and the disk region of interest (ROI) that is usually selected.

The extrapolation technique can be a source of ambiguity as it requires an assumption about the PSF shape. This might lead to strong influence in the final results. Moreover, it does not give information about the spatial distribution of the scatter, which is useful when developing algorithms to correct for it. [15]

3.1.2.3 Scatter medium reposition methodology:

This method was created to try to overcome the problems arising from the extrapolation function in the beam stop methodology. The SPR is calculated by subtracting a primary image (P) to an image that combines primary and scattered radiation (I).

Image I can be obtained by placing a lead sheet with a hole in it, a few centimetres in diameter, on top of the detector and a phantom on top of the lead, leaving a few centimetres air gap. The distance from the detector to the source must be large, i.e. a couple of metres.

Moving the phantom closer to the X-ray focal spot and keeping the rest of the geometry constant will give image P. When the air gap is large, only a small amount of scattered radiation is recorded. [13]

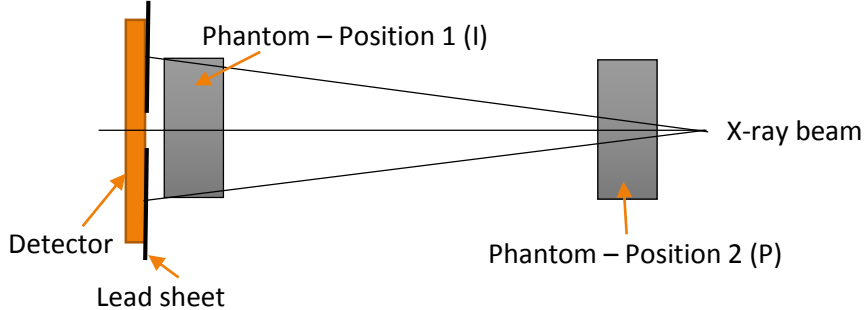


Figure 15: The image shows the geometry of the scatter medium reposition method with the two possible positions of the phantom (named position 1 (I) and position 2 (P) in the image).

3.1.2.4 Slat methodology:

This method gives the SPR measurement across the image. A narrow steel slat is placed between the X-ray beam and the detector + phantom, centred with the beam. Two images, one without and one with the slat, have to be acquired. The first one gives the primary and scattered image (I), while the shadow created by the slat in the second image gives the scatter (S). SPR can be obtained by subtracting the images and evaluating the shadowing area. [13]

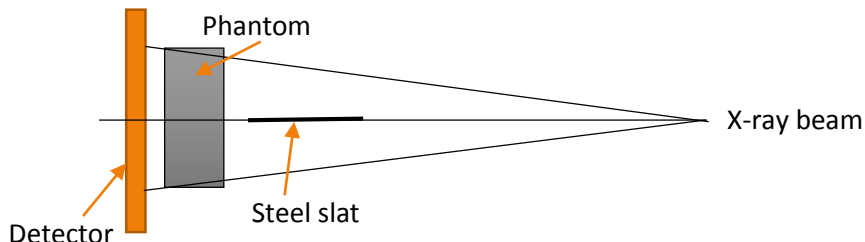


Figure 16: The image shows the geometry of the slat method where a steel slat is placed parallel to the X-ray beam and perpendicular to the phantom and the detector in order to study the SPR measurement across the image.

Although the physical measurements explained above stand as more convincing scatter estimation methods than the simulation techniques, due to the synthetic nature of the latter, they suffer from experimental biases and have not been proven to give better results, i.e. the ambiguity introduced when extrapolating to zero millimetres of diameter in the beam stopper method [13]. Moreover, some of these methods also require a direct measurement of the scatter signal, increasing the delivered radiation dose to the patient, or would need specific set ups in the medical exam. [14] [44]

3.1.3 Simulations

3.1.3.1 Monte Carlo simulations (MC)

Direct MC simulations give very accurate values of the scatter and primary contributions and they are conceptually simpler than the rest of the methods, [13]. However, if the scattering reduction is intended to be extended to all medical exams, it would be necessary to implement one simulation per exam, as these simulations are strongly dependent on the geometry and the part of the body that it is imaged. Moreover, these simulations are computationally expensive, taking up to 10 hours per simulations as reported by Diaz et al., [46].

For all these reasons, this method is usually adopted purely for data verification and methodological validation purposes [13].

3.1.3.2 Scatter convolution methodology:

Convolution-based digital filtration techniques are based on the idea that the scatter in the system is spatially diffuse thus it can be approximated to a two-dimensional low-pass convolution filter of the primary image, Equation 10 [14]. The 2D low pass filters can be simulated (point spread function) or random kernels can be employed:

Point spread function kernels

PSF kernels are obtained from MC simulation where the X-ray beam is a normally incident delta function, i.e. the X-ray tube is simulated following the narrow pencil beam method as a monochromatic point source [13] [47] [48]. This method is useful for accurate assessment of the SPR for small apertures and large field of views, as it reduces the computation time [13].

The program computes the point spread function (PSF) of scattered radiation for different energy steps, for example from 9.5 to 31.5 keV in 1keV steps for mammography applications [47], and then the monochromatic data, stored in a precomputed library [49], is combined to form the desired X-ray spectra. This step in the calculation is commonly performed in polar coordinates, however it can be studied just as a radial-dependent function if the angular distribution is assumed isotropic [13]. Once the PSF is obtained, it can be convolved with the field of view (FOV) in order to obtain the scatter distribution [50].

Results from MC simulations show that the PSF distribution can be taken as rotationally symmetric [2]. However, the assumption of symmetry can be argued. Wang et al., [1], suggest that it would be better to adapt the kernel to local variations in object thickness and attenuation. The authors proved that asymmetric kernels give better results than symmetric kernels, especially in areas close to the edge of the breast, where the symmetric ones tend to overcorrect for the scatter. The idea behind the asymmetric kernels is to account for elevated or depressed scatter due to thinner or thicker neighbouring regions,

respectively. Wang et al. propose a fast adaptive scatter kernel superposition method (fASKS) in the frequency domain:

Moreover, if the kernel is chosen spatially invariant, it will risk overestimation of scattering around the edge area of the breast, leading to up to 50% of discrepancies when compared with pure Monte Carlo simulations [46].

Random shape kernels

The kernel, $h(x,y)$, used to convolve the output image can be calculated following the point spread function method, as explained above, or it can be a pre-defined low-pass filter kernel. Authors like Love [43], Ducote and Mollo [14] or Boone and Seibert [51] use this last option in their studies.

Love and Kruger [43] studied four generic kernel shapes, 2D boxes, pyramid, Gaussian and exponential profiles, limiting their investigation to closed form functions to simplify the process and allow reproducibility. They used kernels that were functionally separable in the x and y directions, so instead of applying a 2D convolution they applied two consecutive 1D convolutions in order to speed up the process. Their study focused on finding the optimal kernel shape and size and their findings suggested that an exponential shape gave slightly better results when the size was big enough, i.e. 75 x 75 pixel kernel.

Ducote and Mollo [14], and Boone and Seibert [44], [51] made use of a radially symmetric scattering kernel in order to have a better approximation to physical reality. The formula that describes the kernel used by Ducote and Mollo has a first term with a delta function, that represents the mapping of the primary component, and a second term that is a function of the scatter fraction (SF) and the scatter radial extent or the mean propagation distance (k):

$$g_{si}(r) = \frac{\delta(r)}{r} + \frac{SF}{(1-SF)2kr} e^{-r/k} \quad \text{Equation 21}$$

To obtain the values of the SF and k both Ducote and Mollo, and Boone and Seibert used the beam stopping physical method.

These methods using random kernel shapes was always combined with the use of anti-scatter grids, so they were focused on further reductions in the scatter. The results in the absence of an anti-scatter grid could be completely different to the ones presented in the papers above. In fact, a recently published paper by Leon and Wagner, [45], combines the kernel shape proposed by Ducote and Mollo with the simulated PSF method, which they use to calculate the SF and the mean propagation distance (k or MRE). They applied this method with and without anti-scatter grid and studied different dependencies, like breast glandularity, size and thickness, or X-ray spectra. Their results show a perfect fit between the kernel shape and the grid data. However, when applied to grid-less measurements, the reported PSF form turned out to be less accurate, and they found that a bi-exponential PSF shape would be better fit. Their explanation is related to the Compton scattering contribution. The grid absorption of the scatters makes coherent scattering dominate over the Compton scattering. However, without the grid the Compton contribution is bigger and so the bi-exponential equation would account for both factors.

The 2D low pass filters, independently of how they have been obtained, can be assumed to be shift invariant, i.e. the same kernel is used to convolve the whole image, or can be optimised in shape and size and operated on a pixel by pixel basis [14], [2].

Size optimization can be performed by selecting a kernel with radial dependency, as explained in the Ducote and Molloï method. These authors also present a way of taking into account the breast thickness variations.

For breast thickness corrections, the authors create a look up table with kernels calculated at different thicknesses, $g_s(t)$, for example using 1mm steps. After the mammogram is acquired, the apparent breast thickness can be estimated in a pixel by pixel basis and 1mm thickness masks can be created, i.e. one mask for 1mm thickness, a second mask for 2mm and so on until the nth mask is created, corresponding to the maximum breast thickness. Each mask is then convolved with its corresponding kernel and n partial primary images are obtained. The primary image is finally obtained by adding all the partial images. [14]

Ahn and Cho, [2], also present an algorithm to account for the thickness contribution. They also create look up tables with the PSF simulated as a function of the thickness. They later used them to correct the image in a pixel by pixel basis: starting from pixel (0,0) the thickness is estimated and the image is convolved with the PSF of that thickness; the process is repeated for all pixels. Their algorithm also takes into account possible errors in the thickness estimation, as they report that the scattering affects the estimations when using general dual-energy algorithms. They propose an iterative method that recalculates the thickness estimation with the scattered corrected image obtained from the first iteration. A second scattered corrected image is obtained from the new estimation and the difference between the first and second correction is analysed. If the difference is smaller than a value specified by the user, the algorithm stops. If the difference is higher, a new iteration is produced and the second image is compared with the third one, etc.

Convolution-based techniques do not require a direct measurement of the scatter signal so do not cause an increase in the radiation dose. As they are applied after the image acquisition, it is possible to use them in tomosynthesis and it is not necessary to change the acquisition method or increase the image acquisition time [14] [44]. Their main limitation is in the simulation itself: if the geometries are idealised and simplified some of the dependencies will not be taken into account, leading to over or under estimate of the scatter contribution [48].

Siemens has recently introduced a software-based scatter correction for grid-less mammography acquisitions, Mammomat Inspiration PRIME [3]. They affirm that if the detector air kerma (DAK) values are modified, something that was not possible in film-screen mammography but that does not affect the results in digital radiography, the dose delivered to the patient can be significantly reduced.

3.1.4 Scattering dependencies

The dependencies in the distribution of the scatter, in the absence of anti-scatter grid, have been largely studied in the literature, [11, 12, 14, 15, 47-50, 52, 54 – 58]. The way most of the authors carry out this study is by modifying the PSF simulations, i.e. modifying the X-ray beam energies to study the energy dependency, simulating different breast phantoms changing breast glandularity or thickness, varying the air gaps or changing the shape and size of the field of view (FOV) are some examples [50]. The parameters studied were:

3.1.4.1 X-ray energy:

The method used by Boone et al., [50], calculates mono-energetic PSFs from 5 to 120 keV in 1keV increments and then weights them using the poly-energetic X-ray spectra. The authors found that the scatter properties are approximately constant at the energy range used in diagnostic mammography. The maximum scatter to primary ratio (SPR) relative difference when comparing 40kVp and 22kVp energies (obtained with a Mo/Mo anode/filter combination) was found for a 6 cm breast thickness (12.7%). The difference was reduced to 7% for a 4cm breast thickness, 1% for 2cm and to 2% for 8cm.

Similar results were found by Sechopoulos et al. [47].

3.1.4.2 Position in the field of view (FOV):

Boone et al., [50], found that the SPR depends strongly on the position within the FOV, being maximum in the centre of the breast and dropping off towards the edges.

3.1.4.3 Air gap and FOV:

Again Boone et al., [50], found that the PSF fall off depends on the air gap, becoming more gradual as the air gap is increased. The scatter to primary ratio dependency with the air gap is dependent on the FOV that you use in the convolution. If the FOV is large enough, i.e. 15cm, there will be little variation with the air gap (0-30mm), even at different breast thicknesses. However, for smaller FOVs, i.e. 10cm or smaller, the SPR will fall off when the air gap and the breast thickness are increased. For very small FOVs this trend will approximately follow the inverse square law. This dependency is explained studying the scatter at the exit surface of the breast. For small air gaps the scatter concentrates in the central position but, as the air gap increases, the scatter spreads to larger areas. If the FOV is small, the SPR will not include the larger areas thus it will decrease.

Oliver et al., [46] [48], present a second air gap contribution, present between the lower curved breast edge and the detector. The authors believe that the extended path length of the photons is the main cause of the discrepancies that appear close to the breast edge, reported when using a spatial invariant kernel. It is therefore important to correct for this contribution, as the scattered photons that pass through the skin to the air gap do not encounter the same scattering and attenuation path than the ones that go through the breast directly to the support paddle.

In cases where the breast is simulated, the breast curvature is a known parameter. However, if this correction is to be applied to clinical data, the breast curvature will need to be estimated during the exam [46].

3.1.4.4 Breast thickness:

It has been found that the SPR is nearly linear as a function of breast thickness. The slope of this function being dependent on the air gap and the selected FOV diameter [50] [44] [47].

It is therefore essential to estimate the breast thickness with accuracy. The compression thickness that is reported by the mammography unit can be used as an initial reference measurement but the thickness calibration is sometimes inaccurate, and the breast thickness changes towards the periphery. A software based algorithm to calculate the thickness will be necessary for obtaining reliable results [45] [52] [53].

The breast compression in general mammography allows the achievement of a relatively constant breast thickness, excluding the periphery where the thickness decreases. However, the pressure applied to the

compression paddles ends up deforming them and creating a tilt in the area without breast [53]. This effect introduces variations in the breast thickness.

If the thickness variations are assumed to be negligible within the compressed breast, the thickness calculation is then reduced to an estimate of the averaged value, [52] [54] [55]. However, this assumption introduces some errors that add up in the final scattering simulation. For this reason, some other authors calculate a pixel by pixel thickness map and use kernels that are a function of the thickness, $K(t)$, [53] [45].

Highnam, Brady and Shepstone, [52] [54], introduce a method to estimate the average value of the breast thickness. Their method is focused on delimiting the periphery of the breast from the interior of the breast. They call the periphery the “breast edge”, and they assume that is formed entirely of fat and it is smooth and homogeneous. Within the breast edge, the points that are closer to the transition to the “interior area” can be considered to have a thickness similar to the average thickness (H). As those points are composed only by fat, the thickness H can be estimated using the density/intensity information of the pixel:

$$H = h_{\text{fat}} + h_{\text{int}}$$

$$\text{If } h_{\text{int}}=0 \rightarrow H=h_{\text{fat}}$$

From the pixel intensity information, it is possible to map the pixels with attenuation equal or lower to the one produced by H mm of fat tissue; the lower values are due to those areas close to the edge that are thinner than the average breast thickness. The map created, will have h_{int} values equal to 0 for those pixels, and $h_{\text{int}}>0$ for the rest of the pixels, mapping each pixel density with a value of h_{int} .

With the information of the estimated thickness, plus the knowledge of the polyenergetic X-ray source, anti-scatter grid, intensifying screen, X-ray tube settings and attenuation coefficient values it would be possible to estimate the real h_{int} values, giving as well an idea of the breast tissue composition.

Pixel by pixel thicknesses maps are reported by several authors. Leon et al., [45], use the ratio between an attenuated exposure and a flat image exposed with the same dose. They then compare the ratio with a database of ratios generated from known thicknesses of a BR-12 phantom with 50/50 glandular/adipose composition, database reported by White et al., [56].

3.1.4.5 Breast tissue composition:

The study of breast tissue composition has been commonly carried out by using phantoms with different glandular percentage, with 0, 50 and 100% being the most common choices, although other percentages have also been evaluated. The literature presents very little dependency between SPR changes and breast composition, [50] [47]. The major impact has been found to be in the apparent thickness calculation [45].

Due to the small glandular contribution it is possible to use a PSF simulated for a homogeneous breast [47]. The scatter kernel can be calculated, for example, as the linear combination of the scatter response with 0% and 100% of glandularity [48].

3.1.4.6 Detector cover plate, detector compression plate and breast support plate:

The detector cover plate and the compression and breast support plates were found to have a significant contribution to the scattered signal, [14] [47] [48], especially for thicker breasts, i.e. 5-7cm, close to the

edges of the compressed breast. The reason found by Sechopoulos et al., [47], and studied further by Diaz et al., [48], was related to the scattering contribution of the plates in the area without breast tissue. Some of that scatter is detected under the shadow of the breast, producing a high contribution due to the absorption of the primary photons by the breast tissue. If the breast is thin enough, that absorption is decreased and the SPR is therefore reduced.

This contribution can be pre-corrected by simulating the measurements at zero thickness [14]. A more precise method, reported by Oliver et al., [48], would include the plates in the simulations. To account for the scattering contribution of the area without breast, i.e. system contribution, a second simulation can be done keeping the same geometry but removing the scattering material, i.e. breast phantom. The system kernel will be applied to the areas outside the breast, while the breast kernel (that has been calculated taking the plates into account) is applied within the breast areas.

However, an additional correction is needed. The scattered photons produced outside, but near, the breast, might be scattered towards the breast. In that case, the system scattered radiation will be attenuated by the breast tissue. In order to compensate for this effect, Oliver et al. proposed to weight the system kernel with a weight map, α , where $\alpha=1$ outside the scattering material and $\alpha<1$ when the beam passes through the breast.

It is therefore very important not to exclude the plates in the simulation. If they are not taken into account the scatter will be underestimated by as much as 31% [47], [48].

3.1.4.7 *Source to image distance (SID)*

The SID does not seem to affect the scattered radiation distribution [13].

3.1.5 Typical general mammography parameters for MC simulations:

As mentioned before, the main limitation with convolution-based techniques is the simulation itself. Simplifications in the dependencies mentioned above or in the geometry of the mammographic exam will lead to underestimations of the scatter.

Some of the parameters found in the literature that have been assumed to be used in general mammography exams are described below:

Table 2: The table shows the general geometry parameters used in mammography medical examinations.

SIMULATION PARAMETERS		Value/Range	Material	Comments	Source
ANATOMY	Breast Thickness	2-8 cm			[50]
GEOMETRY	SID	65-66 cm			[45], [47]
	Air gap	≈ 15mm		Values vary between manufacturers	[50]
	Breast support plate to detector distance	2 cm		Grid might be included in the distance. Depends on application	[45]
	Compression plate	2mm thick	Polycarbonate		[45], [47]
	Breast support plate	3.3mm thick	Carbon fibre		[47]
	Divergence angle	8 deg. Maximum		For 8cm breast	[13]
	Anode/Filter		Mo/Mo or Mo/Rh (*)		[50]
SETTINGS	Energy	24-32 KeVp (2-8cm breast thickness)		The typical energies depend on the breast thickness	[50]
	Current x Exposure time	200mAs			[50]

(*) Molybdenum/Molybdenum (Mo/Mo) or Molybdenum/Rhodium (Mo/Rh).

Other factors to take into account in the simulations: [47]

- Backscatter
- Heel effect and the inverse square law
- Detector: simulated to be able to differentiate between primary and scattered photons. If the simulated detector is assumed to have an ideal response, the results should be encompassed for their non-ideal performance.

3.1.6 Monte Carlo PSF simulation – GEANT4 simulation toolkit

There are several particle physics MC software packages available that allow the study of interactions in the medical physics range: GEANT4, Penelope, FLUKA, EGSx/EGSnrc and MCNP/MCNPX, [57]. GEANT4, in particular, has been chosen by many authors, i.e Feng et al. [49], Wang et al. [1], Diaz et al. [46] [48] [57] and Sechopoulos et al. [58], as it is a free software supported by the European Organization for Nuclear Research (CERN), where it is possible to obtain active assistance, [57] [59].

GEANT4 provides detector and physics modeling, simulating the interaction and passage of particles through matter. This simulation toolkit includes all aspects of the simulation process, i.e. the system geometry and materials, the fundamental particles of interest, including a tracking system of them and their interactions, the detector response, etc. [59] [60]. Although GEANT4 was initially designed for high energy physics, its object-oriented structure has allowed its adaptation to a wider range of energies, including medical physics, i.e. mammography, brachytherapy or hadron therapy, and radiation protection [57].

When applied to mammography, GEANT4 has been validated in a number of publications. Sechopoulos, [58], modified the code to simulate X-rays passing through only breast tissue, activating and deactivating the interaction process to study each individual case. That way, the attenuation coefficients were calculated and compared to the values reported by the National Institute of Standards and Technology (NIST) and by other authors finding excellent agreements in all cases. Feijó and Hoff, [61], also validated the software comparing results to previously published data. They report less than 5% difference between the compared values. Also Diaz, [57], validated the toolkit with published and clinical data, arriving to the conclusion that GEANT4 is suitable for modeling X-ray mammography systems.

Computation time reduction: Variance reduction method [47]:

The idea of this method, based in the concept of importance sampling, is to use fewer photons at the beginning of the simulation to reduce the number of primary X-rays simulated, but increase the number of scattering events. In doing so, the Rayleigh and Compton scattering events have to be modified so each scatter event results in more than one output photon. To compensate for this multiplication, each resulting photon is assigned with a relative weight, i.e. if the input photon (weight = 1) undergoes a Compton scattering and 5 photons are scattered, each of the photons will be assigned $1/5^{\text{th}}$ of the weight. When one of those photons (weight = 0.2) is then scattered another 5 times, the weight of the resulting photons will be 0.04. By the time the photons arrive at the imager, the number that is recorded is the photon energy multiplied by its relative weight. This method does not affect the output of the PSF and reduces the computation time.

3.2 PROJECT GOALS

Scattering reduction is one of the main open research topics in radiography, especially in the digital mammography area. To date, anti-scatter grids have been the best solution to this problem and their use has been extended to all general mammography applications. However, the emergence of new mammography examinations, such as digital breast tomosynthesis, where the anti-scatter grids cannot be used, have allowed the development of new scatter reduction techniques and thus the use of the anti-scatter grid as the best solution has been questioned.

The post-processing method for scattering reduction that is going to be followed in this project uses point spread function (PSF) kernels, simulated with the Geant4 Monte Carlo toolkit, to convolve the output image. The main objective is to prove that it would be valid to use this method in diagnostic applications as an alternative to anti-scatter grids, without losing image quality and potentially reducing the delivered dose, [3]. The work shall follow the findings of Oliver Diaz, [46] [48] [57], with whom PerkinElmer is collaborating, and adapt them to mammography examination applications using CMOS X-ray detector technology.

The literature review has been completed. The research was focused on the study of scattering reduction methods in mammography as an alternative to the anti-scatter grid. The dependencies of the scatter with the geometry of the mammography exam were also investigated and a Monte Carlo simulation toolkit, Geant4, was presented, as well as its uses in the literature.

3.3 PSF EVALUATION USING MC SIMULATIONS

3.3.1 Methodology

The work with Geant4 has been started; the following months will be focused on simulating a CMOS X-ray detector with the Geant4 toolkit and to start setting up the appropriate geometry for the simulations. Once this is complete, the data set can start to be filled with the simulated PSFs.

The different PSFs forming the data set will be simulated at different energies and thicknesses, with and without breast simulated phantom. The narrow beam method simplifies the PSF simulations by assuming a mono-energetic X-ray beam and then integrates for all energies, the data set will have to include energies from 6-8 keV to 35keV. Breast thicknesses, after compression, usually comprise a range between 2 and 8 cm but the thickness around the edges might be smaller than 2cm. Therefore, range between 0-8 or 9 cm will have to be simulated.

3.3.2 Technique validation

The first step will be to validate that the geometry set up is correct and the detector is properly simulated. This has to be done before starting to collect the PSF data set. For doing so, complete MonteCarlo simulations can be acquired and the results can be compared with images acquired in house with PerkinElmer's mammography X-ray system. The simulations and validations of this first stage will be done without the presence of an anti-scatter grid.

Once the geometry has been accepted to be accurate, the PSF data set can start to be obtained.

3.4 BREAST THICKNESS ESTIMATION

3.4.1 Methodology

A parallel study with regards breast thickness estimation will have to be carried out. It was found in the literature review that the scattering contribution is highly affected by the breast thickness value. For this reason, an accurate estimation of this parameter is essential to be able to successfully reduce the scattering contribution.

The PSF data set acquisition does not depend on this estimation, as it will be simulated for different thickness steps. Therefore, the method can be developed while the data set is being acquired.

The literature review showed two opposite approaches to this calculation; some authors calculated a pixel by pixel thickness map while others assumed that the breast thickness was homogeneous due to the breast compression. Both approaches will need to be tested and the one giving the best outcome will be adopted in the study.

3.4.2 Technique validation

The thickness estimation method will be evaluated on-site with a set of phantoms of known thicknesses. After this first validation, the method can be tested further by using it to estimate breast thicknesses of real mammograms and the results can be compared with other methods or published results.

3.5 SCATTER REMOVAL USING THE PSF POST-PROCESSING TECHNIQUE

3.5.1 Methodology

Once the PSF data set has been acquired and an appropriate thickness estimation method has been developed, it will be possible to post-process images, acquired without anti-scatter grid, according with the PSF scattering reduction method.

3.5.2 Technique validation

The images obtained at this stage will have to be thoughtfully evaluated before this method can be considered to be used as a valid substitute of the anti-scatter grids.

The first stage of the evaluation can be done by comparing the resultant image with the one obtained with a full Monte Carlo simulation.

The second stage will involve comparing the quality of the processed images with images that have been acquired using anti-scatter grids. PerkinElmer's mammography system does not include a grid so external collaboration will be needed. Phantom images obtained with the same system with and without the use of a grid would be a good starting point for the validation. Phantom and grid simulation could also be used at this stage.

If the results obtained at this point prove to be of comparable or better quality than the images obtained using the grid, a third and final validation stage could be considered necessary. Due to the impossibility of carrying a study with patients, as it would involve irradiating the patient twice with and without the use of grid, and the necessity of obtaining the most realistic results possible, it would be an option to approach hospitals in order to carry on the final study with the use of cadavers.

4 CONCLUSIONS AND FUTURE WORK

The main advances in the first year and a half were made in the image characterization project. The image processing project was re-defined towards the second half of the second year as the company was no longer interested in the initial idea. This change however, did not have major consequences on the progress of the project, as the work done so far had been focused on the acquisition of general image processing knowledge. Moreover, the change is going to facilitate carrying out some external collaborations and, research wise, is more interesting and will have more applications.

4.1 STRUCTURE OF THE FIRST TWO YEARS

Year 1:

- Image Characterization
 - Literature Review
 - Measurement and Analysis methodology for MTF, NPS and DQE measurements
 - Define the measurement method
 - Define the analysis method
 - Acquisition of first set of data and validation of measurement and analysis methods
 - Optimization of the method
 - Methodology established – methodology procedure defined and approved by QA
 - PerkinElmer new CMOS sensors – Sensor evaluation.
- Image Enhancement
 - Study C++ programming
 - Study basic concepts of Image Processing

Year 2:

- Image Characterization
 - Complete the Literature Review
 - Define the whole detector characterization methodology, paying special attention to detector issues
 - Start the image acquisition following the methodology previously defined using detector prototypes with potential design issues.
 - Analysis of the acquired data.
 - PerkinElmer new CMOS sensors – Sensor evaluation
- Image Enhancement
 - Literature review in scattering reduction techniques.
 - Start to define the methodology.
- Write the Transfer document.

4.2 ENGD PROJECT PLAN

4.2.1 Project structure

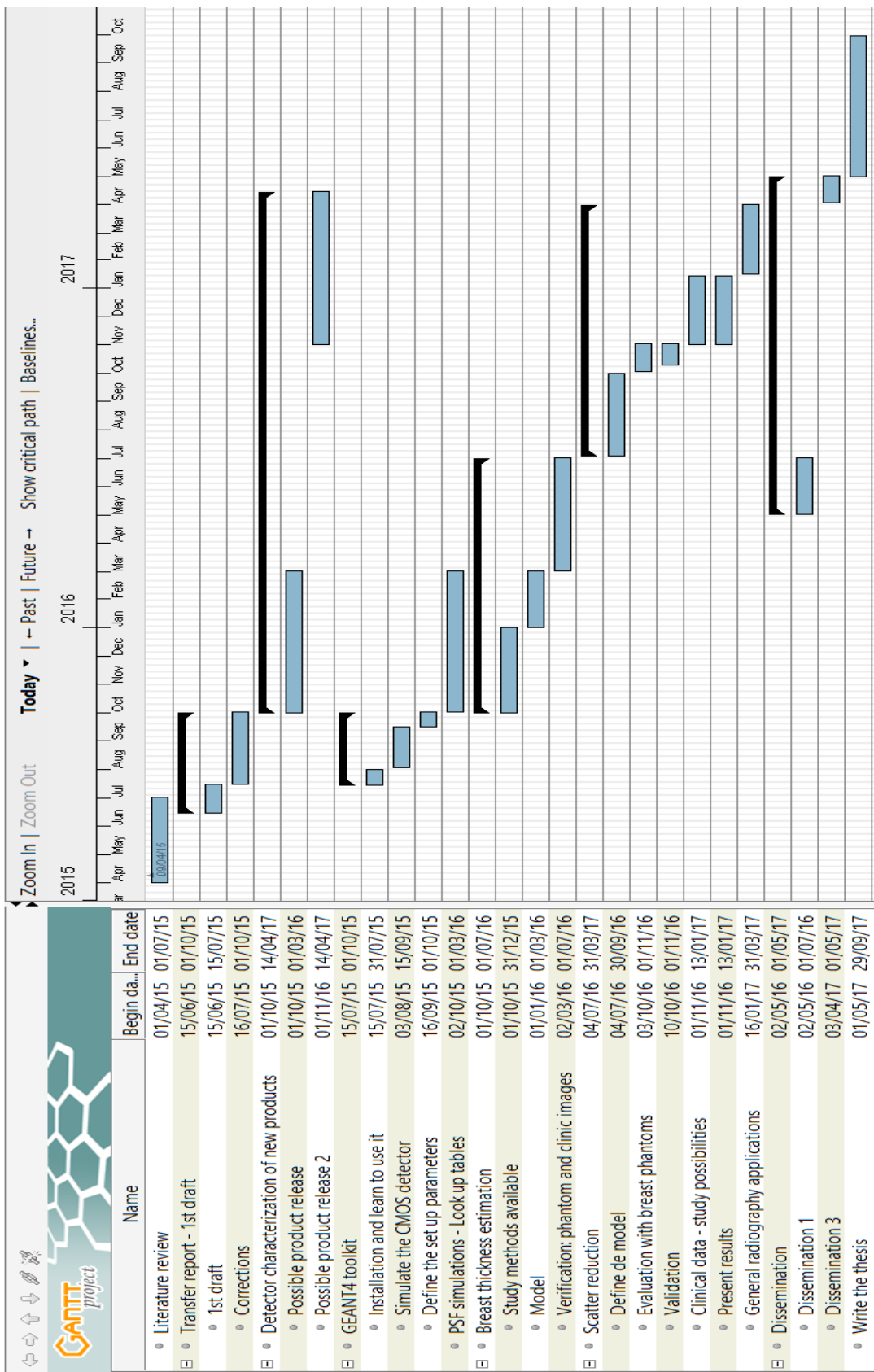
Year 3:

- Image Characterization
 - Continue the acquisition and analysis of data if more sensors/components become available or if new products are released.
- Image Enhancement
 - Finish defining the methodology: simulations and breast thickness estimation.
 - Validation of the methodology.
 - Start to simulate the kernels for scattering corrections
 - Start to disseminate the work done up to date.

Year 4:

- Image Characterization
 - Continue the acquisition and analysis of data if more sensors/components become available or if new products are released.
- Image Enhancement
 - Method evaluation with breast phantoms
 - Study the possibility of extending the mammography scatter reduction method into general radiography
 - Dissemination of the work done up to date
- Write the final version of the Thesis.

4.2.2 Project timeline - Gantt chart



5 BIBLIOGRAPHY

- [1] A. Wang et al, "Asymmetric Scatter Kernels for Software-Based Scatter Correction of Gridless Mammography," *SPIE Medical imaging*, vol. 9412, pp. 1I-1-7, 2015.
- [2] S. K. Ahn, G. Cho and H. Jeon, "A scatter correction using thickness iteration in dual-energy radiography," *IEEE Transactions on Nuclear Science*, vol. 53, no. 1, pp. 133-138, 2006.
- [3] J. Binst et al, "Evaluation of automated CDMAM readings for non-standard CDMAM imaging conditions: Grid-less acquisitions and scatter correction," *Oxford University Press - Radiation Protection Dosimetry*, pp. 1-4, 2015.
- [4] A. Krol et al, "Scatter reduction in mammography with air gap," *Medical Physics*, vol. 23, no. 7, pp. 1263-1270, 1996.
- [5] Kodak Health Sciences, *Introduction to Medical Radiographic Imaging*, Kodak, 1994.
- [6] J. Bushberg, A. Seibert, E. Leidholdt and J. Boone, *The Essential Physics of Medical Imaging*. Third Edition, Wolters Kluwer, 2012.
- [7] M. Hoheisel, "Review of medical imaging with emphasis on X-ray detectors," *Nuclear Instruments & Methods in Physics Research. Section A Elsevier*, vol. 563, pp. 215-224, 2006.
- [8] J. M. Dixon, *ABC of breast diseases*, 1999, First Ed. .
- [9] J. Tobias and D. Hochhauser, *Cancer and its management. Chapters 2 and 13*, 2010 - 6th Ed. .
- [10] A. Waugh and A. Grant, *Ross and Wilson Anatomy and Physiology in Health and Illness*, Ninth Ed., 2001.
- [11] N. c. s. programmes, "www.cancerscreening.nhs.uk," NHS. [Online]. [Accessed 30th June 2015].
- [12] D. J. Dowsett, P. ... Kenny and R. E. Johnston, *The physics of diagnostic imaging*, 2006 - 2nd Ed. .
- [13] J. M. Boone and V. N. Cooper, "Scatter/primary in mammography: Monte Carlo validation," vol. 27 (8), 2000.
- [14] J. L. Ducote and S. Mollo, "Scatter correction in digital mammography based on image deconvolution," *IOP - Physics in Medicine and Biology*, vol. 55, pp. 1295-1309, 2010.
- [15] V. N. Cooper III, J. M. Boone, J. A. Seibert and C. J. Pellet-Barakat, "An edge spread technique for measurement of the scatter-to-primary ratio in mammography," *Medical Physics*, vol. 27, no. 5, pp. 845-853, 2000.

- [16] G. Barnes and G. Frey, "Screen film mammography: Imaging considerations and medical physics responsibilities," *Medical Physics Publishing*, vol. 184, no. 3, p. 242, 1991.
- [17] J. James, "The current status of digital mammography," *Clinical Radiology*, vol. 59, pp. 1-10, 2004.
- [18] S. Muller, "Full-field digital mammography designed as a complete system.," *European Journal of Radiology*, vol. 31, pp. 25-34, 1994.
- [19] G. J. Bansal, "Digital radiography. A comparison with modern conventional imaging.," *Postgraduate Medical Journal.* , vol. 82(969), pp. 425-428, 2006.
- [20] A. Noel and F. Thibault, "Digital detectors for mammography: the technical challenges," *Eur Radiol*, vol. 14, pp. 1990-1998, 2004.
- [21] A. G. Farman et al, "A comparison of 18 different X-ray detectors currently used in dentistry," *OOOOE*, vol. 99, no. 4, pp. 485-489, 2005.
- [22] M. Bigas et al, "Review of CMOS image sensors," *Microelectronics Journal*, ELSEVIER, vol. 37, pp. 433-451, 2006.
- [23] E. Fossum, "CMOS Image Sensors: Electronic Camera-On-A-Chip," *IEEE Transactions on Electron Devices*, vol. 40, no. 10, pp. 1689-1698, 1997.
- [24] J. Tang, "4T CMOS Active Pixel Sensors under Ionizing Radiation - Thesis," Delft University, The Netherlands, 2013.
- [25] A. Konstantinidis and e. all, "X-ray Performance Evaluationo of the Dexela CMOS APS X-ray Detector Using Monochromatic Synchrotron Radiation in the Mammographic Energy Range," *IEEE Transactions on Nuclear Science*, vol. 60, no. 5, pp. 3969-3980, 2013.
- [26] G. F. Knoll, *Radiation Detection and Measurement*. Third edition., John Wiley & Sons, Inc. , 1999.
- [27] J. E. Turner, *Atoms, Radiation and Radiation Protection*. 2nd Edition., John Wiley & Sons, Inc. , 1995.
- [28] T. T. Farman et al, "Effects of scintillator on the modulation transfer function (MTF) of a digital imaging system," *Oral Surg Oral Med Oral Pathol Oral Radiol Oral Endod*, *OOOOE*, vol. 99, pp. 608-613, 2005.
- [29] T. T. Farman et al, "Effects of scintillator on the detective quantum efficiency (DQE) of a digital imaging system," *Oral Surf Oral Med Oral Pathol Oral Radiol Endod*, *OOOOE*, vol. 101, pp. 219-223, 2006.
- [30] J.-P. Moy, "Image quality of scintillator based X-ray electronic imagers," *Part of the SPIE Conference on Physics of Medical Imaging. San Diego, California*, vol. 3336, 1998.

- [31] R. Aufrichtig and P. R. Granfors, "DQE(f) of an Amorphous Silicon Flat Panel X-ray Detector: Detector Parameter Influences and Measurements Methodology," *Proc. of SPIE, Physics of Medical Imaging*, vol. 3977, 2000.
- [32] A. C. Konstantinidis et al, "The Dexela 2923 CMOS X-ray detector: A flat panel detector based on CMOS active pixel sensors for medical imaging applications," *Nuclear Instruments and Methods in Physics Research. Section A*, vol. 689, pp. 12-21, 2012.
- [33] G. Zanella, "Gray levels, dynamic range, contrast and DQE in imaging detectors," *Nuclear Instruments & Methods in Physics Research. Section A*, vol. 481, pp. 691-695, 2002.
- [34] I. E. C. P. (IEC 62220-1), "Medical Electrical Equipment - Characteristics of Digital X-ray Imaging Devices - Part 1: Determination of the Detective Quantum Efficiency," Geneva, 2003.
- [35] I. E. C. P. (IEC 62220-1-2), "Medical Electrical Equipment - Characteristics of Digital X-ray Imaging Devices - Part 1-2: Determination of the Detective Quantum Efficiency - Detectors used in mammography," Geneva, 2007.
- [36] E. Samei, N. Ranger and J. T. Dobbins, "Intercomparison of methods for image quality characterization. I. Modulation Transfer Function," *Medical Physics*, vol. 33, no. 5, pp. 1454-1465, 2006.
- [37] J. Dobbins et al, "DQE(f) of four generations of computed radiography acquisition devices," *Medical Physics*, vol. 22, pp. 1581-1593, 1995.
- [38] E. Samei et al, "A method for measuring the presampled MTF of digital radiographic systems using an edge test device," *Medical Physics*, vol. 25, pp. 102-113, 1998.
- [39] P. Monnin et al, "A comparison of the performance of digital mammography systems," *Medical Physics*, vol. 34, pp. 906-914, 2007.
- [40] A. Konstantinidis, "Evaluation of digital X-ray detectors for medical imaging applications," UCL, London, 2011.
- [41] M. Hoheisel, "Review of medical imaging with emphasis on X-ray detectors," *Nuclear Instruments & Methods in Physics Research - Elsevier*, vol. A 563, pp. 215-224, 2006.
- [42] A. Smith, "Fundamentals of Digital Mammography: Physics, Technology and Practical Considerations," *Radiology Measurements*, vol. 25(5), pp. 18-31, 2003.
- [43] L. A. Love and R. A. Kruger, "Scatter estimation for a digital radiographic system using convolution filtering," *Medical Physics*, vol. 14, no. 2, pp. 178-185, 1987.
- [44] J. Seibert and J. Boone, "X-ray scatter removal by deconvolution," *Medical Physics*, vol. 15, no. 4, pp. 567-575, 1988.

- [45] S. M. Leon, L. F. Brateman and L. K. Wagner, "Characterization of scatter in digital mammography from use of Monte Carlo simulations and comparison to physical measurements," *Medical Physics*, vol. 41, no. 11, pp. 111914-1-10, 2014.
- [46] O. Diaz et al, "A fast scatter field estimator for digital breast tomosynthesis," *Proc. SPIE Medical Imaging*, vol. 8313, 2012.
- [47] I. Sechopoulos et al, "Scatter radiation in digital tomosynthesis of the breast," *Medical Physics*, vol. 34, no. 2, pp. 564-576, 2007.
- [48] O. Diaz et al, "Estimation of scattered radiation in digital breast tomosynthesis," *IOP Physics in Medicine and Biology*, vol. 59, pp. 4375-4390, 2014.
- [49] S. S. J. Feng et al, "X-ray scatter correction in breast tomosynthesis with a precomputed scatter map library," *Medical Physics*, vol. 41, no. 3, pp. 031912-1-7, 2014.
- [50] J. Boone et al, "Scatter/primary in mammography: Comprehensive results," *Medical Physics*, vol. 27, no. 10, pp. 2408-2416, 2000.
- [51] J. M. Boone and V. N. Cooper, "An analytical model of the scattered radiation distribution in diagnostic radiology," *Medical Physics*, vol. 15, pp. 721-5, 1988.
- [52] R. P. Highnam, J. M. Brady and B. J. Shepstone, "Estimation of compressed breast thickness during mammography," *The British Journal of Radiography*, vol. 71, pp. 646-653, 1998.
- [53] G. E. Mawdsley et al, "Accurate estimation of compressed breast thickness in mammography," *Medical Physics*, vol. 36, no. 2, pp. 577-586, 2009.
- [54] R. Highnam et al, "Robust Breast Composition Measurement - Volpara," in *10th International Workshop, IWDM, LNCS 6136*, 2010.
- [55] G. Trotter and E. Dinko et al, "Thickness-dependent scatter correction algorithm for digital mammography," *Proceedings of SPIE*, vol. 4682, pp. 469-478, 2002.
- [56] D. R. White, R. J. Martin and R. Darlison, "Epoxy resin based tissue substitutes," *Brit. J. Radiol.*, vol. 50, pp. 814-821, 1977.
- [57] O. Diaz et al, Scattered radiation in projection X-ray mammography and digital breast tomosynthesis. PhD Thesis, University of Surrey, 2013.
- [58] I. Sechopoulos, Investigation of physical processes in digital X-ray tomosynthesis imaging of the breast. PhD thesis., Georgia Institute of Technology, 2007.
- [59] S. Agostinelli et al, "GEANT4 - a simulation toolkit," *Nuclear instruments & methods in physics research. Section A*, vol. 506, pp. 250-303, 2003.

- [60] J. Allison et al, "GEANT4 developments and applications," *IEEE Transactions on nuclear science*, vol. 33, no. 1, pp. 270-278, 2006.
- [61] P. V. Feijó and G. Hoff, "Geant4 Validation on Mammography Applications," in *IEEE Nuclear Science Symposium* , 2008.
- [62] NASA, "NASA," [Online]. Available: <http://imagine.gsfc.nasa.gov/science/toolbox/emspectrum1.html>. [Accessed 11 September 2015].
- [63] U. Bick and F. Diekmann, "Digital mammography: what do we and what don't we know?," *Eur Radiol*, vol. 72, pp. 1931-1942, 2007.
- [64] D. Evans et al, "A comparison of the imaging properties of CCD-based devices used for small field digital mammography," *Physics in Medicine and Biology*, vol. 47, pp. 117-135, 2002.
- [65] J. Dobbins and E. Samei et al, "Intercomparison of methods for image quality characterization. II. Noise Power Spectrum," *Medical Physics*, vol. 33, no. 5, pp. 1466-1475, 2006.
- [66] J. S. J. T. Bushberg, *The Essential Physics of Medical Imaging*, 3rd edition, Lippincott Williams & Wilkins, 2012.
- [67] M. Bigas and a. et, "Review of CMOS image sensors," *Microelectronics Journal - Elsevier*, vol. 37, pp. 433-451, 2006.
- [68] A. Noel and F. Thibault, "Digital detectors for mammography: the technical challenges.," *European Radiology*, Vols. 14, No.11, pp. 1990-1998, 2004.
- [69] E. Pisano et al, "Image Processing Algorithms for Digital Mammography: A pictorial Essay," *RadioGraphics*, vol. 20, pp. 1479-1491, 2000.

APPENDIX A

This appendix complements the literature review of Chapter 2, section 2.1. Section A.1 presents the main characteristics, advantages and drawbacks of the main radiography technologies. Sections A.2 and A.3 expand on the theory behind the Modulation Transfer Function and the Noise Power Spectrum respectively.

A.1 X-RAY DETECTOR TECHNOLOGIES

Screen-Film and CR technology

Screen-film detector technology

In general, film-screen cassettes consist of a film emulsion layer located between two fluorescent screens and loaded into a light-tight cassette. The fluorescent screens, made of scintillator material, convert the incident X-ray photons into visible or ultraviolet photons that are detected by the film, see Figure 17 to understand the differences between types of Electromagnetic (EM) radiation, in particular the X-ray and visible or ultraviolet radiation. The film is a sheet of thin plastic with a photosensitive silver halide emulsion coated onto both sides and it is the part of the detector that forms the latent image when the detector is exposed with the X-rays, i.e. it records the X-ray intensity pattern. The final image is obtained by chemically processing of the film, reducing the silver halide into metallic silver grains [6].

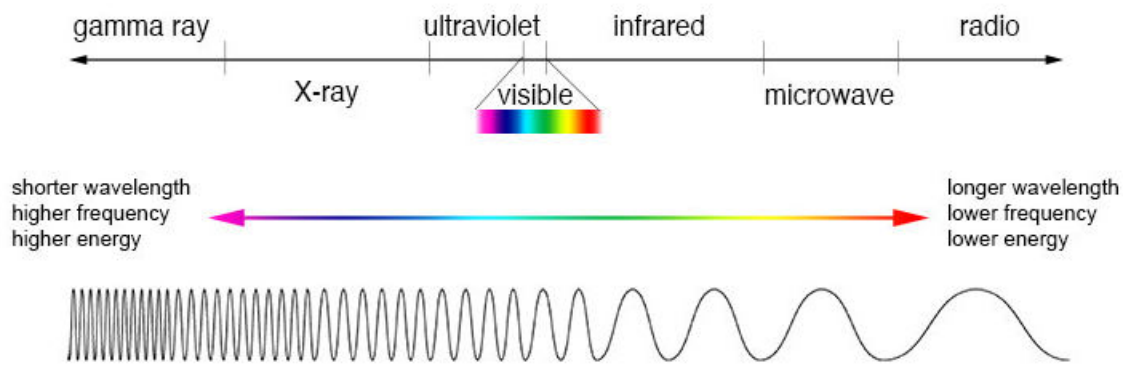


Figure 17: Schematic of the Electromagnetic (EM) spectrum. This figure shows that the X-ray photons and the visible or ultraviolet photons are both EM radiation of different energies, frequencies or wavelengths. The figure was taken from the NASA website, [62].

For mammography applications, this configuration is changed to a single high definition screen, used as a back screen, in contact with a single emulsion film, which acts simultaneously as an image acquisition detector, as a storage medium and as a display device [18]. This combination reduces the light diffusion, which is one of the main causes of blurring [16].

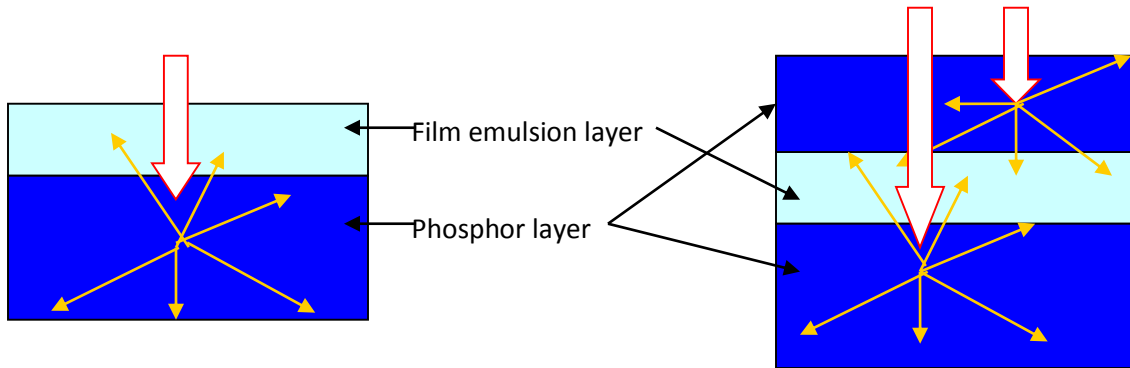


Figure 18: Diagrams comparing configurations for two screen-film combinations. The left figure shows a back screen in contact with a single emission film, combination employed in mammography. The right figure shows an emission film sandwiched between two intensifying screens, the combination employed for general medical radiography.

The choice of the type of film and screen, the processing conditions (i.e. chemical formulation of the solutions employed), the time of exposure, the dose employed and even the ambient conditions (temperature or humidity) will affect the performance of the detector [16]. It is, therefore, very important to choose correctly between materials and ways of operations, so the outcome is optimized.

The principal advantage of film-screen imaging systems is its excellent spatial resolution. The films are also physically handled, allowing the radiographer to display more than one image at the same time, for comparative analysis, and can be stored for long periods of time suffering almost no degradation. The detectors can be large and continuously sensitive surfaces and are directly sensitive to the impact of the X-ray beam. [18] [20]

On the other hand, the main drawback is in image quality; film-screen systems usually have low SNR and low dynamic range. There is a compromise between the spatial resolution and the detection efficiency of the X-ray image and between the dynamic range and the contrast resolution that limits the quality of the images. Moreover, the film layer is fragile and cannot be duplicated without loss of quality [18] [20]. There are applications such as mammography, where conventional film-screen imaging is not precise enough, missing approximately 10% of the breast cancers that can be detected by physical examinations [18].

Photostimulable storage phosphor computed radiography (PSP CR)

In this system the screen-film combination is replaced by a storage phosphor imaging plate, also contained inside a cassette. Irradiation excites electrons in the phosphor and the crystalline structure traps them, keeping them stable until the exposure is finished. The number of excited electrons is proportional to the intensity of the beam so, after the exposure, the phosphor plate can be processed and the pattern of the absorbed X-rays read. For the processing, the phosphor plate is inserted into a reader and scanned by a laser beam of appropriate wavelength. The phosphor plate can be reused after the residual latent image is erased [17] [20].

The main advantage that CR systems have over completely digital radiography systems, is the lower investment cost required, as it is possible to re-purpose existing, conventional radiography systems just by changing the screen and film of the cassettes by the CR phosphor plates. However, if new installations are required, the cost difference between CR and other digital mammography systems would not be

significant. On the other hand, CR needs higher dose to obtain an acceptable image quality, mainly due to lower overall DQE and to the impossibility of changing and optimizing the exposure parameters [63].

Solid State X-ray Detectors

Thin-film transistor (TFT) based detectors or Active Matrix Flat Panel Imagers

TFT panels have been used extensively for medical imaging applications since the 1990s. There are two main types: Amorphous Silicon detectors and Amorphous Selenium detectors, which are direct and indirect conversion detectors respectively.

Amorphous silicon-based technology:

Amorphous silicon (a-Si) detectors are indirect conversion detectors, the X-rays are converted into visible light photons by a scintillator, usually a layer of thallium-activated caesium iodide (CsI:Tl). The scintillator plate is combined with an array of photodiodes and a thin film transistor (TFT) made with amorphous silicon material, which converts the photons into electronic charges before the analogue-to-digital conversion is performed, see Figure 19-left [17] [20].

These detectors, also called integrated area detectors, have favourable spatial resolution, good DQE and the images can be obtained in relatively short sequences. The pixel size of these systems is, however, larger than the average (100mm). A reduction of the pixel size is difficult, as it reduces the DQE and increases the required dose exposure to the patient [17] [63].

Amorphous selenium-based technology:

The detector consists of a thin layer of photoconductive material, amorphous selenium (a-Se), deposited on an imaging plate and with a uniform positive charge built up on the surface. The incident X-ray photons strike the surface of the material freeing electrons. The partial discharge produced has the form of a charge distribution pattern, as the discharge is related to the local radiation exposure. The latent image can then be read out and digitalized, resulting in an unprocessed radiography, see 19-right [17] [20].

The main advantage of this technology over other digital radiography systems is the direct conversion of the X-rays into electrical charge. This allows the avoidance of the conversion losses characteristic of X-rays being converted into light and light into electrical charge. Direct conversion detectors have lower signal to noise ratio and a higher degree of sharpness, so they generally have good DQE values. The main drawbacks are longer image lag and ghosting. [17]

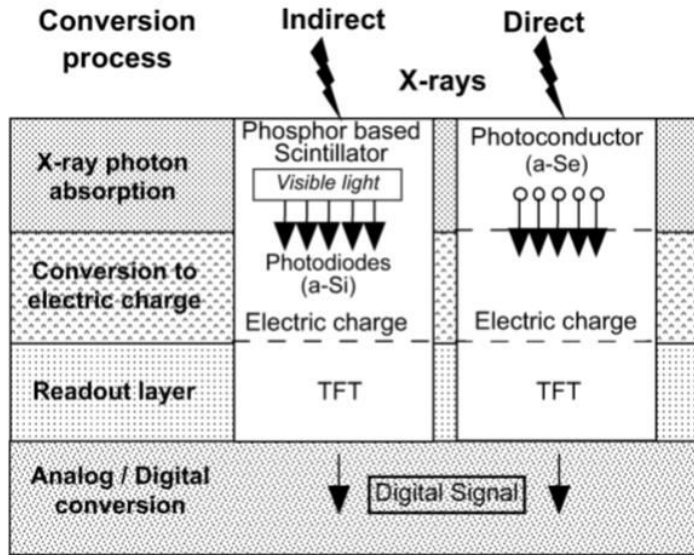


Figure 19: Image obtained from A. Noel and F. Thibault [20]. The figure shows the schematic of both the direct conversion a-Se TFT (right) and the indirect conversion a-Si TFT (left) detectors. It shows the main characteristics of both detectors and the detection process.

The main advantages of these two types of detectors are their high performance, radiation hardness and the possibility of achieving large active areas, making them a good choice for general radiography applications.

However, these detectors have high read noise, which results in a reduction of the DQE at low doses. They suffer from ghosting, an excess of image lag and baseline drifts (caused by the amorphous structure) at high frame rates and the pixel size is too big for some applications, usually restricted to 100-130 μ m. [25]

Charge Couple Device (CCD)

A CCD is another type of indirect solid-state detector. A scintillator, usually CsI:Tl, is used to convert the X-rays into visible photons. Optical focusing devices, such as lenses or fibre optics, are usually used for demagnification in order to match the scintillator size with the CCD size and, finally, a silicon CCD chip is used to detecting the light photons, converting them into electronic signal and digitizing them.

A schematic of a CCD chip can be seen in Figure 20-middle. When the light strikes the pixel, electron-hole pairs are formed and the electrons are constrained to an area by electrostatic forces. See Figure 20-left which shows the pixel structure with the typical 3 electrode structure. The charge is then moved down the columns (Full Frame readout method, see Figure 20-right) to the readout row using voltage sign changes, then is moved out from that row, amplified and digitized. [21] [64]

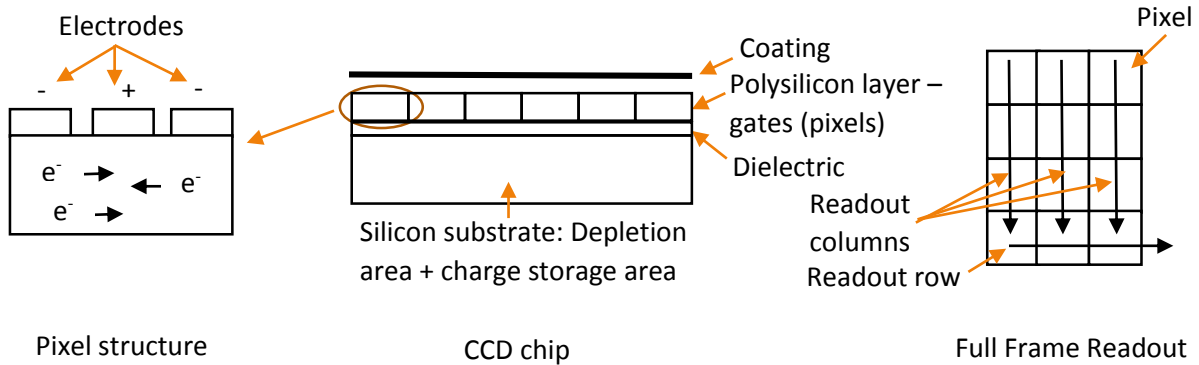


Figure 20: From left to right: Typical 3 electrodes pixel structure, CCD chip layout and typical Full Frame Readout schematics.

CCDs have a wide dynamic range (65-70dB), a low fix-pattern noise, high light sensitivity, high spatial resolution and a 100% Fill Factor with full frame readout technology. It also presents a linear response, small pixel sizes ($\leq 25\mu\text{m}$), high Signal-to-Noise Ratio (SNR) and, therefore, high image quality.

The main drawbacks of this technology are the size limitation of the sensor, being usually limited to $5 \times 5 \text{ cm}^2$, significantly increasing the cost with the size. The small active area combined with the impossibility to increase the pixel size reduces the applications that the CCD technology can target. It can achieve high frame rates but the read noise increases with it, limiting its performance for CT, tomosynthesis or fluoroscopy applications. It also requires relatively high power and it is susceptible to temperature changes and radiation damage. The demagnification mentioned above, however, is the major concern as the light collection efficiency is affected and it can also lead to geometric distortion, light scattering and a bad coupling efficiency might create secondary quantum sink. Special care has to be taken in the demagnification process to minimize these effects [32] [25].

A.2 MODULATION TRANSFER FUNCTION

Conceptually, if an image system is stimulated spatially with a pure sinusoidal wave of frequency f and amplitude 1, it will produce another sinusoidal wave with same frequency but lower contrast, i.e. amplitude smaller than 1, showing the system resolution losses. Calculating the Fourier transform of the resulting signal, a peak at frequency f and height equal to the amplitude of the wave will be obtained. If instead of one pure sinusoidal wave, the input signal contains more than one wave, the Fourier transform will separate the result for every frequency. The MTF will be the curve evolving each one of the frequency peaks.

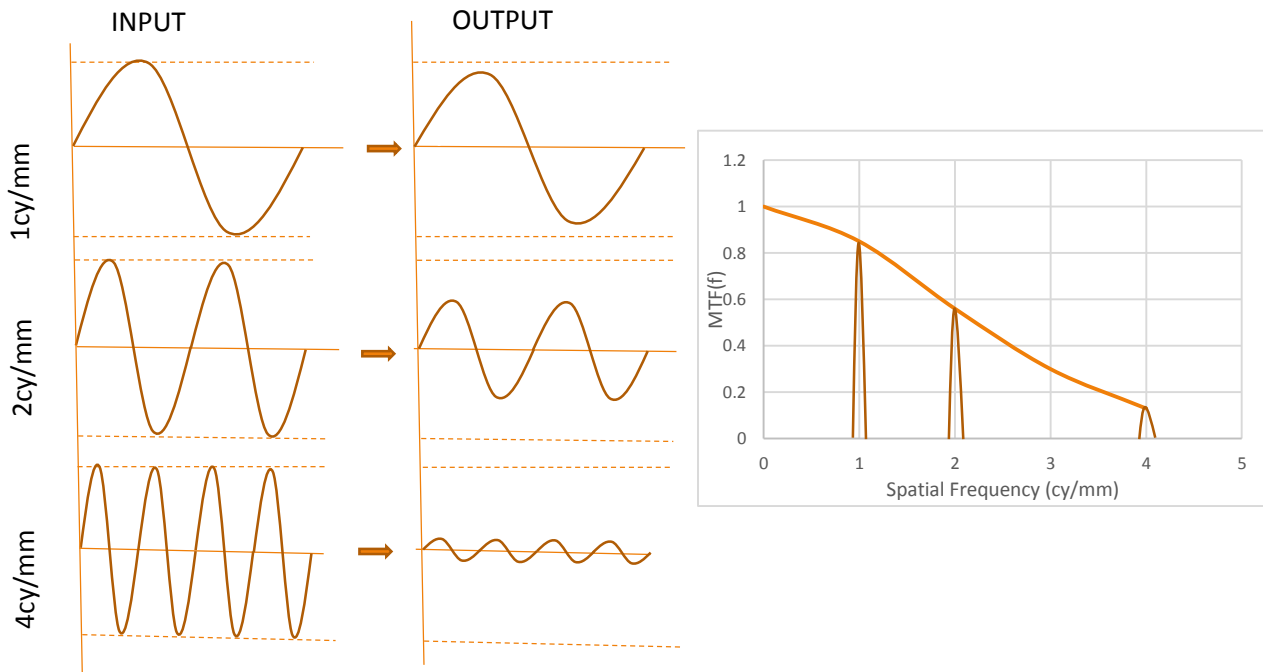


Figure 21: Description of the effect that the imaging system has over pure sinusoidal waves (left) and visual explanation of how the MTF is obtained (right).

The values of the MTF are between 0 and 1, where 1 means a complete transmission of the object's contrast over the image and 0 means no transmission of the contrast. High spatial resolution results in an improvement of image sharpness and a better detection of small details (very useful in analysis of microcalcifications, for example); therefore the MTF is desired to be as high as possible.

While the MTF describes the spatial resolution in the frequency domain, there are three other functions that describe it in the spatial domain: point spread function (PSF), line spread function (LSF) and edge spread function (ESF). There is a direct relationship between these four parameters (22-24) so it is possible to choose the simplest and easier function to measure and calculate the MTF from the results obtained.

PSF is the response of the system to a point source that is five to ten times smaller than the pixel pitch.

LSF describes the response of the system to a test device that has a narrow slit.

ESF is the response of the detector to a sharp edge. A straight edge is an easier device to make so the MTF is usually obtained from a measurement of the ESF.

$$LSF(x) = \int_{y=-\infty}^{\infty} PSF(x, y) dy \quad \text{Equation 22}$$

$$ESF(x) = \int_{x', -\infty}^{\infty} LSF(x') dx' \quad \text{Equation 23}$$

$$MTF = \text{FFT}(LSF) \quad \text{Equation 24}$$

A.3 NOISE POWER SPECTRUM

The IEC 62220-1 [34] states that an accurate measurement requires 4 million of individual pixels, distributed between the ROIs per frame and the frames required. As the ROIs are overlapping, see Figure 22 and Appendix C-Methodology for further analysis, each ROI introduces 128×128 individual pixels. Assuming 16 ROIs per frame, it will be necessary to calculate the averaged NPS of at least 15 frames.

$I(x,y)$ is the flat field image.

$S(x,y)$ is the correction applied to each captured image to compensate the presence of background trends and non-linearity, see discussion below.

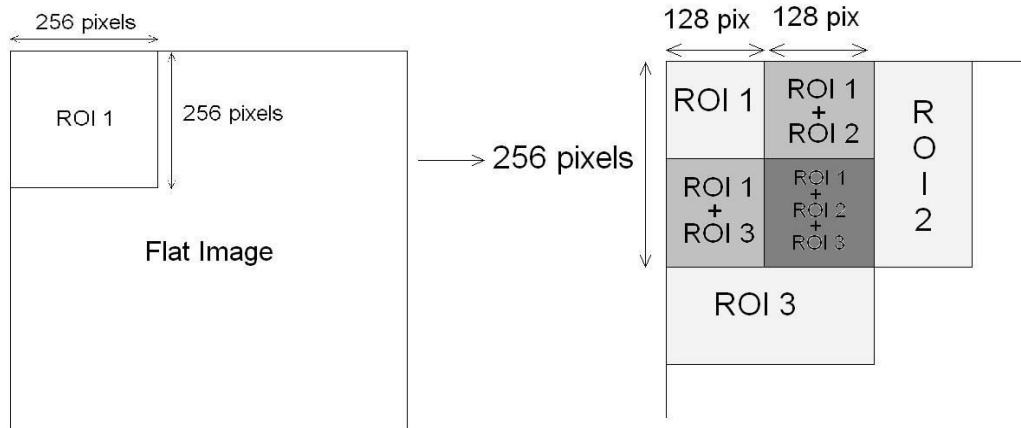


Figure 22: Distribution of region of interest (ROIs) in a flat image-one frame.

It is important to evaluate the two-dimensional NPS (2D-NPS) as well as the one-dimensional NPS (1D-NPS) as some artefacts, usually related with electronic problems, would not show up in the 1D plot. The 1D-NPS can be obtained selecting one-dimensional profiles from the 2D-NPS function. [40] [34] [65]

The NPS curve is constant as a function of spatial frequency for uncorrelated or white noise, i.e. the noise value of one pixel is independent of its neighbours. However, it typically decreases with the spatial frequency when the noise is correlated, i.e. there is noise leak into adjacent elements. [6]

Document Title	Document Number	Revision
Detector Imaging Testing – Work Instructions	DX-001818	A
This document is confidential and proprietary to PerkinElmer Medical Imaging		

APPENDIX B

1.0 SCOPE

This document is applicable to all detectors being tested at PerkinElmer Medical Imaging London

2.0 PURPOSE

The document defines the test method to be followed for the collection of image data to be used in turn for detector characterisation and qualification. It also defines analysis methods in the second half of the document. At the end of the document are appendices which contain a detector imaging test request form and other information pertinent to detector image testing.

3.0 PREREQUISITES

Before any testing or data collection can occur of 'Engineering detectors', an imaging test request must be submitted and signed by a Design Engineer. It is the Test Engineer's responsibility to begin testing only when this test request form is complete. See Appendix A for a copy of the imaging test request form.

The Test Engineer needs to be trained in the use of X-ray systems and image analysis tools as a minimum.

4.0 REFERENCE DOCUMENTS

- 4.1 DX-001538 Conversion Function, Modulation Transfer Function and Detective Quantum Efficiency Measurements
- 4.2 International Standard IEC62220-1: Medical equipment – Characteristics of digital X-ray imaging devices – Part1: Determination of the detective quantum efficiency

5.0 DEFINITIONS

Define uncommon words, terms and/or acronyms used within the document.

DQE	Detective Quantum Efficiency
MTF	Modulation Transfer Function
PC	Personal Computer (typically running Microsoft Windows)
DUT	Device (detector) Under Test
NNPS	Normalised Noise Power Spectrum

Document Title	Document Number	Revision
Detector Imaging Testing – Work Instructions	DX-001818	A
This document is confidential and proprietary to PerkinElmer Medical Imaging		

6.0 RESPONSABILITY

Department	Responsibility
Engineering	Definition of the work instructions
Engineering (independent reviewer)	Verification / review that the tests are appropriate.
Engineering Manager	Review that the work instruction is appropriate
Quality and Regulatory Affairs	Review that the work instruction is appropriate

Document Title	Document Number	Revision
Detector Imaging Testing – Work Instructions	DX-001818	A
This document is confidential and proprietary to PerkinElmer Medical Imaging		

7.0 TABLE OF CONTENTS

1.0	SCOPE	55
2.0	PURPOSE	55
3.0	PREREQUISITES.....	55
4.0	REFERENCE DOCUMENTS	55
5.0	DEFINITIONS	55
6.0	RESPONSABILITY.....	56
7.0	TABLE OF CONTENTS	57
8.0	LIST OF DATA COLLECTION ACTIVITIES.....	60
9.0	LIST OF DATA ANALYSIS ACTIVITIES	60
10.0	MATERIALS AND AQUIPMENT REQUIRED	61
11.0	MEASUREMENT PRECISION	61
12.0	BEFORE TESTING	61
12.1	ROOM TEMPERATURE	61
12.2	FORMAL ENGINEERING TEST REPORT FORM	61
12.3	DETECTOR STATUS	61
13.0	DARK IMAGE CORRECTION.....	62
13.1	DARK IMAGE PERFORMANCE AS A FUNCTION OF TEMPERATURE	62
13.2	DARK IMAGE PERFORMANCE AS A FUNCTION OF TIME.....	63
14.0	OPTICAL IMAGE COLLECTION.....	64
14.1	MEASUREMENTS FOR LINEARITY ANALYSIS.....	64
14.2	MEASUREMENTS OF SENSOR RESPONSE TIME.....	66
15.0	X-RAY IMAGE COLLECTION	67
15.1	SENSOR (TILE) GAP MEASUREMENT DATA COLLECTION	67

Document Title	Document Number	Revision
Detector Imaging Testing – Work Instructions	DX-001818	A
This document is confidential and proprietary to PerkinElmer Medical Imaging		

15.2	SENSOR IMAGE ARTEFACT MEASUREMENTS, BASED ON IMAGING WITH A UNIFORM X-RAY EXPOSURE	68
15.3	SENSOR IMAGE ARTEFACT MEASUREMENTS (USING X-RAY PHANTOMS)	69
15.4	COIN TEST	71
15.5	SENSITIVITY, MODULATION TRANSFER FUNCTION, NORMALISED NOISE POWER SPECTRUM AND DETECTIVE QUANTUM EFFICIENCY.....	72
15.6	UNIFORMITY	73
16.0	DATA ANALYSIS.....	74
16.1	OFFSET VARIATION WITH TEMPERATURE	74
16.2	OFFSET VARIATION WITH TIME.....	75
16.3	STATIC NOISE	76
16.4	TEMPORAL NOISE	78
16.5	LINEARITY.....	79
16.6	SENSOR RESPONSE TIME	81
16.7	SENSOR GAP MEASUREMENT	83
16.8	IMAGE LAG.....	84
16.9	IMAGE AFTERGLOW	85
16.10	PIXEL CROSSTALK	86
16.11	SENSOR GLOW EFFECT	88
16.12	“COIN” TEST	90
16.13	UNIFORMITY	91
16.14	SENSITIVITY	92
16.15	CONVERSION FUNCTION	93
16.16	MTF.....	94
16.17	NNPS.....	95
16.18	DQE.....	96

Document Title	Document Number	Revision
Detector Imaging Testing – Work Instructions	DX-001818	A
This document is confidential and proprietary to PerkinElmer Medical Imaging		

17.0	REVISION HISTORY	97
18.0	APPENDIX A – FORMAL ENGINEERING REQUEST FORM	98
19.0	APPENDIX B – GAIN AND OFFSET CORRECTIONS.....	99
20.0	APPENDIX C– IMAGE AND IMAGE SEQUENCE FILE FORMATS, AND TEST DATA STORAGE LOCATION	100
20.1	DATA FORMAT	100
20.2	LOCATION.....	100
21.0	APPENDIX D – REFERENCE IMAGES FOR IMAGE ARTEFACT ANALYSIS	101
21.1	ARTEFACT 1	101
21.2	ARTEFACT 2	103
21.3	ARTEFACT 3	106
21.4	ARTEFACT 4	107
21.5	ARTEFACT 5	108
21.6	ARTEFACT 6	109
21.7	ARTEFACT 7	109

Document Title	Document Number	Revision
Detector Imaging Testing – Work Instructions	DX-001818	A
This document is confidential and proprietary to PerkinElmer Medical Imaging		

8.0 LIST OF DATA COLLECTION ACTIVITIES

ID	Description of tests	Section
1	Dark image collection - Dark image performance as a function of temperature	13.1
2	Dark image collection - Dark image performance as a function of time	13.2
3	Dark image collection - Noise	13.2
4	Optical image collection - Linearity	14.1
5	Optical image collection – Sensor response time	14.2
6	X-ray image collection – Gap measurements	15.1
7	X-ray image collection – Image artefacts with flood images	15.2
8	X-ray image collection – Image artefacts with phantom images	15.3
9	X-ray image collection – “Coin” test	15.4
10	X-ray image collection – Sensitivity, MTF, NPS and DQE	15.5
11	X-ray image collection – Uniformity	15.6

9.0 LIST OF DATA ANALYSIS ACTIVITIES

ID	Description of tests	Section
1	Offset variation with temperature	16.1
2	Offset variation with time	16.2
3	Static noise	16.3
4	Temporal noise	16.4
5	Linearity	16.5
6	Sensor response time	16.6
7	Sensor gap measurement	16.7
8	Image lag	16.8
9	Image afterglow	16.9
10	Pixel crosstalk	16.10
10	Sensor glow effect	16.11
11	“Coin” test	16.12
12	Uniformity	16.13
14	Sensitivity	16.14
15	Conversion function	16.15
16	MTF	16.16
17	NNPS	16.17
18	DQE	16.18

Document Title	Document Number	Revision
Detector Imaging Testing – Work Instructions	DX-001818	A
This document is confidential and proprietary to PerkinElmer Medical Imaging		

10.0 MATERIALS AND EQUIPMENT REQUIRED

See the 'Materials required' section of each test for the specific materials and equipment needed for that particular test. This list collates all of the materials required for all of the tests.

- 10.1 PC with appropriate software for running the detector under test
- 10.2 X-ray generator with an operating energy range applicable to the detector under test
- 10.3 Detector cooling equipment. This may consist of power supplies, fans, fan/heatsink aggregates etc., which will be specific to the detector under test
- 10.4 Power supplies. Each detector will require a specific power supply to provide power to the electronic printed circuit boards
- 10.5 A temperature sensor / logging instrument with suitable probes. For example the PicoScope TC-08
- 10.6 Fast-rise-time LED, bright enough to saturate the detector at minimum exposure time, with appropriate driving electronics to ensure a switch on time of 1ms or faster
- 10.7 MTF edge test device (phantom)
- 10.8 X-ray hand phantom
- 10.9 Calibrated radiation dose meter (eg. RTI piranha meter)
- 10.10 Set of Aluminium X-ray filters (thicknesses: 0.2mm x2, 0.5mm x 4, 4.28mm x1, 15mm x1)
- 10.11 Resolution Mesh
- 10.12 ImageJ software (<http://imagej.nih.gov/ij/> - version 1.48 or later)
- 10.13 Matlab version 8 (R2012b) or later

11.0 MEASUREMENT PRECISION

- 11.1 Temperatures to be measured to within an accuracy of $\pm 0.1^\circ\text{C}$
- 11.2 Exposure times to be measured to within an accuracy of $\pm 100\mu\text{s}$

12.0 BEFORE TESTING

- 12.1 Room temperature

The room temperature has to be measured and stated for each test.

- 12.2 Formal engineering test report form

Ensure that the Detector Test Request form has been completed and signed, paying particular attention to ensure that firmware versions, voltage references and current source settings, and anything else that could influence the performance of the detector have been noted

- 12.3 Detector status

Ensure that the offset of the dark images is high enough to avoid any clipping in the image, i.e. 0 pixel values in non-dead pixels.

Document Title	Document Number	Revision
Detector Imaging Testing – Work Instructions	DX-001818	A
This document is confidential and proprietary to PerkinElmer Medical Imaging		

13.0 DARK IMAGE CORRECTION

13.1 Dark image performance as a function of temperature

Materials required
<ol style="list-style-type: none"> 1) PC with the appropriate software for running the detector under test 2) Detector cooling equipment (if appropriate for this detector) 3) A power supply appropriate for the detector (typically the Dexela +4/+6/-6 multi-rail or 24V power supply) 4) Temperature sensor / temperature logger

Test method
<ol style="list-style-type: none"> 1) Place the temperature sensors around the detector as indicated by the Design Engineer's instructions 2) Take photographs of the location of each of the thermocouples, clearly showing the location of the thermocouple in relation to the rest of the detector. Label the associated image files with thermocouple label. (Labels could just be simply thermocouple1.jpg, thermocouple2.jpg etc., as long as they are unique) 3) Connect the detector to the measurement PC and start any temperature data acquisition software (if the temperature is to be automatically logged) 4) Power on the detector 5) Set the detector exposure time to its minimum value 6) Collect a sequence of 20 dark images or collect 20 individual dark images, use the naming convention defined in Appendix C – Image and image sequence file formats and test data storage location. 7) Note the temperature at which this sequence is collected 8) Using any specific temperature sensor as a master reference, wait for the temperature to rise by 2 – 3 degrees 9) Repeat steps 6 - 8 10) Continue to collect sequences of 20 images for even temperature steps of 2 – 3 degrees until the time interval between measurements exceeds 20 minutes or the temperature has risen to its maximum specified operating temperature.

Outputs
<ol style="list-style-type: none"> 1) Set of pictures of the detector (in JPG format) showing the location of each of the thermocouples 2) A sequence of images (either in a single file (typically SMV format) or as individual TIFF files) clearly showing the detector type, serial number, exposure time and temperature (see Appendix C for more information). Eg: 2321_00003_80ms_35deg_Dark.smv

Document Title	Document Number	Revision
Detector Imaging Testing – Work Instructions	DX-001818	A
This document is confidential and proprietary to PerkinElmer Medical Imaging		

13.2 Dark image performance as a function of time

Materials required

- 1) PC with the appropriate software for running the detector under test
- 2) Detector cooling equipment (if appropriate for this detector)
- 3) A power supply appropriate for the detector (typically the Dexela +4/+6/-6 multi-rail or 24V power supply)

Test method

- 1) Connect the detector to the measurement PC
- 2) Power on the detector
- 3) Warm up the detector until a stable temperature is reached.
- 4) Set the detector exposure time to its minimum value
- 5) Collect a sequence of 20 dark images or collect 20 individual dark images including a reference to the exposure time in the file name of the image
- 6) Save these images using the naming and storage convention described in Appendix C – Image and image sequence file formats and test data storage location.
- 7) Increase the exposure time to 100ms
- 8) Repeat step 4
- 9) Increase the exposure time in the sequence 200ms, 500ms, 1000ms, 2000ms, 5000ms, 10 000ms... (until all pixels of the detector have saturated or the maximum exposure time has been reached.)

Outputs

- 1) A sequence of images (either in a single file (typically SMV format) or as individual TIFF files) clearly showing the detector type, serial number and exposure (see Appendix C for more information).

Eg: 2321_00003_80ms_Dark.smv

Document Title	Document Number	Revision
Detector Imaging Testing – Work Instructions	DX-001818	A
This document is confidential and proprietary to PerkinElmer Medical Imaging		

14.0 OPTICAL IMAGE COLLECTION

NOTE: If the detector does not have a removable (press-on) scintillator then tests 14.1 and 14.2 will have to be performed with X-ray exposure instead of optical illumination. See the individual tests for more instructions.

14.1 Measurements for linearity analysis

Materials required
<ol style="list-style-type: none"> 1) PC with the appropriate software for running the detector under test 2) Detector cooling equipment (if appropriate for this detector) 3) A power supply appropriate for the detector (typically the Dexela +4/+6/-6 multi-rail or 24V power supply) 4) Fast-rise-time LED with stabilised light output, bright enough to saturate the detector at minimum exposure time, with appropriate driving electronics to ensure a switch on time of 1ms or faster OR X-ray system if the detector does not have a removable (press-on) scintillator.

Test method
<ol style="list-style-type: none"> 1) Connect the detector to the measurement PC 2) Remove the scintillator plate and the carbon cover. 3) Place the detector facing the light source. 4) Power on the detector 5) Warm up the detector until a stable temperature is reached 6) Select the minimum exposure time 7) Select the light intensity values that gives a percentage of the dynamic range of: 0 (Dark image), 2, 3, 5, 8, 12, 18, 25, 32, 40, 50, 60, 70, 80, 90 and 100% 8) For each intensity step acquire 20 bright images 9) Save these images using the naming and storage convention described in Appendix C – Image and image sequence file formats and test data storage location. <p>NOTE1: If the detector uses a FOS and the scintillator is not removable the intensity steps will be limited to the 11 current steps that the X-ray generator offers, range from 10-100mA. The voltage should be selected so the detector is partially saturated when the current is 100mA.</p> <p>NOTE2: The data collection and the data analysis tests are defined for detectors that do not present shadowing areas.</p>

Outputs

Document Title	Document Number	Revision
Detector Imaging Testing – Work Instructions	DX-001818	A
This document is confidential and proprietary to PerkinElmer Medical Imaging		

- 1) A sequence of images (either in a single file (typically SMV format) or as individual TIFF files) clearly showing the detector type, serial number, exposure time and temperature (see Appendix C for more information).
Eg: 2321_00003_80ms.smv

Document Title	Document Number	Revision
Detector Imaging Testing – Work Instructions	DX-001818	A
This document is confidential and proprietary to PerkinElmer Medical Imaging		

14.2 Measurements of sensor response time

Materials required

- 1) PC with the appropriate software for running the detector under test
- 2) Detector cooling equipment (if appropriate for this detector)
- 3) A power supply appropriate for the detector (typically the Dexela +4/+6/-6 multi-rail or 24V power supply)
- 4) Fast-rise-time LED, with stabilised light output, bright enough to saturate the detector at minimum exposure time, with appropriate driving electronics to ensure a switch on time of 1ms or faster.

Test method

- 1) Connect the detector to the measurement PC
- 2) Remove the scintillator plate and the carbon cover.
- 3) Place the detector facing the light source.
- 4) Power on the detector
- 5) Warm up the detector until a stable temperature is reached
- 6) Select the settings that give low exposure (around 500ADU after dark subtraction), mid exposure (8000 ADU) and high exposure (15000 ADU) levels.
- 7) Note down the settings used
- 8) For each exposure level, acquire a set of 50-100 images in the following way:
 - a. Start the acquisition with the led source turned off to acquire some dark images (5-10 darks).
 - b. After 5-10 darks have been acquired turn on the led source (during the same sequence of 50-100 images) and acquire 20-30 bright images.
 - c. Turn off the led source and finish the sequence with dark images.
- 9) Save these images using the naming and storage convention described in Appendix C – Image and image sequence file formats and test data storage location.

NOTE: If the detector uses a FOS and the scintillator is not removable this test must be skipped. A similar test will be done in test 15.2

Outputs

- 1) A sequence of images (either in a single file (typically SMV format) or as individual TIFF files) clearly showing the detector type, serial number, exposure time and light intensity or exposure level (see Appendix C for more information).
Eg: 2321_00003_80ms_8000ADU.smv

Document Title	Document Number	Revision
Detector Imaging Testing – Work Instructions	DX-001818	A
This document is confidential and proprietary to PerkinElmer Medical Imaging		

15.0 X-RAY IMAGE COLLECTION

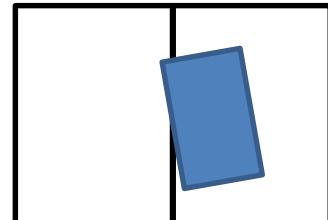
15.1 Sensor (tile) gap measurement data collection

Materials required

- 1) PC with the appropriate software for running the detector under test
- 2) Detector cooling equipment (if appropriate for this detector)
- 3) A power supply appropriate for the detector (typically the Dexela +4/+6/-6 multi-rail or 24V power supply)
- 4) X-ray system
- 5) MTF edge test device

Test method

- 1) Connect the detector to the measurement PC
- 2) Place the detector under the X-ray source and align with the use of the collimator
- 3) Turn on the detector
- 4) Place the MTF edge test device across the tiled sensor gap area with a small angle (< 5°) relative to the gap between the sensors (as shown in the image).
- 5) Acquire an image.
- 6) Move to another gap in the tiled sensor array and Repeat 4 and 5 for all the gaps.
- 7) Name the images as stated in the Output section of this test. Save them following using the storage convention described in Appendix C – Image and image sequence file formats and test data storage location. See the outputs section to see naming convention.



Outputs

- 1) A series of TIFF images, one image for each gap, clearly stating the sensors that define the gap.
E.g. : Sensor1_Sensor2_Gap.TIFF

Document Title	Document Number	Revision
Detector Imaging Testing – Work Instructions	DX-001818	A
This document is confidential and proprietary to PerkinElmer Medical Imaging		

15.2 Sensor image artefact measurements, based on imaging with a uniform X-ray exposure

Materials required
<ol style="list-style-type: none"> 1) PC with the appropriate software for running the detector under test 2) Detector cooling equipment (if appropriate for this detector) 3) A power supply appropriate for the detector (typically the Dexela +4/+6/-6 multi-rail or 24V power supply) 4) X-ray system

Test method
<ol style="list-style-type: none"> 1) Connect the detector to the measurement PC 2) Place the detector under the X-ray source and align it with the collimator 3) Turn on the detector 4) Select the settings that give low exposure (around 500ADU after dark subtraction), mid exposure (8000 ADU) and high exposure (15000 ADU) levels. 5) Make note of the settings 6) For each exposure level, acquire a set of 50 images in the following way: <ol style="list-style-type: none"> i. Start the acquisition with the X-ray source turned off in order to acquire some dark images (5-10 dark). ii. After the 5-10 darks have been acquired turn on the X-ray source and acquire the rest of the sequence with bright images. 7) Save these images using the naming and storage convention described in Appendix C – Image and image sequence file formats and test data storage location. <p>NOTE: Before starting the irradiation, make sure the X-ray tube is ready for irradiation. To do so, before starting the irradiation half press the triggering button and wait until the machine warms up (it will be indicated with a noise). If the irradiation is started without the warm up, the first couple of images will have higher response, i.e. if you are irradiating at 7000 ADU you will get a couple of images with 10000 ADU.</p>

Outputs
<ol style="list-style-type: none"> 1) A sequence of images (either in a single file (typically SMV format) or as individual TIFF files) clearly showing the detector type, serial number, voltage, exposure time and current (see Appendix C for more information). Eg: 2321_00003_40kV_80ms_32mA.smv 2321_00003_40kV_80ms_32mA_01.TIFF

Document Title	Document Number	Revision
Detector Imaging Testing – Work Instructions	DX-001818	A
This document is confidential and proprietary to PerkinElmer Medical Imaging		

15.3 Sensor image artefact measurements (using X-ray phantoms)

Materials required

- 1) PC with the appropriate software for running the detector under test
- 2) Detector cooling equipment (if appropriate for this detector)
- 3) A power supply appropriate for the detector (typically the Dexela +4/+6/-6 multi-rail or 24V power supply)
- 4) X-ray system
- 5) Hand phantom (or similar)

Test method

- 1) Connect the detector to the measurement PC
- 2) Place the detector under the X-ray source and align with the use of the collimator
- 3) Turn on the detector
- 4) Select the settings that give low exposure (around 500ADU after dark subtraction), mid exposure (8000 ADU) and high exposure (15000 ADU) levels.
- 5) Make note of the settings
- 6) For each exposure level, acquire a set of 50 images in the following way:
 - i. Start the acquisition with the X-ray source turned on, in order to acquire some bright images (5-10 bright).
 - ii. After the 5-10 bright images have been acquired turn off the X-ray source and acquire the rest of the sequence with dark images.
- 7) For each exposure level, acquire a set of 50 images in the following way:
 - i. Start the acquisition with the X-ray source turned off, in order to acquire some dark images (5-10 darks).
 - ii. After the 5-10 dark images have been acquired turn on the X-ray source and acquire the rest of the sequence with bright images.
- 8) Remove the phantom and acquire 20 flat images for each exposure level.
- 9) Acquire a set of 20 dark images.
- 10) Save these images using the naming and storage convention described in Appendix C – Image and image sequence file formats and test data storage location.

NOTE: Before starting the irradiation, make sure the X-ray tube is ready for irradiation. To do so, before starting the irradiation half press the triggering button and wait until the machine warms up (it will be indicated with a noise). If the irradiation is started without the warm up, the first couple of images will have higher response, i.e. if you are irradiating at 7000 ADU you will get a couple of images with 10000 ADU.

Document Title	Document Number	Revision
Detector Imaging Testing – Work Instructions	DX-001818	A
This document is confidential and proprietary to PerkinElmer Medical Imaging		

Outputs

- 1) A sequence of images (either in a single file (typically SMV format) or as individual TIFF files) clearly showing the detector type, serial number, voltage, exposure time and current. Specify if the sequence is of darks (adding at the end _Dark), phantoms (adding at the end _Hand) or flats (not adding anything). See Appendix C for more information.

Eg: 2321_00003_40kV_80ms_32mA_Dark.smv
2321_00003_40kV_80ms_32mA_01.TIFF

Document Title	Document Number	Revision
Detector Imaging Testing – Work Instructions	DX-001818	A
This document is confidential and proprietary to PerkinElmer Medical Imaging		

15.4 Coin test

Materials required
<ol style="list-style-type: none"> 1) PC with the appropriate software for running the detector under test 2) Detector cooling equipment (if appropriate for this detector) 3) A power supply appropriate for the detector (typically the Dexela +4/+6/-6 multi-rail or 24V power supply) 4) X-ray system 5) 30x30x04 mm of lead

Test method
<ol style="list-style-type: none"> 1) Place the detector under the X-ray source and align with the use of the collimator 2) Turn on the detector 3) Cover the centre area of one of the sensors with a 30 x 30 x 4 mm piece of lead. 4) Acquire a set of 20 darks. 5) Acquire a set of 20 bright images at three different exposure levels (around 1000-2000 ADU, 7000-8000 ADU and 15000-16000 ADU). 6) Acquire a second set of 20 darks. 7) Save these images using the naming and storage convention described in Appendix C – Image and image sequence file formats and test data storage location.

Outputs
<ol style="list-style-type: none"> 2) A sequence of images (either in a single file (typically SMV format) or as individual TIFF files) clearly showing the detector type, serial number, voltage, exposure time and current. Specify if the sequence is of darks (adding _Dark) or flats (not adding anything). See Appendix C for more information. Eg: 2321_00003_40kV_80ms_32mA_Dark.smv 2321_00003_40kV_80ms_32mA_01.TIFF

Document Title	Document Number	Revision
Detector Imaging Testing – Work Instructions	DX-001818	A
This document is confidential and proprietary to PerkinElmer Medical Imaging		

- 15.5 Sensitivity, Modulation Transfer Function, Normalised Noise Power Spectrum and Detective Quantum Efficiency

Materials required

All details are given in document DX-001538 Revision B

Test method

All details are given in document DX-001538 Revision B

Outputs

All details are given in document DX-001538 Revision B

Document Title	Document Number	Revision
Detector Imaging Testing – Work Instructions	DX-001818	A
This document is confidential and proprietary to PerkinElmer Medical Imaging		

15.6 Uniformity

Materials required
<ol style="list-style-type: none"> 1) PC with the appropriate software for running the detector under test 2) Detector cooling equipment (if appropriate for this detector) 3) A power supply appropriate for the detector (typically the Dexela +4/+6/-6 multi-rail or 24V power supply) 4) X-ray system 5) Resolution mesh

Test method
<ol style="list-style-type: none"> 1) Connect the detector to the measurement PC 2) Place the detector under the X-ray source and align with the use of the collimator 3) Turn on the detector 4) Acquire a set of 20 darks. 5) Acquire a set of 20 bright images at a mid-exposure level (around 7000-8000 ADU). 6) Place the resolution mesh covering the detector surface. 7) Acquire a set of 20 phantom images keeping constant the settings. 8) Save these images using the naming and storage convention described in Appendix C – Image and image sequence file formats and test data storage location.

Outputs
<ol style="list-style-type: none"> 3) A sequence of images (either in a single file (typically SMV format) or as individual TIFF files) clearly showing the detector type, serial number, voltage, exposure time and current. Specify if the sequence is of darks (adding at the end –Dark), phantom (adding at the end –Mesh) or flats (not adding anything). See Appendix C for more information. Eg: 2321_00003_40Kv_80ms_32mA_Dark.smv

Document Title	Document Number	Revision
Detector Imaging Testing – Work Instructions	DX-001818	A
This document is confidential and proprietary to PerkinElmer Medical Imaging		

16.0 DATA ANALYSIS

16.1 Offset variation with temperature

Data inputs and tools required

- 1) ImageJ software or Matlab.
- 2) Data set from 13.1.

Analysis method

- 1) Select the first temperature step and calculate the mean pixel value of a 100x100 pixels² area centred in each sensor. If the chosen area is not smooth, move the area up or down to avoid the non-uniformities, i.e. the Cerberus and Hercules sensors have a circular mark in the middle of the sensor, avoid to include that area. Avoid including read-out columns, stitching blocks or dead columns/rows into the selected area.
- 2) Repeat step 1 for each image of the sequence and average.
- 3) Repeat steps 1 and 2 for each temperature step.
- 4) Plot the mean pixel value vs. the temperature steps and study the trend.
- 5) Identify any discontinuities or any deviation from smooth variation.

Outputs

- 1) Graph of mean pixel value vs. temperature

NOTE – Look out for:

Abrupt changes in the graph, the offset level should change smoothly with temperature.

Document Title	Document Number	Revision
Detector Imaging Testing – Work Instructions	DX-001818	A
This document is confidential and proprietary to PerkinElmer Medical Imaging		

16.2 Offset variation with time

Data inputs and tools required
<ol style="list-style-type: none"> 1) ImageJ software or Matlab. 2) Data set from 13.2.

Analysis method
<ol style="list-style-type: none"> 1) Select the first temperature step and calculate the mean pixel value of a 100x100 pixels² area centred in each sensor. If the chosen area is not smooth, move the area up or down to avoid the non-uniformities, i.e. the Cerberus and Hercules sensors have a circular mark in the middle of the sensor, avoid to include that area. Avoid including read-out columns, stitching blocks or dead columns/rows into the selected area. 2) Repeat step 1 for each image of the sequence and average. 3) Repeat steps 1 and 2 for each time step. 4) Plot the mean pixel value vs. the time steps and study the trend. 5) Plot the variance, square of the standard deviation, vs time steps and study the trend. 6) Check that the increments of time that double the mean pixel value should double the variance as well. Report if it does not follow this trend. 7) Select a row and repeat steps 2 to 4 to study individual pixel performances.

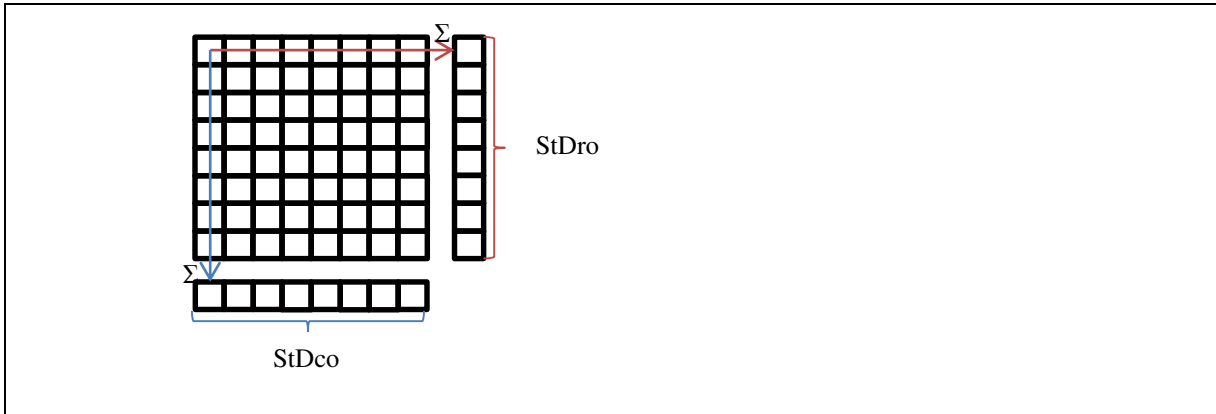
Outputs
<ol style="list-style-type: none"> 1) Graph of mean pixel value vs. time <p>NOTE- Look out for:</p> <ul style="list-style-type: none"> - Pixels that have different response with time than the average pixel response. - Abrupt changes in the graph, the offset level should increase (or decrease) linearly with integration time.

Document Title	Document Number	Revision
Detector Imaging Testing – Work Instructions	DX-001818	A
This document is confidential and proprietary to PerkinElmer Medical Imaging		

16.3 Static noise

Data inputs and tools required
<ol style="list-style-type: none"> 1) ImageJ software or Matlab. 2) Data set from 13.1
Analysis method
<ol style="list-style-type: none"> 1) Add a 1000ADU offset to the first image of the sequence, Dark1 + 1000ADU. 2) Subtract the 19 remaining images from the image resulting from step 1. This will result in 19 noise images (*). 3) To quantify the noise of the image: <ol style="list-style-type: none"> i. For each noise image, calculate the noise value (**) using a 100x100 pixel² area centred on each individual sensor in the sensor array. This results in a matrix of 19 times the number of sensors in the array. ii. Calculate the average of the 19 images and number of sensors and calculate the standard deviation to determine the rms noise in each case. iii. With ImageJ, open the 19 noise images and create a stack of images. Check that the images look flat and there is no image to image variation (flickering, see 16.4 for more information). <p>NOTE1 (*): The noise image can be obtained with the formula: $\text{NoiseImage} = (\text{Dark1} + 1000 \text{ ADU}) - \text{Dark2}$ Where Dark1 and Dark2 are individual dark images and the 1000ADU offset is an arbitrary value to ensure that values are not clipped due to the integer image space.</p> <p>NOTE2 (**): The noise is obtained from the standard deviation of an area of the noise image divided by the square root of 2.</p> $\text{Noise} = \frac{\text{StD(Noise Image)}}{\sqrt{2}}$ <ol style="list-style-type: none"> 4) To quantify the row and column noise: <ol style="list-style-type: none"> i. Select an area (MxN) for each sensor and noise image. Where M is the number of rows and N the number of columns. ii. Sum de values of each row of the MxN matrix, obtaining a Mx1 matrix, and calculate the standard deviation of that matrix, StD rows, see image below. iii. Sum de values of each column of the MxN matrix, obtaining a Nx1 matrix, and calculate the standard deviation of that matrix, StD cols, see image below. iv. Average the results of the 19 images.

Document Title	Document Number	Revision
Detector Imaging Testing – Work Instructions	DX-001818	A
This document is confidential and proprietary to PerkinElmer Medical Imaging		



Outputs
<ol style="list-style-type: none"> 1) 19 noise images (static) 2) Table with the standard deviation values for every sensor and image, the averages and the noise value with its correspondent tolerance value. 3) Table with the row and column standard deviations values for every sensor. <p>NOTE: See Section 21.0, Appendix D – Artefact 1, for more information regarding interpreting the data collected and see examples where the noise image showed problems with the detector electronics.</p>

Document Title	Document Number	Revision
Detector Imaging Testing – Work Instructions	DX-001818	A
This document is confidential and proprietary to PerkinElmer Medical Imaging		

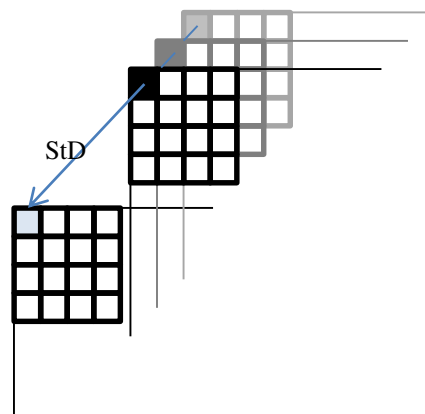
16.4 Temporal noise

Data inputs and tools required

- 1) ImageJ software or Matlab.
- 2) Data set from section 13.1 – 20 darks obtained at the minimum exposure time.

Analysis method

- 1) Calculate the temporal standard deviation image, i.e. Noise image, with a sequence of 20 dark images, see image on the right.
- 2) Calculate the mean pixel value, the median and the mode of a 100×100 pixel² area centred in each sensor in the sensor array. Select a different area if the chosen one is not smooth; make sure non-uniformities are avoided, i.e. the Cerberus and Hercules sensors have a circular mark centred in the sensor, avoid including that area.
- 3) Average to obtain the noise value (median) and calculate the standard deviation to calculate the rms noise.
- 4) Check if the median, mean and mode values are comparable (Gaussian distribution).
- 5) Make sure the image is flat.



Note: The noise value obtained for static images should be similar to the value obtained in this section.

Outputs

- 1) Noise image (temporal)
- 2) Table with the median, mean and mode values for each sensor.
- 3) Noise value (temporal) and tolerance values

NOTE: See Section 21.0, Appendix D – Artefact 2, for more information regarding interpreting the data collected and see examples where the noise image showed problems with the detector electronics.

Document Title	Document Number	Revision
Detector Imaging Testing – Work Instructions	DX-001818	A
This document is confidential and proprietary to PerkinElmer Medical Imaging		

16.5 Linearity

Data inputs and tools required
<ol style="list-style-type: none"> 1) ImageJ software or Matlab. 2) Data set from 14.1

Analysis method
<p>Linearity test:</p> <ol style="list-style-type: none"> 1) Average each set of images. 2) Calculate the mean pixel value of a 100x100 pixels² area centred in each sensor. If the chosen area is not smooth, move the area up or down to avoid the non-uniformities, i.e. the Cerberus and Hercules sensors have a circular mark in the middle of the sensor, avoid to include that area. Avoid including read-out columns, stitching blocks or dead columns/rows into the selected area. 3) Plot the mean pixel value versus the intensity steps. 4) Fit a linear curve and obtain the y-intercept and the slope values. 5) Calculate the theoretical mean pixel values with the coefficients obtained from the fit. 6) Calculate the deviation from linearity by subtracting the theoretical and experimental mean pixel values. 7) Compare the result with pre-defined tolerance limits. <p>NOTE1: The data collection and the data analysis tests are defined for detectors that do not present shadowing areas.</p> <p>Quick linearity check:</p> <ol style="list-style-type: none"> 1) Select the set of images at three exposure levels: low (\approx500-1000ADU), mid (\approx5000-8000ADU) and high (\approx10000) 2) Gain and offset correct the images (See Appendix B for gain correction explanation) using a different gain-map: <ol style="list-style-type: none"> a. Gain and offset correct the low and mid-range images with the high range gain-map. b. Gain and offset correct the low and high range images with the mid-range gain-map. c. Gain and offset correct the mid and high range images with the low range gain-map. 3) Check that the gain and offset corrected images look smooth and homogeneous. Report otherwise.

Outputs
<p>Linearity test:</p> <ol style="list-style-type: none"> 1) Table with the mean pixel values for the different intensity steps 2) Plot of the mean pixel value vs. intensity steps 3) Table with theoretical mean pixel values for the different intensity steps

Document Title	Document Number	Revision
Detector Imaging Testing – Work Instructions	DX-001818	A
This document is confidential and proprietary to PerkinElmer Medical Imaging		

- 4) Table with the deviation from linearity
- 5) Graph of the deviation from linearity

Quick linearity check:

- 1) Set of gain and offset corrected images using different gain-maps.

NOTE: See Section 21.0, Appendix D – Artefact 3, for more information regarding interpreting the data collected and see examples where linearity issues are seen in gain and offset corrected images using different gain-maps (See Analysis method – NOTE2).

Document Title	Document Number	Revision
Detector Imaging Testing – Work Instructions	DX-001818	A
This document is confidential and proprietary to PerkinElmer Medical Imaging		

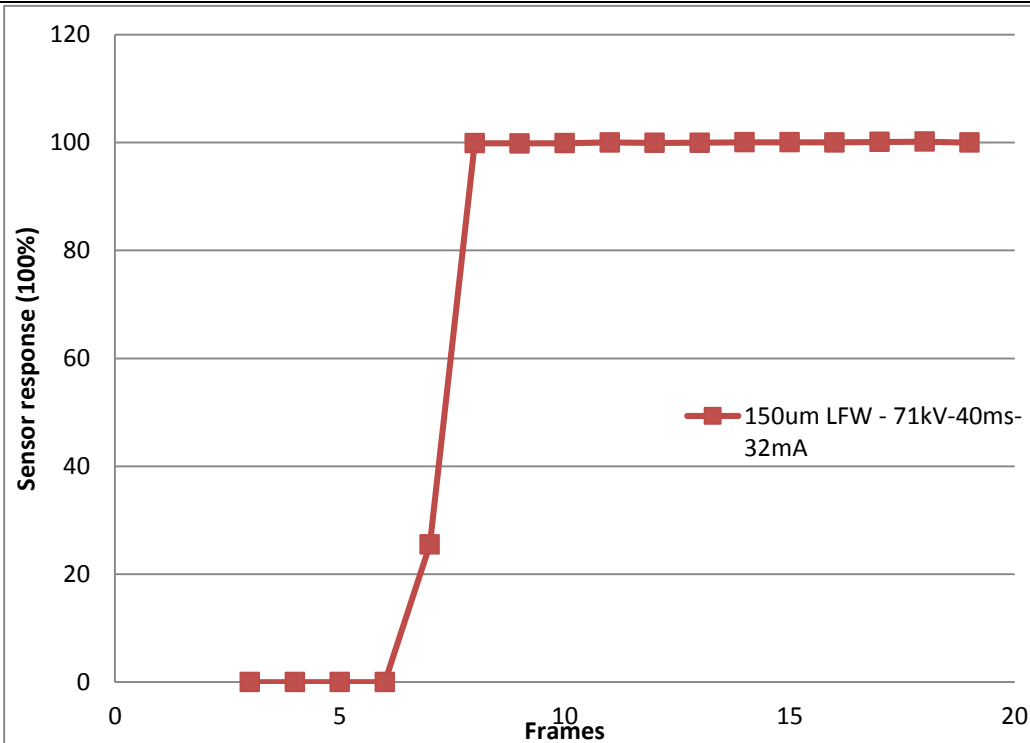
16.6 Sensor response time

Data inputs and tools required
<ol style="list-style-type: none"> 1) ImageJ software or Matlab. 2) Data set from 14.2

Analysis method
<ol style="list-style-type: none"> 1) Calculate the mean pixel value of each frame of a 100x100 pixel² area centred on the imaging area of the detector. If the chosen area is not smooth, move the area up or down to avoid the non-uniformities, i.e. the Cerberus and Hercules sensors have a circular mark in the middle of the sensor, avoid to include that area. Avoid including read-out columns, stitching blocks or dead columns/rows into the selected area. 2) Plot the mean pixel value versus the number of frames 3) Evaluate the sensor rise and decay time (or number of frames)

Outputs
<ol style="list-style-type: none"> 1) Table with the mean pixel value (ADU) of each frame 2) Graph of mean pixel value vs. frames (or time), see example below.

Document Title	Document Number	Revision
Detector Imaging Testing – Work Instructions	DX-001818	A
This document is confidential and proprietary to PerkinElmer Medical Imaging		



NOTE: See Section 21.0 , Appendix D – Artefact 4, for more information regarding interpreting the data collected and see examples where the response time of the detector showed issues.

Document Title	Document Number	Revision
Detector Imaging Testing – Work Instructions	DX-001818	A
This document is confidential and proprietary to PerkinElmer Medical Imaging		

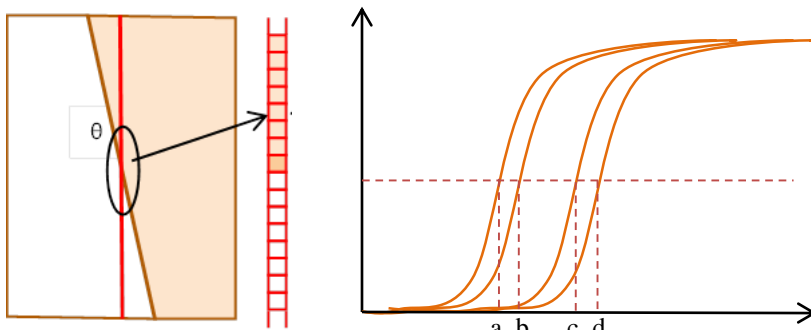
16.7 Sensor Gap Measurement

Data inputs and tools required

- 1) ImageJ software or Matlab.
- 2) Data set from section 15.1

Analysis method

- 1) Plot the intensity profile of ten consecutive columns, including the area of the gap, see image below. In the plot, skip the gap column and its neighbouring columns. The graph below shows the intensity profile of 4 columns; a-b and c-d are consecutive columns, but b-c have the three skipped columns between them.
- 2) In the graph, extrapolate the distance that corresponds to half the maximum intensity value for the 10 columns (values a, b, c and d in the image below). The difference between distances should be comparable between consecutive columns, i.e. b-a or d-c in the figure, and bigger between the columns that include the skipped columns, i.e. c-b.
- 3) Calculate the average of the distances between the consecutive columns and multiply by three.
- 4) Subtract result from step 3 to the bigger distance, i.e. $D(c-b) - 3 \times D(a-b)$, if only one consecutive column is taken into account.
- 5) Multiply the value obtained in step 4 by the pixel pitch and the tangent of the edge angle to obtain the gap distance.



Outputs

- 1) Sensor gap distance for all the gaps.

Document Title	Document Number	Revision
Detector Imaging Testing – Work Instructions	DX-001818	A
This document is confidential and proprietary to PerkinElmer Medical Imaging		

16.8 Image Lag

Data inputs and tools required
<ul style="list-style-type: none"> 1) ImageJ software or Matlab. 2) Data set from 15.2
Analysis method
<ul style="list-style-type: none"> 1) Follow the analysis described in section 16.6: Sensor response time
Outputs
<ul style="list-style-type: none"> 1) Graph of mean pixel value vs. frames (or time) 2) Table with the mean pixel value (ADU) of each frame <p>NOTE1: See section 16.6 to see an example of the expected outputs.</p> <p>NOTE: See Section 21.0 , Appendix D – Artefact 4, for more information regarding interpreting the data collected and see examples where the response time of the detector showed issues.</p>

Document Title	Document Number	Revision
Detector Imaging Testing – Work Instructions	DX-001818	A
This document is confidential and proprietary to PerkinElmer Medical Imaging		

16.9 Image Afterglow

Data inputs and tools required

- 1) ImageJ software or Matlab.
- 2) Data set from 12.3

Analysis method

- 1) Gain and offset correct the phantom images (bright and dark).
- 2) For each exposure, count the amount of dark frames that show the phantom image, i.e. ghosting.
- 3) Multiply the frame number of the last dark that shows the phantom by the exposure time to calculate the duration of the afterglow.

Outputs

- 1) Graph of mean pixel value vs. time
- 2) Duration of the afterglow effect

Document Title	Document Number	Revision
Detector Imaging Testing – Work Instructions	DX-001818	A
This document is confidential and proprietary to PerkinElmer Medical Imaging		

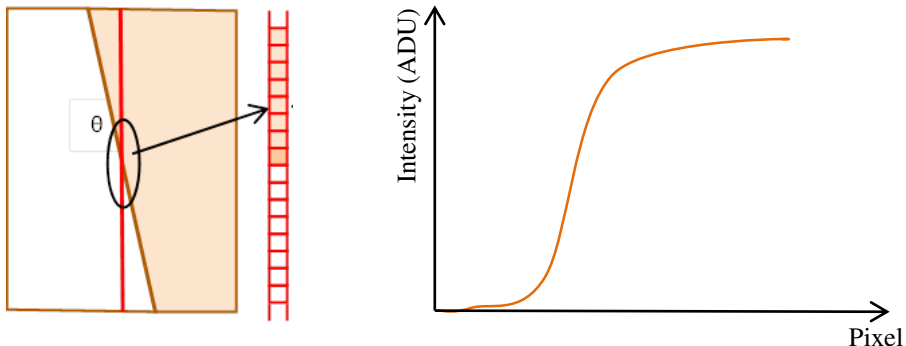
16.10 Pixel Crosstalk

Data inputs and tools required

- 1) ImageJ software or Matlab.
- 2) Data set from 15.2 and 15.5

Analysis method

- 1) With the images obtained in section 15.2:
 - a. Find the rows and columns that have a defective (or absent) column next to them, i.e. columns/rows next to the edges, read out columns or defective column/row.
 - b. Check the ADU difference between those columns and the average value of the sensor.
 - c. Repeat step 3 at different exposure levels
 - d. Check that there are no differences between the sensors mean pixel value and the mean pixel value of the studied row/columns. Report otherwise.
- 2) With the images obtained in section 15.5:
 - a. Gain and offset correct one of the edge images.
 - b. Plot the intensity profile across the edge for ten consecutive columns, i.e. pixel value (ADU) vs. pixel.
 - c. Check that the pixel distance between the profiles at a constant intensity value is always constant. Report otherwise, see Appendix D.



Outputs

From section 1

- Table with the mean pixel value of the sensor and of the studied rows/columns

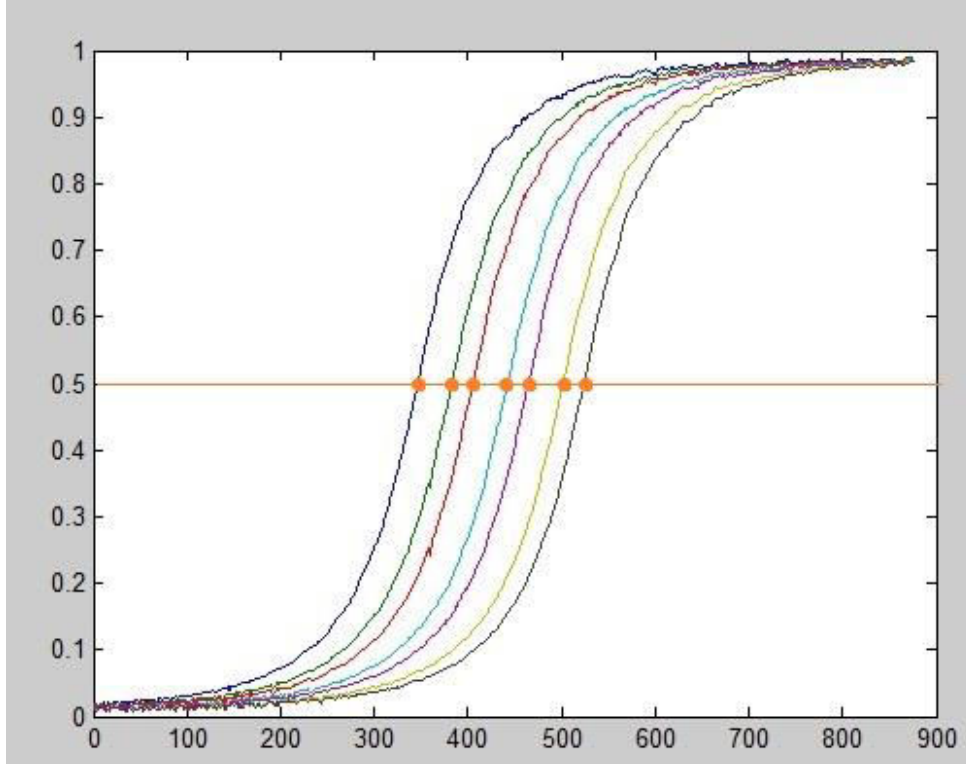
From section 2

Document Title	Document Number	Revision
Detector Imaging Testing – Work Instructions	DX-001818	A
This document is confidential and proprietary to PerkinElmer Medical Imaging		

- Plot of the intensity profile of 10 consecutive columns across the edge.

NOTE - Look out for:

Line pairing between the intensity curves: The distances between consecutive lines at a specific intensity level, i.e. 50%, should be constant. If the distances vary every second line between two distances D_1 and D_2 , as shown in the figure below, that will indicate that there is a pixel crosstalk every 2 pixels.



Document Title	Document Number	Revision
Detector Imaging Testing – Work Instructions	DX-001818	A
This document is confidential and proprietary to PerkinElmer Medical Imaging		

16.11 Sensor Glow Effect

Data inputs and tools required
<ol style="list-style-type: none"> 1) ImageJ software or Matlab. 2) Data set from section 0
Analysis method
<ol style="list-style-type: none"> 1) Find the rows and columns that have a defective (or absent) column next to them, i.e. columns/rows next to the edges, read out columns or defective column/row. 2) Study their lag behaviour in comparison with the rest of the sensor, see section 16.8. The results should be comparable. Report otherwise. 3) Gain and offset correct the low exposure images acquired in section 0, using a gain-map acquired at mid-range (6000-8000 ADU). Make sure to include all the irradiated images. 4) Change the contrast in the image and check that the rows/columns under study do not show in the first frames to fade away after several frames. Report otherwise – “glow effect”.
Outputs
<ol style="list-style-type: none"> 1) Graph of mean pixel value vs. frames comparing the average sensor response and the response of rows and columns that have a defective (or absent) column next to them. 2) Table with the values of the graph in 1) NOTE1 - Look out for: Different lag behaviour in the rows and columns that have a defective (or absent) column next to them when compared with the average sensor response. 3) Set of gain and offset corrected phantom images. NOTE2 - Look out for: “Glowing effect” appearing in the studied column/row. Compare the first frame with following ones and check if the column/row is visible and fade after several frames. See image below.

Document Title	Document Number	Revision
Detector Imaging Testing – Work Instructions	DX-001818	A
This document is confidential and proprietary to PerkinElmer Medical Imaging		



Document Title	Document Number	Revision
Detector Imaging Testing – Work Instructions	DX-001818	A
This document is confidential and proprietary to PerkinElmer Medical Imaging		

16.12 "Coin" test

Data inputs and tools required
<ol style="list-style-type: none"> 1) ImageJ software or Matlab. 2) Data set from section 15.4

Analysis method
<ol style="list-style-type: none"> 1) Select a 100×100 pixel² area centred in the lead area of the first set of bright images. 2) Calculate the mean pixel value for each image of the set and average. 3) Repeat steps 1 and 2 for the rest of bright image sets. 4) Select the same 100×100 pixel² area in the sets of dark images. 5) Repeat step 2 for both sets. 6) Compare the mean pixel values of the dark and bright images.

Outputs
<ol style="list-style-type: none"> 1) Table with the mean pixel value of an area for several set of images. <p>NOTE - Look out for:</p> <ul style="list-style-type: none"> - Different offset levels between the lead area of the bright images and the dark images. - Afterglow in the second set of dark images. If that is the case, report linking with section 16.9.

Document Title	Document Number	Revision
Detector Imaging Testing – Work Instructions	DX-001818	A
This document is confidential and proprietary to PerkinElmer Medical Imaging		

16.13 Uniformity

Data inputs and tools required
<ol style="list-style-type: none"> 1) ImageJ software or Matlab. 2) Data set from section 15.6

Analysis method
<ol style="list-style-type: none"> 1) Gain and offset correct the mesh image (M,N) acquired in section 12.6 2) Find a region of interest (ROI) close to 50x50 pixel², so the detector size is a multiple of that value. 3) Place the first ROI in the top left corner of your image. 4) Calculate the division between the standard deviation and the mean value of that ROI, $\frac{\sigma_{ROI}}{\mu_{ROI}}$. Record that value in a new matrix, location (1,1). 5) Move the ROI to the right by half the ROI length, i.e. if the ROI is 50pixels in length move it by 25 pixels. 6) Repeat step 4 and 5 until the whole matrix length is covered. 7) Go back to left and move down by half the ROI length 8) Repeat steps 4 to 7 until the whole image area is covered and a resolution matrix is created, size (M/ROIx, N/ROIy). 9) The overall non-uniformity can be defined as: $\text{Non-uniformity (\%)} = 100 * \frac{\max(\text{Resolution}) - \min(\text{Resolution})}{\mu(\text{Resolution})}$ <p>NOTE: The $\frac{\sigma_{ROI}}{\mu_{ROI}}$ measurement is a measurement of the resolution of the detector so it is proportional to the MTF at certain spatial frequency, which varies depending of the pixel size and the mesh. This measurement gives an idea of the resolution of the whole detector area.</p>

Outputs
<ol style="list-style-type: none"> 1) Resolution matrix (image) 2) Percentage of overall non-uniformity 3) MTF value at a certain frequency. To be compared with section 16.16

Document Title	Document Number	Revision
Detector Imaging Testing – Work Instructions	DX-001818	A
This document is confidential and proprietary to PerkinElmer Medical Imaging		

16.14 Sensitivity

Data inputs and tools required

- 1) ImageJ software or Matlab.
- 2) Data set from section 12.5

Analysis method

All details are given in document DX-001538 Revision B

Outputs

- 1) Dose table
- 2) Table of the Mean pixel value (MPV) as a function of the dose
- 3) MPV vs. dose plot

Document Title	Document Number	Revision
Detector Imaging Testing – Work Instructions	DX-001818	A
This document is confidential and proprietary to PerkinElmer Medical Imaging		

16.15 Conversion Function

Data inputs and tools required

- 1) Data set from section 12.5

Analysis method

- 1) From the sensitivity curve, select a dose at mid-range and its correspondent signal.
- 2) Calculate the Incident X-rays multiplying the SNR_{IN2} value, 30174 photons/(uGy mm²) - given in the IEC-62220-1 International Standard, by the chosen dose in uGy and the square of the pixel size.
- 3) Calculate the number of electrons multiplying the number of counts given by the chosen dose by the gain (e-/counts).
- 4) Divide the number of electrons by the number of incident X-rays:

$$CF = \frac{Counts(D) * Gain(\frac{e^-}{counts})}{D * SNR_{IN}^2 * pp^2}$$

Outputs

- 1) Conversion function value

Document Title	Document Number	Revision
Detector Imaging Testing – Work Instructions	DX-001818	A
This document is confidential and proprietary to PerkinElmer Medical Imaging		

16.16 MTF

Data inputs and tools required

- 1) Matlab
- 2) Data set from section 12.5

Analysis method

All details are given in document DX-001538 Revision B

Outputs

- 1) Table of the MTF as a function of the spatial frequency at mid exposure
- 2) Plot of the MTF vs. the spatial frequency

NOTE: See Section 21.0, Appendix D – Artefact 5, for more information regarding interpreting the data collected and see examples where the MTF values showed problems in the detector.

Document Title	Document Number	Revision
Detector Imaging Testing – Work Instructions	DX-001818	A
This document is confidential and proprietary to PerkinElmer Medical Imaging		

16.17 NNPS

Data inputs and tools required
<ul style="list-style-type: none"> 1) Matlab 2) Data set from section 12.5
Analysis method
All details are given in document DX-001538 Revision B
Outputs
<ul style="list-style-type: none"> 1) Table of the NNPS values as a function of the spatial frequency at three exposure levels. <p>NOTE: See Section 21.0 Appendix D – Artefact 6, for more information regarding interpreting the data collected and see examples where the NNPS values showed problems in the detector.</p>

Document Title	Document Number	Revision
Detector Imaging Testing – Work Instructions	DX-001818	A
This document is confidential and proprietary to PerkinElmer Medical Imaging		

16.18 DQE

Data inputs and tools required

- 1) Analysed data from 13.14, 13.16 and 13.17
- 2) Data set from section 12.5

Analysis method

All details are given in document DX-001538 Revision B

Outputs

- 1) Table of the DQE as a function of the spatial frequency at three exposure levels
- 2) Plot of the DQEs vs. the spatial frequency

NOTE: See Section 21.0, Appendix D – Artefact 7, for more information regarding interpreting the data collected and see examples where the DQE values showed problems in the detector.

Document Title	Document Number	Revision
Detector Imaging Testing – Work Instructions	DX-001818	A
This document is confidential and proprietary to PerkinElmer Medical Imaging		

17.0 REVISION HISTORY

Note that the revision history is only used when the document is captured into document control. This is a requirement for formal verification against requirements. Informal verification may be versioned in a revision control system such as SharePoint.

Revision	Sections Changed	Originator	ECO No.	ECO Date
A	Creation	EMM & PM		

Document Title	Document Number	Revision
Detector Imaging Testing – Work Instructions	DX-001818	A
This document is confidential and proprietary to PerkinElmer Medical Imaging		

18.0 APPENDIX A – FORMAL ENGINEERING REQUEST FORM

All items are required to be filled in

Detector Type	
Detector Serial Number	
Requested by	
Firmware Version Numbers (DAQ, MUX, ADC, Sensor FPGAs etc.)	
If the detector has any specific reference voltage (e.g. reset voltage, etc), current source values or any other customised / customisable configuration (linearity correction, gain settings, etc), note it here or attach external configuration document to this request.	
Test temperatures required (tick as applicable – obviously not applicable for tests performed as a function of temperature)	<input type="checkbox"/> Room temperature <input type="checkbox"/> Minimum operating temperature <input type="checkbox"/> Maximum operating temperature
List of tests required (refer to test number)	
Signature of requester AND date	

Document Title	Document Number	Revision
Detector Imaging Testing – Work Instructions	DX-001818	A
This document is confidential and proprietary to PerkinElmer Medical Imaging		

19.0 APPENDIX B – GAIN AND OFFSET CORRECTIONS

To gain and offset correct the images apply the formula below:

$$Image_{Offset_Gain_corr} = (Image - Offset_{Avg}) \frac{(Flat_{Avg} - Offset_{Avg})}{(Flat_{Avg} - Offset_{Avg})}$$

Where,

$Image_{Offset_Gain_corr}$ is the gain and offset corrected image. It can be a flat or a phantom image.

$Image$ is the image to be corrected. It can be a flat or a phantom image.

$Offset_{Avg}$ is the offset image obtained by averaging a set of at least 20 images.

$Flat_{Avg}$ is the flat image obtained by averaging a set of at least 20 images.

$(Flat_{Avg} - Offset_{Avg})$ is the mean pixel value of the offset corrected flat.

- Use the same exposure time for the dark and gain reference image.
- The image to correct can be a flat image or a phantom image.
- The averaged flat used to correct the image can be acquired at the same exposure level (correction using a gain-map with the same exposure level) or at a different exposure level (correction using a gain-map with different exposure level).
- Correcting using a gain-map with different exposure level helps to highlight the presence of non-linearity in the images. The normal set up is to correct with a gain-map acquired at mid-exposures.

Document Title	Document Number	Revision
Detector Imaging Testing – Work Instructions	DX-001818	A
This document is confidential and proprietary to PerkinElmer Medical Imaging		

20.0 APPENDIX C– IMAGE AND IMAGE SEQUENCE FILE FORMATS, AND TEST DATA STORAGE LOCATION

To provide the ability for automated data collection and analysis in the future, data must be collected in a very specific place and stored in a very specific location.

20.1 Data format

NEEDS TO BE CLEARLY DEFINED TO BE BACKWARDS AND FORWARDS COMPATIBLE

<detector type>_<serial number><voltage>kV_<exposure time>ms_<current>mA_<intensity>int_<temperature>deg _<exposure level>ADU_Dark/Flat/Phantom.tiff

<detector type>_<serial number><voltage>kV_<exposure time>ms_<current>mA_<intensity>int_<temperature>deg _<exposure level>ADU_Dark/Flat/Phantom.smv

- 1) The name stated below includes all possible variations for every test. If the test do not use one specific parameter delete it and pass to the next one in the list, i.e. the names of optical tests do not need to specify voltage or current.
- 2) Select Dark, Flat or Phantom depending on the type of image acquired. If the image is a phantom, specify the type: Hand, Coin, Mesh, Edge...

Eg: 2321_00003_80ms_35deg_Flat.smv

20.2 Location

All data to be stored here:

\\\emealonf02\Project\<ProjectName>\<detector type>\<serial no>

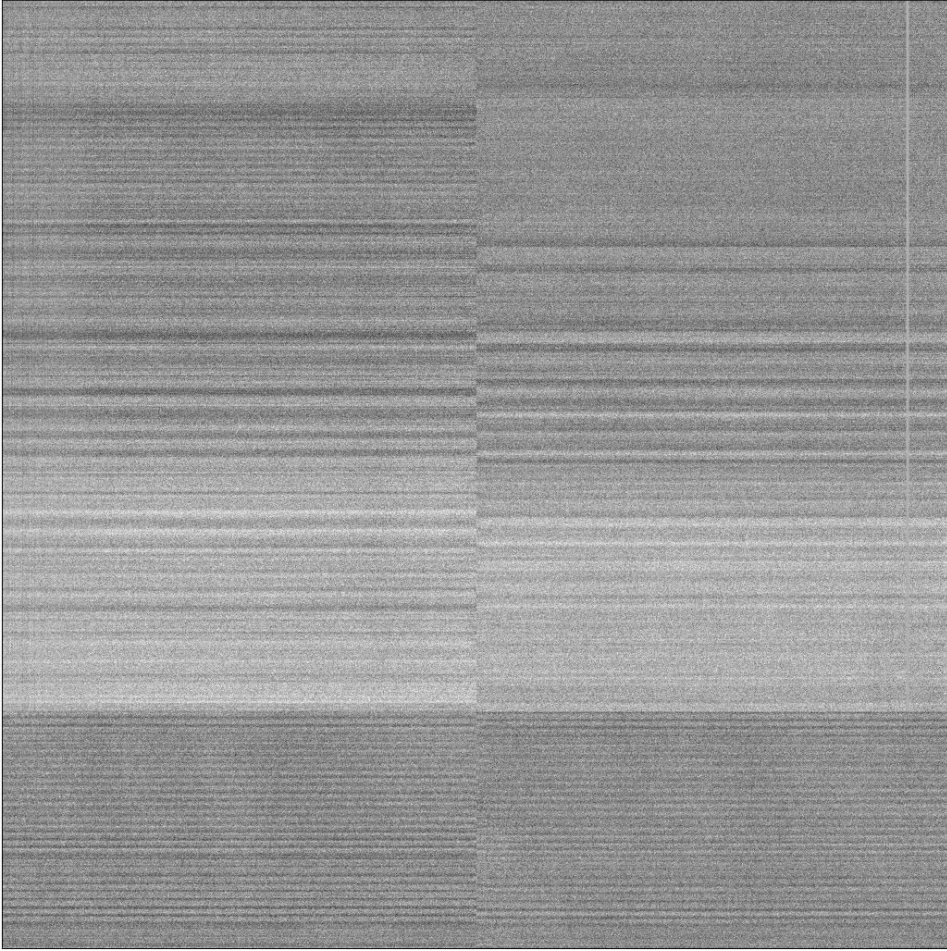
E.g: \\\EMEALONF02\Project\3030, 2020 ZIEHM IMAGE DATA\3030, UNIT IMAGE DATA\3030, UNIT1

Document Title	Document Number	Revision
Detector Imaging Testing – Work Instructions	DX-001818	A
This document is confidential and proprietary to PerkinElmer Medical Imaging		

21.0 APPENDIX D – REFERENCE IMAGES FOR IMAGE ARTEFACT ANALYSIS

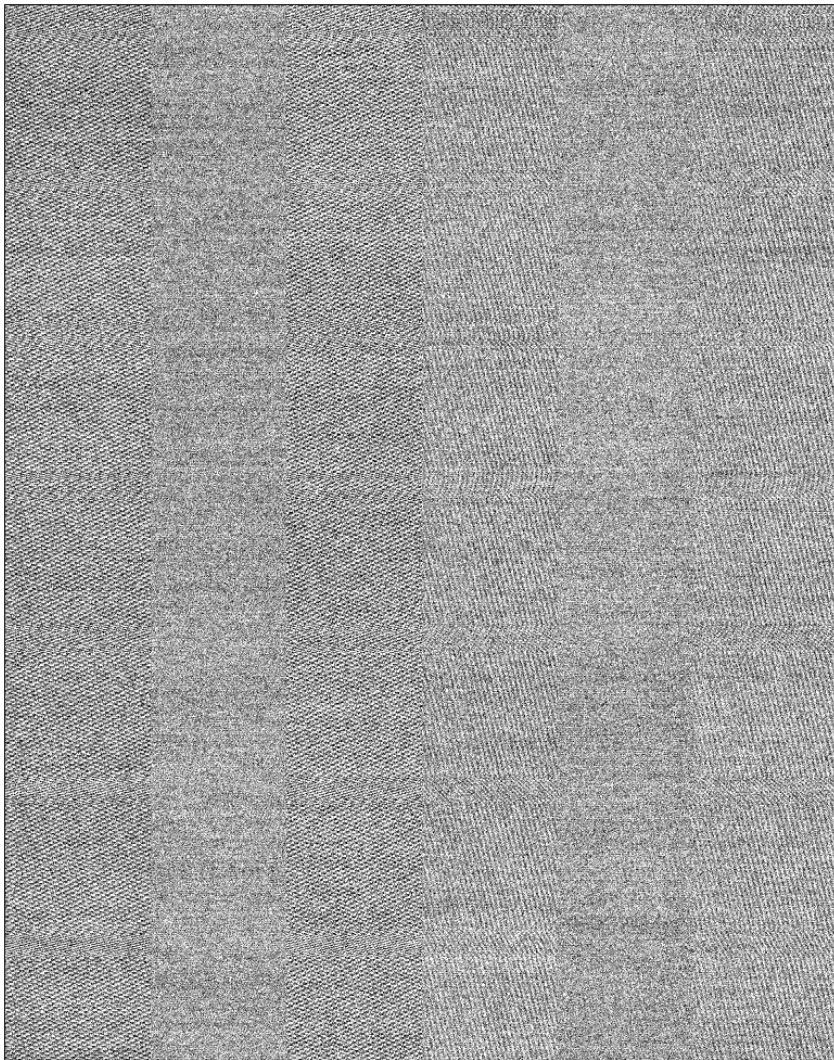
The purpose of this section is to illustrate how image artefacts have manifested themselves in the past and to provide techniques to identify them.

21.1 Artefact 1

Reference Test	16.3 – Static Noise
Description	Non-flatness of the static noise image, i.e. row noise, noise frequency variations...
Consequences	If the noise has high variations it can lead to clipping in the NNPS
Example 1: Row noise	 <p>Note: The row noise can be quantified by comparing row and columns standard deviation, as explained in Section 16.3. If there is row noise, as the one shown above, the StDrow will be higher than the StDcols.</p>

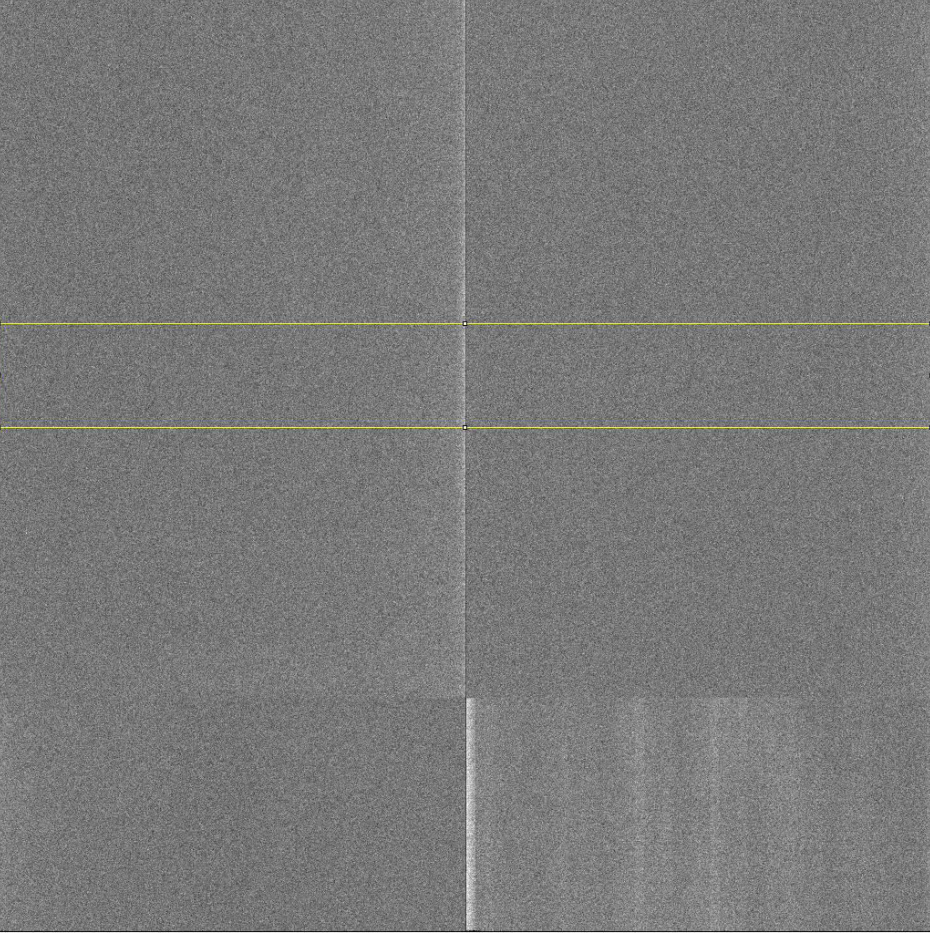
Document Title	Document Number	Revision
Detector Imaging Testing – Work Instructions	DX-001818	A
This document is confidential and proprietary to PerkinElmer Medical Imaging		

Example 2:
Clipping and high
frequency noise

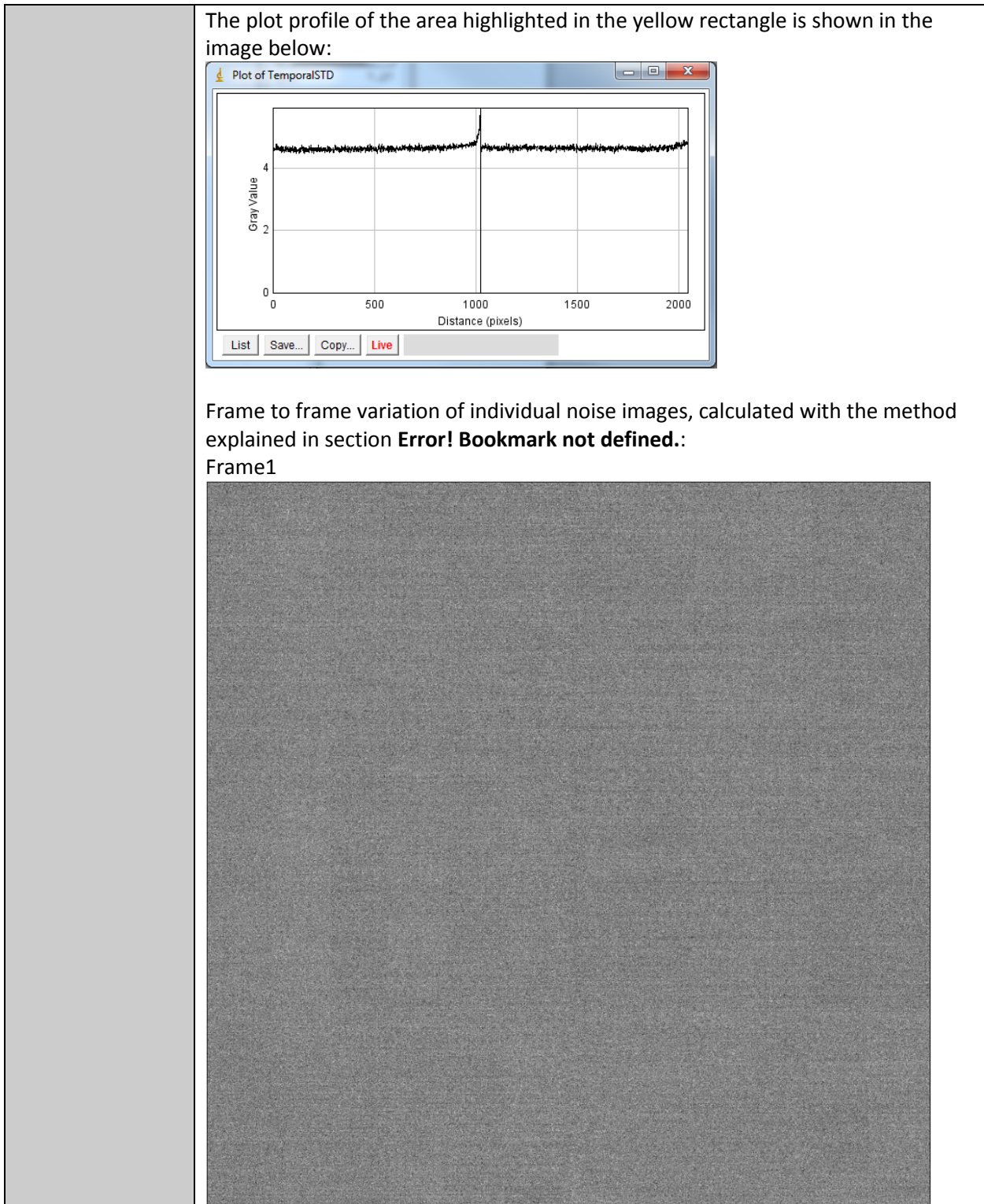


Document Title	Document Number	Revision
Detector Imaging Testing – Work Instructions	DX-001818	A
This document is confidential and proprietary to PerkinElmer Medical Imaging		

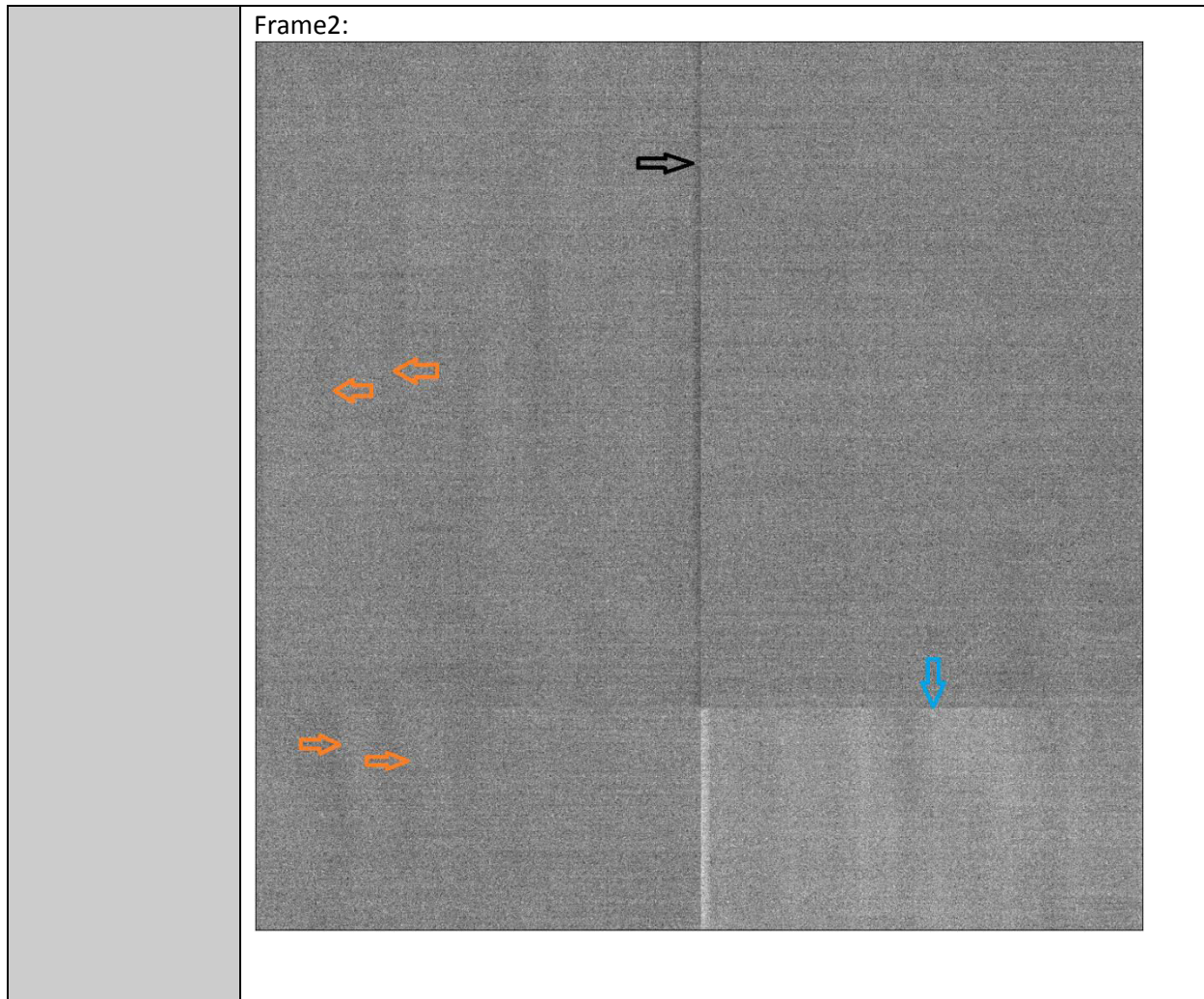
21.2 Artefact 2

Reference Test	16.4 – Temporal Noise
Description	<ul style="list-style-type: none"> - Any variations in the temporal noise image indicates an unusual change in the pixel between different frames, it is an indication of the “flickering” effect. - If the noise determined using the static noise and the temporal noise methods differ significantly, this may indicate flicker or other frame to frame variations. <p>NOTE: If the effect needs to be quantified, the images to be analysed are the 19 noise images obtained in section 13.3. The temporal noise image will not be entirely accurate: if the flicker increases and decreases in respect to the mean value, the standard deviation will be reduced as a consequence of this variation.</p>
Consequences	Variations between frames due to the “flickering effect” might affect the gain and offset corrections.
Example 1:	<p>Temporal noise image:</p> 

Document Title	Document Number	Revision
Detector Imaging Testing – Work Instructions	DX-001818	A
This document is confidential and proprietary to PerkinElmer Medical Imaging		

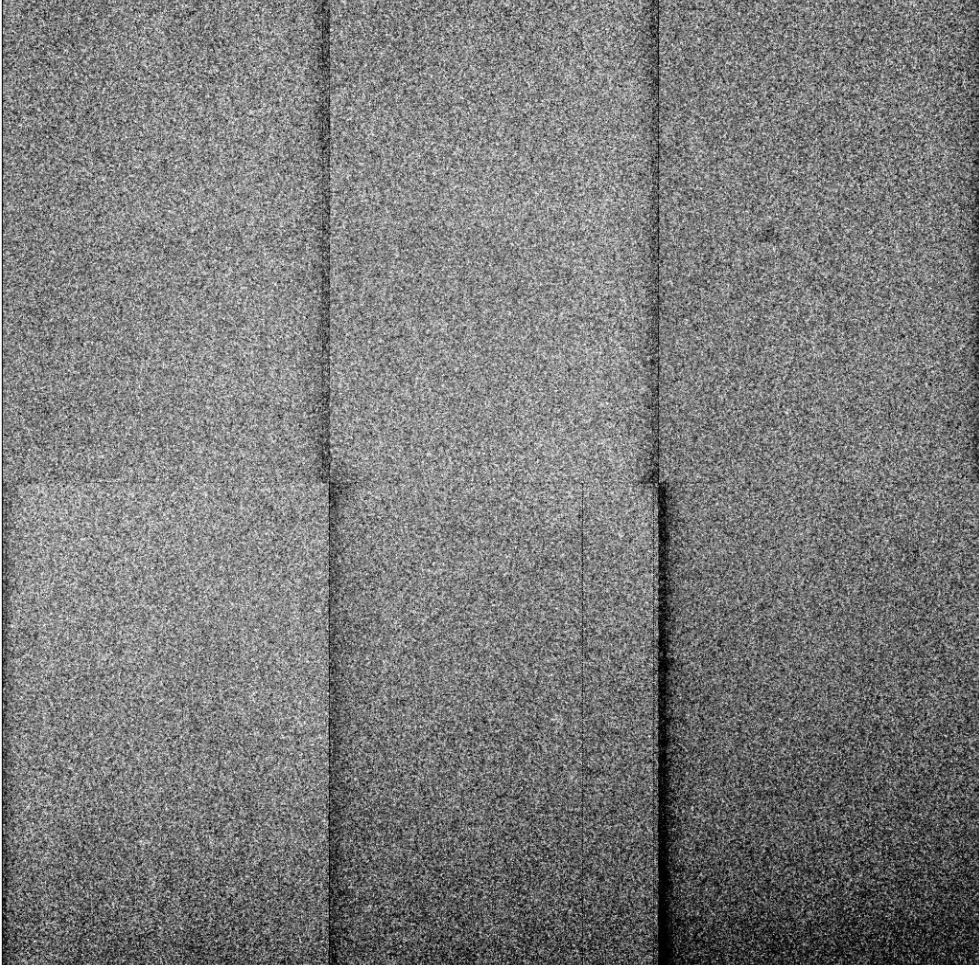


Document Title	Document Number	Revision
Detector Imaging Testing – Work Instructions	DX-001818	A
This document is confidential and proprietary to PerkinElmer Medical Imaging		



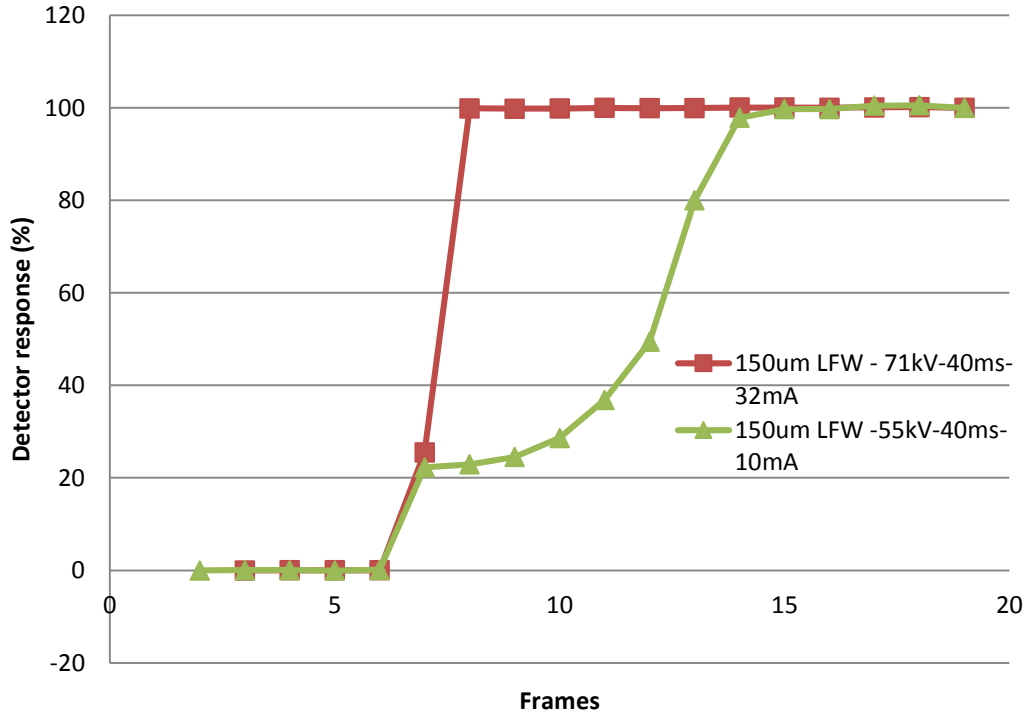
Document Title	Document Number	Revision
Detector Imaging Testing – Work Instructions	DX-001818	A
This document is confidential and proprietary to PerkinElmer Medical Imaging		

21.3 Artefact 3

Reference Test	Section 16.5 – Linearity – Quick linearity check		
Description	Detector non-linearity can be easily spotted when a set of images are averaged and corrected with a gain-map from a different intensity level.		
Consequences	Non-linearity can affect the gain corrected images showing artefacts in the image, affecting the quality of the image.		
Example: Non-linearity – quick linearity check section			

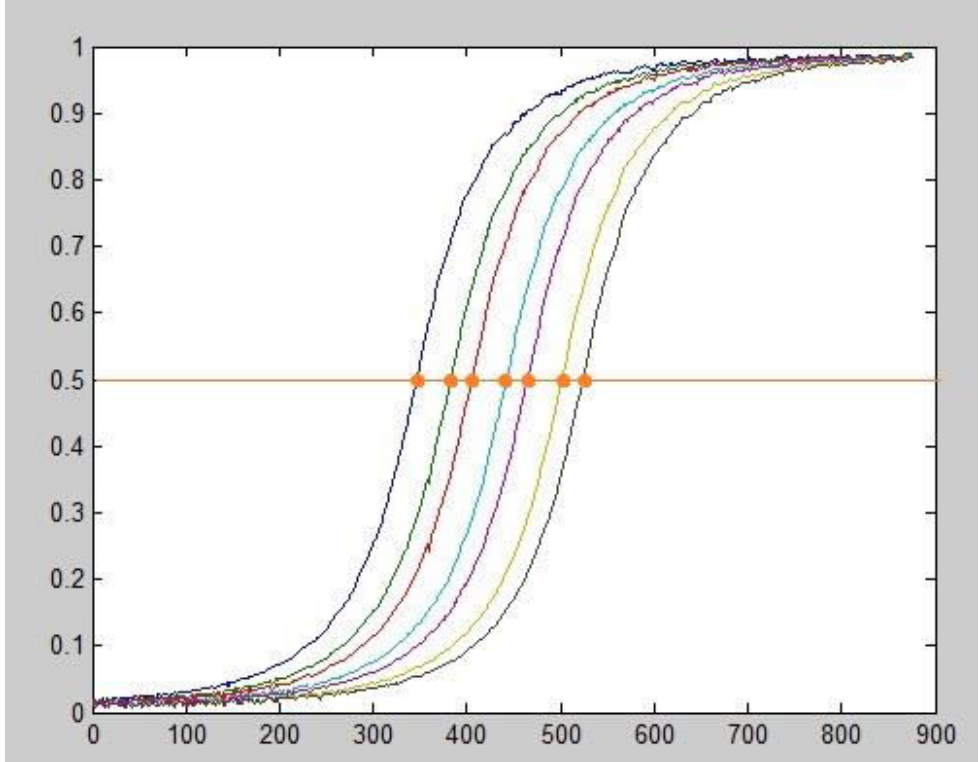
Document Title	Document Number	Revision
Detector Imaging Testing – Work Instructions	DX-001818	A
This document is confidential and proprietary to PerkinElmer Medical Imaging		

21.4 Artefact 4

Reference Test	Section 16.6 and 16.8 – Image lag																																	
Description	<p>Image lag appears when there is delay between the detector response and an input signal, when the signal passes from dark to bright.</p> <p>There is an expected transition of one or two frames when changing from dark to bright, higher values than that will affect the performance of the detector.</p> <p>Pay special attention to lag variation with exposure.</p>																																	
Consequences	<p>Lag can decrease the value of the normalised noise power spectrum (NNPS) leading to unusually large values (sometimes higher than one) of the detective quantum efficiency (DQE).</p>																																	
Example: Lag variation with exposure	 <p>The graph illustrates the detector response (%) over 20 frames for two different exposure settings. The red curve, representing 71kV-40ms at 32mA, shows a sharp rise from frame 6 to 100% response at frame 7. The green curve, representing 55kV-40ms at 10mA, shows a more gradual rise from frame 6 to 100% response at frame 14. Both curves remain at 100% response for the remainder of the frames.</p> <table border="1"> <caption>Estimated data points from the graph</caption> <thead> <tr> <th>Frames</th> <th>150um LFW - 71kV-40ms (32mA) (%)</th> <th>150um LFW - 55kV-40ms (10mA) (%)</th> </tr> </thead> <tbody> <tr><td>0-6</td><td>0</td><td>0</td></tr> <tr><td>7</td><td>100</td><td>25</td></tr> <tr><td>8</td><td>100</td><td>25</td></tr> <tr><td>9</td><td>100</td><td>25</td></tr> <tr><td>10</td><td>100</td><td>30</td></tr> <tr><td>11</td><td>100</td><td>50</td></tr> <tr><td>12</td><td>100</td><td>80</td></tr> <tr><td>13</td><td>100</td><td>100</td></tr> <tr><td>14</td><td>100</td><td>100</td></tr> <tr><td>15-20</td><td>100</td><td>100</td></tr> </tbody> </table> <p>The green curve on the graph above shows an image lag problem (or sensor response problem). For a constant input the detector takes 9 frames to return the 100% of the expected response.</p> <p>The graph also shows how this effect changes with the exposure, when the response delay is reduced to 1 frame at exposures higher to saturation (red curve).</p>	Frames	150um LFW - 71kV-40ms (32mA) (%)	150um LFW - 55kV-40ms (10mA) (%)	0-6	0	0	7	100	25	8	100	25	9	100	25	10	100	30	11	100	50	12	100	80	13	100	100	14	100	100	15-20	100	100
Frames	150um LFW - 71kV-40ms (32mA) (%)	150um LFW - 55kV-40ms (10mA) (%)																																
0-6	0	0																																
7	100	25																																
8	100	25																																
9	100	25																																
10	100	30																																
11	100	50																																
12	100	80																																
13	100	100																																
14	100	100																																
15-20	100	100																																

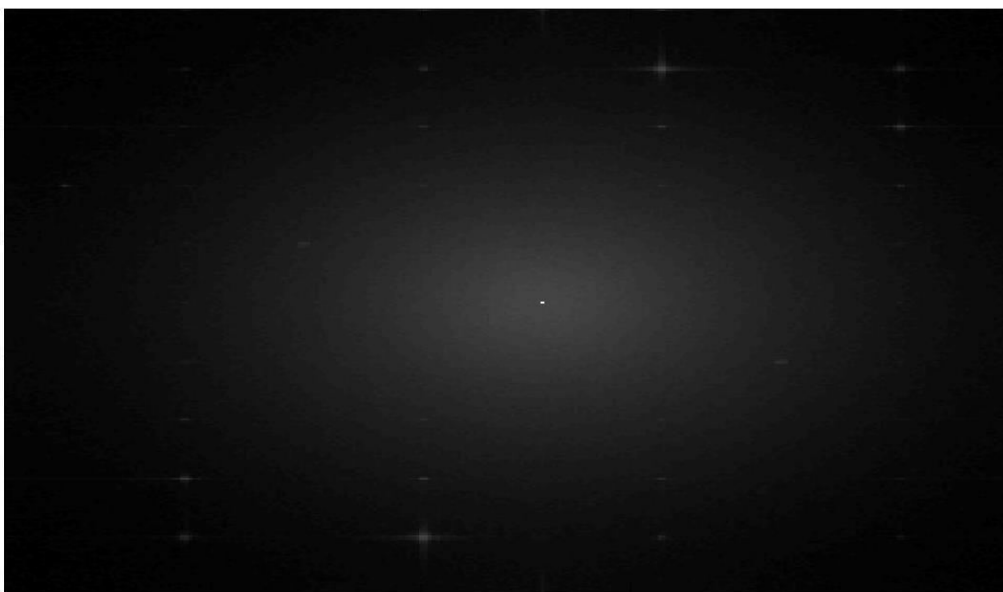
Document Title	Document Number	Revision
Detector Imaging Testing – Work Instructions	DX-001818	A
This document is confidential and proprietary to PerkinElmer Medical Imaging		

21.5 Artefact 5

Reference Test	Section 16.16 - MTF
Description	<ul style="list-style-type: none"> 1) A non-uniform MTF curve 2) Non-uniform edge spread function (ESF) or a function with a wide slope. 3) Pairing of the ESF curves is caused by pixel crosstalk (see example below).
Consequences	<ul style="list-style-type: none"> 1) The DQE is proportional to the square of the MTF. This means that small changes in the MTF uniformity will highly affect the DQE. 2) A non-smooth ESF might indicate that the detector is noisier than it should be. If the function is too wide it will present a drop in the resolution. Both cases will lead to a drop in the expected MTF values. 3) The “pairing” can affect the MTF calculation if it is not taken into account when the ESF samples are shifted and averaged.
Example: ESF “Pairing”	<p>The ESF is the intensity profile of one column across the tilted edge device. For statistical reasons, the ESF that is used in the MTF calculation is the average of 7 consecutive ESF (7 consecutive columns). To calculate the average, the functions must be overlapping so they are shifted a certain amount. The “pairing” means that the distances between 3 consecutive ESF are different. If this is not taken into account in the shifting step, the functions will not be overlapping and it will affect the averaged ESF and therefore the MTF.</p> 

Document Title	Document Number	Revision
Detector Imaging Testing – Work Instructions	DX-001818	A
This document is confidential and proprietary to PerkinElmer Medical Imaging		

21.6 Artefact 6

Reference Test	Section 16.17 - NNPS
Description	<ul style="list-style-type: none"> 1) Non-smooth 2D NNPS. 2) NNPS changes between operation modes when the MTF and the exposure are constant.
Consequences	<ul style="list-style-type: none"> 1) Any feature in the 2D NNPS plot will indicate problems in the detector (see example below). If spotted, start investigating the noise image. 2) This effect it can be related with image lag and will affect the DQE result.
Example: Clipping in the 2D NNPS	

21.7 Artefact 7

Reference Test	Section 16.18 - DQE
Description	The DQE is a very sensitive measurement, any problem in the MTF, NNPS or exposure measurements will affect the DQE, sometimes giving values even higher than 1. This measurement can be used as a red flag.

Document Title	Document Number	Revision
Conversion Function, Modulation Transfer Function and Detective Quantum Efficiency Measurements and Analysis	DX-001538	B
This document is confidential and proprietary to PerkinElmer		

APPENDIX C

1.0 PURPOSE

This procedure outlines the experimental method and analysis that has to be followed to perform Conversion Function (CF), Modulation Transfer Function (MTF) and Detective Quantum Efficiency (DQE) measurements complying with the IEC 62220-1 International Standard at PerkinElmer Medical Imaging (London).

2.0 SCOPE

This document applies to all personnel of PerkinElmer MI London, who intend to perform complete Conversion Function, Modulation Transfer Function and Detective Quantum Efficiency measurements on production detector models or on detector models which are intended to be transferred to production.

3.0 REFERENCE DOCUMENTS

International Standard: IEC 62220-1: Medical electrical equipment – Characteristics of digital X-ray imaging devices – Part1: Determination of the detective quantum efficiency.

International Standard: IEC 62220-1-2: Medical electrical equipment – Characteristics of digital X-ray imaging devices – Part 1-2: Determination of the detective quantum efficiency – Detectors used in mammography.

4.0 DEFINITIONS

Define uncommon words, terms and/or acronyms used within the document.

CF	Conversion Function: The CF is a function that gives the response of the detector to the input signal by relating the measured exposure in pixel value to the exposure value.
MTF	Modulation Transfer Function: The MTF quantifies the spatial resolution of the detector. The values of the MTF are between 0 and 1, where 1 means a complete transmission of the contrast of the object over the image and 0 means no transmission of the contrast.
NNPS	Normalized Noise Power Spectrum: The NPS quantifies the spectral decomposition of the noise variance within an image as a function of the spatial frequency, so it can be used to compare the noise properties of different systems.
DQE	Detective Quantum Efficiency: The parameter DQE describes the ability that an imaging system has to capture information over a range of spatial frequencies. It expresses the efficiency with which the detector uses the input signal (incident photons) to form the image
RQA5	Radiation Quality specified in IEC 62220-1
RQAM	Radiation Quality for Mammography specified in IEC 62220-1-2

Document Title	Document Number	Revision
Conversion Function, Modulation Transfer Function and Detective Quantum Efficiency Measurements and Analysis	DX-001538	B
This document is confidential and proprietary to PerkinElmer		

5.0 RESPONSIBILITY

Department	Responsibility
Operations	Operations Manager (OM) is responsible for following this procedure with regards to performing complete CF, MTF and DQE tests within Operations for the manufacture and supply of Dexela products.
Engineering	Engineering Manager (EM) is responsible for following, updating and revising this procedure with regards to performing complete CF, MTF and DQE tests within Engineering for the design and development of Dexela products.

6.0 SAFETY REQUIREMENTS

Only trained personnel following X-ray safety procedures should perform this procedure.

7.0 MATERIALS AND EQUIPMENT

X-ray tube:

Philips – 2.5mmAl (inherent filtration) - RQA5

Varian – 50µm Rh (inherent filtration) - RQAM

Varian tube Collimator

Aluminium Filters of different thicknesses (from 0.2mm up to 20mm)

Edge Test Device complying with the IEC 62220-1 Standard

Acquisition tool software – SCap

RTI Piranha Radiation Meter

8.0 MEASUREMENTS PROCEDURE

8.1 The use of monitoring and measuring devices is described in Quality Manual to ensure compliance with requirements. Equipment is handled, preserved and stored in a manner that protects its accuracy and fitness for use. If precautions in addition to standard plant practice and standard plant conditions are required, they are outlined in the equipment manual, the calibration or maintenance work instructions or related measuring and monitoring work instructions.

8.2 Measurements for CF, MTF and DQE calculations:

The following procedure shall be followed when accurate CF, MTF or DQE curves are required for either RQA5 or RQAM:

Document Title	Document Number	Revision
Conversion Function, Modulation Transfer Function and Detective Quantum Efficiency Measurements and Analysis	DX-001538	B
This document is confidential and proprietary to PerkinElmer		

Geometry:

Set-up for MTF measurements: The geometry is shown in Figure 1. A collimator has to be placed close to the X-ray tube (Note that in the case of the Philips X-ray tube the collimator is already attached below the X-ray tube) followed by an additional Aluminium Filter (see Radiation Quality specifications in Table 2). The detector has to be aligned with the central axis of the X-ray beam and located at a specific Source-to-Image-Distance (SID) defined in Table 1.

The Edge Test Device has to be placed on top of the detector, aligned vertically (or horizontally) with the X-ray Beam and tilted an angle between 1.5° to 3° (see Figure 2).

If the collimator allows it, i.e. Philips X-ray tube collimator, adjust the irradiated area to the size of the detector surface¹.

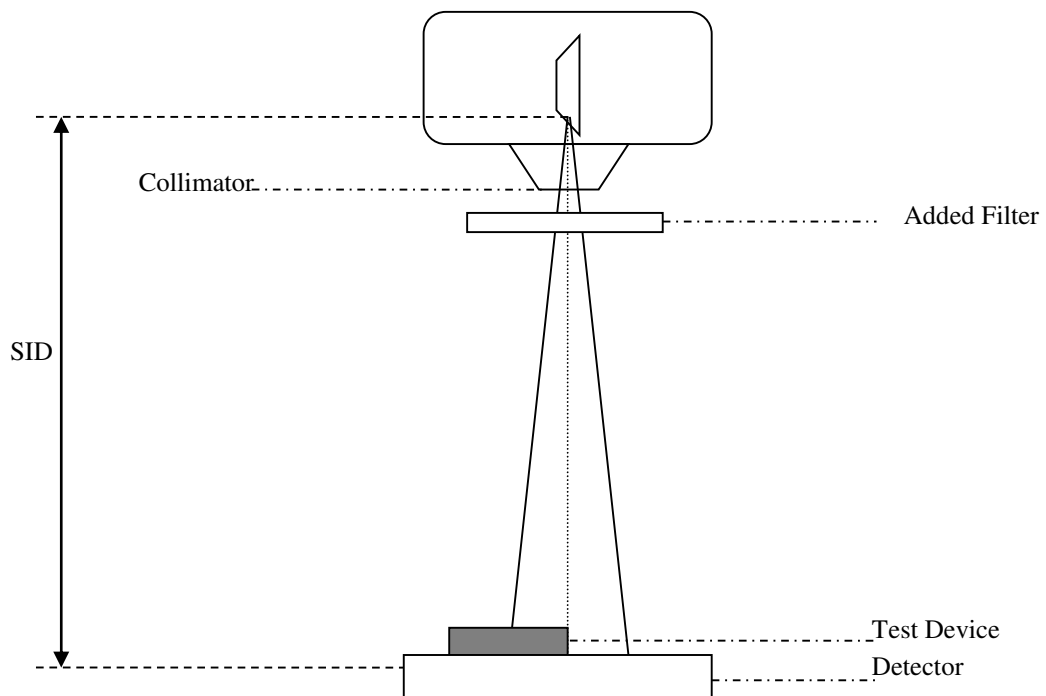


FIGURE 1: SCHEME OF THE GEOMETRY FOR MTF MEASUREMENTS

¹ The International Standard IEC 62220-1 states that the irradiated area has to be collimated to 160 mm x 160 mm for CF measurements and 125 mm x 125 mm for NNPS measurements. However, due to the detector size being sometimes smaller than 160cm and the impossibility to manipulate the collimator in the Varian X-ray tube the irradiated area has been taken equal to the detector surface.

Document Title	Document Number	Revision
Conversion Function, Modulation Transfer Function and Detective Quantum Efficiency Measurements and Analysis	DX-001538	B
This document is confidential and proprietary to PerkinElmer		

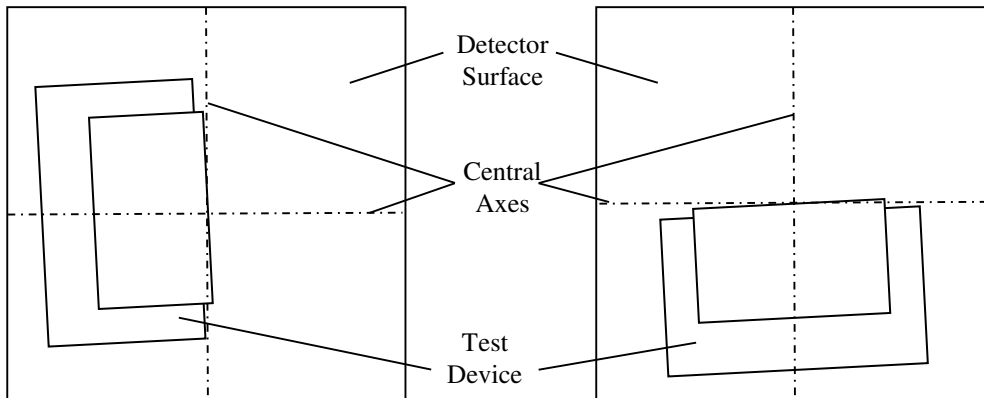


FIGURE 2: TOP VIEW OF THE DETECTOR WITH EDGE TEST DEVICE. THE LEFT IMAGE SHOWS THE VERTICAL POSITION AND THE RIGHT ONE THE HORIZONTAL POSITION.

Set up for CF and NNPS measurements: The geometry has to be kept the same as the one explained in the Set up for MTF Measurements (Figure 1) but the Edge Test Device has to be removed from the detector.

Set up for Dose measurements: the Edge Test Device and the Detector have to be removed from the Set up for MTF Measurements and the RTI Pirahna radiation meter has to be placed in the position of the detector, properly aligned with the X-ray beam. Re-adjust the distance to keep a constant SID.

SID Distances:

TABLE 1: SOURCE-TO-IMAGE-DISTANCE FOR DIFFERENT RADIATION QUALITIES

SID (RQA5) > 1.5 m
0.6 m < SID (RQAM) < 0.7 m

Radiation Quality Settings:

TABLE 2: RADIATION QUALITIES SETTINGS

Radiation Quality	Nominal X-ray tube Voltage (kV)	Nominal Half-Value Layer (mmAl)	Added Filter (mmAl)
RQAM – Varian X-ray tube (W/0.05mm Rh)	28	0.75	2.0
RQA5 – Philips X-ray tube	70	7.1	21.0

The Nominal X-ray tube Voltage, the Added Filter and the SID can be slightly modified in order to comply with the Nominal Half-Value Layer. However, once the values have been selected they will have to be kept constant during the rest of the experiment.

Document Title	Document Number	Revision
Conversion Function, Modulation Transfer Function and Detective Quantum Efficiency Measurements and Analysis	DX-001538	B
This document is confidential and proprietary to PerkinElmer		

Nominal Half-Value Layer calculation and Settings:

- 1- Place the RTI Piranha radiation meter in the Detector position (Dose measurements).
- 2- Keep the voltage specified in Table 2 and select an arbitrary current and exposure time values, i.e. 32mA and 200ms. The added filtration should be the one specified in Table 2.
- 3- Irradiate the radiation meter and obtain a reading of the dose (See Appendix 1). Repeat 5 to 10 times and average to obtain D_0 .
- 4- Increase the added filtration a quantity equal to the Nominal Half-Value Layer specified in Table 2. Repeat step 2 to obtain D_{HVL} .
- 5- If $D_{HVL} = D_0 / 2$ (with a relative difference lower than 5%) keep the values of the voltage and the added filter. Otherwise, modify the SID, the Voltage or the Added filtration and repeat steps 3 to 5.

IMPORTANT! Once the thickness of the added filtration has been selected and the filter has been placed in its appropriate position (see Figure 1) it should not be moved between sets of images with same current. If moved between the flat set of images and the edge set the measurements will have to be repeated. Otherwise the gain correction of the images will be affected and so will be the MTF and DQE results. The same applies to the detector, it should not be moved.

CF, MTF and NNPS Measurements:

- 1- Set up the geometry for CF and DQE measurements keeping the parameters chosen in the Radiation Quality Settings. Choose a current of 100mA.
- 2- Open SCap and find which exposure time gives an ADU value of approximately 90% of saturation (around 14700 ADU), ensuring that there are no areas saturated in the image. The current can be increased to 125mA or decreased to 80mA if necessary. Once selected the exposure time the value will be kept constant during the rest of the experiment.

Note 1: Make sure that SCap does not have the defect, gain and offset corrections selected.

Note 2: The NNPS will be calculated at 3 dose levels. The highest dose level will correspond to the maximum current, the middle dose level to the current obtained dividing the maximum current by 2 for RQAM and by 3.2 for RQA5 and the lowest dose level to the current obtained dividing a second time by the same quantity:

- a) For a maximum current of 100mA the NNPS current levels will be:
 RQAM: 100mA, 50mA and 25mA.
 RQA5: 100mA, 32mA and 10mA.
- b) For a maximum current of 125mA the MTF current level will be:
 RQAM: 125mA, 63mA and 32mA.
 RQA5: 125mA, 40mA and 12mA.
- c) For a maximum current of 80mA the MTF current level will be:
 RQAM: 80mA, 40mA and 20mA.
 RQA5: 80mA, 32mA and 10mA².

² The Philips tube in Radiography Mode cannot be reduced to a current lower than 10mA so the dose values do not follow the standard progression of dividing by 3.2.

Document Title	Document Number	Revision
Conversion Function, Modulation Transfer Function and Detective Quantum Efficiency Measurements and Analysis	DX-001538	B
This document is confidential and proprietary to PerkinElmer		

Note 3: The MTF dose level (called Normal Exposure Level) will correspond to the middle NNPS dose level.

- 3- Reduce the current to the minimum value (see Appendix 2).
- 4- Irradiate the detector and grab a flat image. Make sure that the exposure time selected in the X-ray tube is longer than the one selected in SCap and start to irradiate before 'snap' has been clicked.
- 5- Save the image in 16-bit TIFF format under the name: VkV_Etms_CmA_01.tif, where V is the selected Voltage, Et the selected Exposure time and C the selected Current, i.e. 71kV_200ms_10mA_01.tif.
- 6- Repeat step 4 and save the image increment the final number in the filename, i.e. 71kV_200ms_10mA_02.tif. Repeat until number 20 is reached, i.e. 71kV_200ms_10mA_20.tif.

Note: It is also possible to acquire the images in a set of 20. If this is the case, they have to be saved in .smv format (since it can store multiple images in a single file) and saved under the name: 71kV_200ms_10mA_.smv. Bear in mind that the temperature of the X-ray tube will increase quickly, so it will be necessary to wait a period of time long enough to allow the system to cool down.

- 7- Obtain a set of 20 Dark images and save them in .smv format, under the name: VkV_Etms_CmA_Dark_.smv.

Note: Ensure that the correct Exposure time and quantity are set in the SCap dialog box.

- 8- Repeat steps 4 to 7 increasing the current steps (see Appendix 2). Stop after obtaining the set that corresponds to the Normal Exposure Level.
- 9- Place the Edge Test Device (set up for MTF measurements, see Figure 1) aligned with the X-ray beam in the vertical position (see Figure 2).
- 10- Keeping the current at the Normal Exposure level, irradiate the detector and grab an edge image. Save the image with 16bit .tif format with the name: VkV_Etms_CmA_EdgeVert_01.tif.
- 11- Repeat step10 and save the image increasing the last number in the name, i.e. 71kV_200ms_10mA_EdgeVert_02.tif. Repeat until number 20 is reached, i.e. 71kV_200ms_10mA_EdgeVert_20.tif.
- 12- Place the Edge Test Device aligned with the X-ray beam in the horizontal position (see Figure 2) and repeat steps 10 and 11 changing the word EdgeVert for EdgeHor in the names.
- 13- Remove the Edge Test Device and repeat steps 4 to 7 for the rest of the current steps, see Appendix 2.

Document Title	Document Number	Revision
Conversion Function, Modulation Transfer Function and Detective Quantum Efficiency Measurements and Analysis	DX-001538	B
This document is confidential and proprietary to PerkinElmer		

Exposure Measurements:

- 1- Remove the detector. Place the RTI Piranha radiation meter in the place of the detector, keeping the SID constant and aligning with the X-ray beam. (Dose measurements).
- 2- Keep the settings chosen in the CF, MTF and NNPS Measurements, choosing the first current step, i.e. the minimum current.
- 3- Irradiate the radiation meter and obtain a reading of the dose (See Appendix 1). Repeat 5 to 10 times and average.
- 4- Increase the current one step and repeat Step3.
- 5- Repeat for all currents (see Appendix 2).

9.0 ANALYSIS PROCEDURE

9.1 Gain and Offset corrections

1. Gain and Offset corrected Flat Images

The following formula corrects individual flat images:

$$Flat_{Offset\ and\ Gain\ corrected} = (Flat(x, y) - \overline{Dark(x, y)}) * \frac{(\overline{Flat(x, y)} - \overline{Dark(x, y)})}{(\overline{Flat(x, y)} - \overline{Dark(x, y)})}$$

2. Gain and Offset corrected Edge Images

The following formula corrects an average of edge images:

$$Edge_{Offset\ and\ Gain\ corrected} = (Edge(x, y) - \overline{Dark(x, y)}) * \frac{(\overline{Flat(x, y)} - \overline{Dark(x, y)})}{(\overline{Flat(x, y)} - \overline{Dark(x, y)})}$$

Where,

$Flat(x, y)$ = the individual flat image to be corrected.

$\overline{Edge(x, y)}$ = the average of the 20 edge images to be corrected.

$\overline{Dark(x, y)}$ = Matrix resulting from the average of the 20 Dark images

$\overline{Flat(x, y)}$ = Matrix resulting from the average of the 20 Flat/Flood images

$(\overline{Flat(x, y)} - \overline{Dark(x, y)})$ = Mean pixel value of the matrix $(\overline{Flat(x, y)} - \overline{Dark(x, y)})$

9.2 Conversion Function Curve

1. For each of the twenty offset and gain corrected flat images, obtained at the first exposure level, calculate the mean pixel value of a 100x100 centred area of the image, i.e. for a MxN image select the area (M/2-50, N/2-50, 100, 100).
2. Average the 20 mean pixel values to obtain MeanPixelValue(Exposure1).
3. Repeat for all exposure steps.
4. Plot the mean pixel values versus their correspondent exposures.

9.3 Modulation Transfer Function Curve

1. Read the offset and gain corrected vertical edge image.
2. Crop the image around the edge area and rotate the angle until it is in the same position than Figure 3.
3. Calculate the slope of the edge.
4. Find the position in the x axis of the column that splits the edge in two halves (see Figure 3).

Document Title	Document Number	Revision
Conversion Function, Modulation Transfer Function and Detective Quantum Efficiency Measurements and Analysis	DX-001538	B
This document is confidential and proprietary to PerkinElmer		

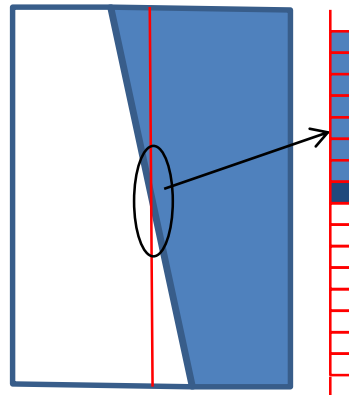


FIGURE 3: EDGE IMAGE ONCE CROPPED AND ROTATED WITH CENTRAL COLUMN HIGHLIGHTED.

5. Get the values of that column and of three previous and posterior columns.
6. Plot the intensity values (pixel value) vs. the correspondent pixel to get 7 samples of the Edge Spread Function (ESF), see Figure 4.
7. Taking the first line as reference, shift the other lines so they end up superimposed. Average the columns to get the ESF, see Figure 4.

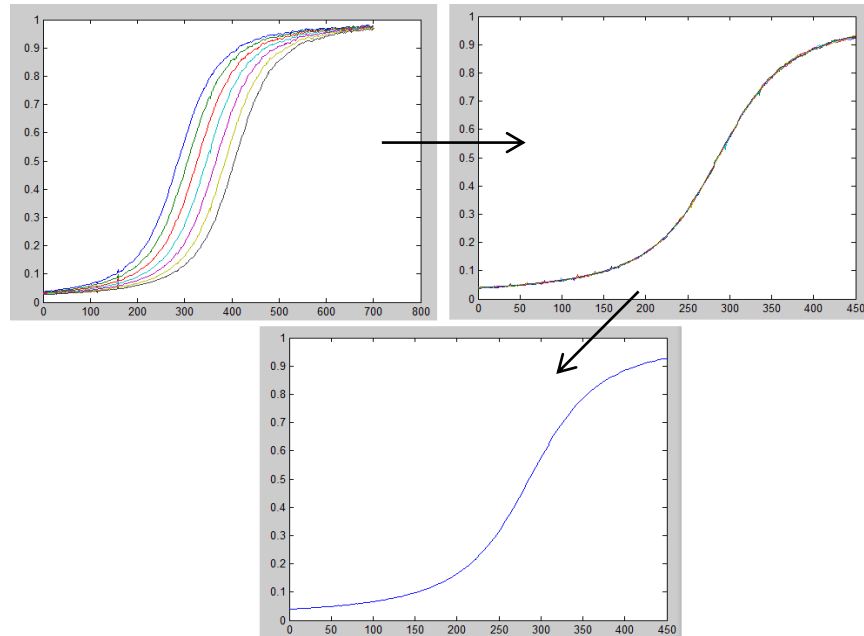


FIGURE 4: THE FIGURE SHOWS ON THE TOP LEFT, AN EXAMPLE OF THE 7 SAMPLES OF THE ESF; ON TOP RIGHT, THE 7 SAMPLES SUPERIMPOSED; ON THE BOTTOM, THE AVERAGED ESF.

8. Obtain the Line Spread Function (LSF) convolving the ESF with a kernel $\left[1, 1, 1, 1, 1, 1, 1\right]$.
9. For better MTF sampling, increase the LSF function by adding 9 times its size of zeros at both ends.
10. Obtain the MTF performing a Fast Fourier Transform of the LSF vector, reorganise the data in a way that the zero frequency component is in the centre of the function and get the absolute values.
- 11.

Document Title	Document Number	Revision
Conversion Function, Modulation Transfer Function and Detective Quantum Efficiency Measurements and Analysis	DX-001538	B
This document is confidential and proprietary to PerkinElmer		

- i. Normalise the MTF function and situate the unit value in the origin of the X-axis.
- ii. Take the positive values of the MTF function.
- iii. To get the right units (spatial frequency) in the x-axis divide by the absolute value of the slope of the edge, by the pixel pitch and the size of the MTF vector.
12. Obtain the MTF values up to the Nyquist frequency (inverse of twice the pixel pitch) in steps of 0.5lp/mm.
13. Plot the MTF values versus its correspondent spatial frequency.
14. Repeat 1 to 13 with the corrected horizontal edge image.
15. Average the Horizontal and Vertical MTF.
- 9.4 Normalised Noise Power Spectrum Curve
1. Select three exposure levels covering approximately the whole dynamic range.
 2. For one of the levels get the 20 gain and offset corrected flat images.
 3. Select the first image and select a central area of at least 512x512 pixel size. The area has to be a multiple of 128.
 4. Starting from the top left corner of that area, select a Region of Interest, ROI, of 256x256 pixel size, Figure 5-A.
 5. Select a second ROI of the same size moving the area 128pixels to the right, i.e. overlapping the first ROI by an area of 128x256, Figure 5-B.
 6. Repeat step 5 until the whole row is completed, Figure 5-C.

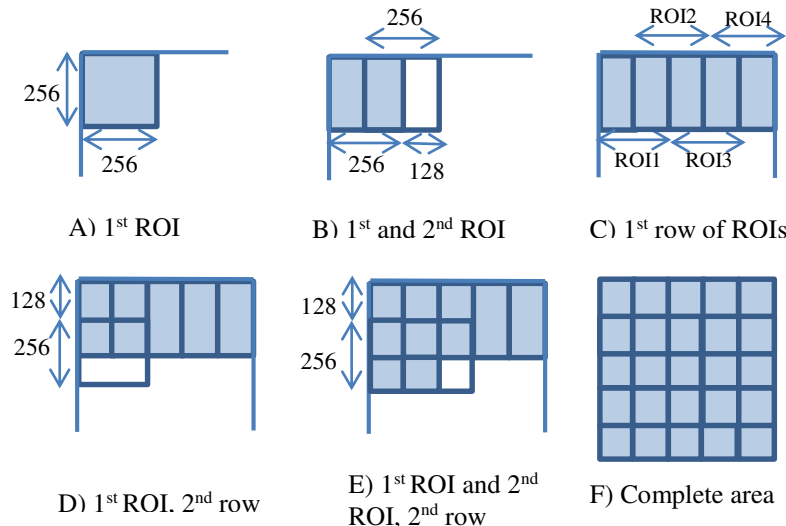


FIGURE 5: ROI SELECTION PROCESS FOR A SELECTED AREA OF 640X640 PIXELS.

7. From the first ROI, select another ROI of the same size moving the area 128pixels down, i.e. overlapping the first ROI by an area of 256x128, Figure 5-D.
8. For this new row, repeat steps 5 and 6 until row is complete, Figure 5-E.
9. Repeat steps 7 and 8 until all the rows are covered, Figure 5-F.
10. For every ROI:
 - Calculate the mean pixel value.

Document Title	Document Number	Revision
Conversion Function, Modulation Transfer Function and Detective Quantum Efficiency Measurements and Analysis	DX-001538	B
This document is confidential and proprietary to PerkinElmer		

- ii. Calculate the 2D Fast Fourier Transform, reorganise the data in a way that the zero frequency component is in the centre of the function and get the square of the absolute values, FFT^2 .
- 11. Average the results from steps 10.i. and 10.ii. for all the ROIs.
- 12. Repeat steps 3 to 11 with the left 19 frames.
- 13. Average the results from step 11 for all the frames obtaining the mean pixel value (MPV) and the 2D Noise Power Spectrum (2DNPS). For calculating the 2DNPS, the averaged result has to be multiplied for the square of the pixel pitch and divided by the vertical and horizontal ROI dimensions.

Equations 1 and 2 summarize steps 10 to 13.

EQUATION 1

$$MPV = \frac{1}{F} \sum_{Frame=1}^F \left\{ \frac{1}{R} \sum_{ROI=1}^R (Mean\ Pixel\ Value)_{ROI} \right\}_{Frame}$$

where,

F= Number of frames, i.e. 19 flat images.

R= Number of ROIs for frame.

EQUATION 2

$$2DNPS = \frac{pp^2}{N_x N_y} \left[\frac{1}{F} \sum_{Frame=1}^F \left\{ \frac{1}{R} \sum_{ROI=1}^R (FFT^2)_{ROI} \right\}_{Frame} \right]$$

where,

pp= Pixel Pitch

Nx=ROI width in pixels = 256

Ny=ROI height in pixels = 256

- 14. Axis dimensions: Normalise dividing by the size of the vector and get the right dimensions dividing by the pixel pitch. Bear in mind that we are working with double variable function (2D) so the dimensions of both axes has to be corrected:

$$u = \frac{\left[\frac{-N_x}{2} : \frac{N_x - 1}{2} \right]}{N_x} \frac{1}{pp}$$

$$v = \frac{\left[\frac{-N_y}{2} : \frac{N_y - 1}{2} \right]}{N_y} \frac{1}{pp}$$

Note: The zero frequency component has been shifted to the centre of the function.

- 15. Get the 1D NPS Vertical and Horizontal profile from the 2DNPS:

- i. Horizontal NPS: Average the values of the 14 rows that surround the horizontal axis. Take only the values that correspond to the positive frequencies from the vector u.
- ii. Vertical NPS: Average the values of the 14 columns that surround the vertical axis. Take only the values that correspond to the positive frequencies from the vector v.

Document Title	Document Number	Revision
Conversion Function, Modulation Transfer Function and Detective Quantum Efficiency Measurements and Analysis	DX-001538	B
This document is confidential and proprietary to PerkinElmer		

- iii. 1D axis dimensions: $f = \sqrt{u^2 + v^2}$
16. Get the Horizontal and Vertical NPS values that correspond to the frequencies 0.5 to the Nyquist frequencies in 0.5 steps.
17. Calculate the Normalised Noise Power Spectrum (NNPS) by dividing the vector obtained in step 16 by the squared MPV value (see Equation 1).
18. Plot the Vertical, Horizontal and Averaged NNPS as a function of the frequency and get the values.
19. Repeat steps 2 to 18 for the other exposure levels selected in step 1.
- 9.5 Detective Quantum Efficiency Curve

The Detective Quantum Efficiency (DQE) can be calculated with Equation 3:

$$DQE = \frac{MTF^2}{k_a SNR_{in}^2 NNPS}$$

where,

MTF= Values obtained in step 9.3. MTF should be exposure independent.

NNPS=Values obtained in step 9.4.

K_a = Measured air kerma, i.e. exposure level employed to calculate the NNPS.

SNR_{in}^2 = Squared signal to noise ratio per air kerma. Tabulated value given in the IEC-62220-1 and dependant on the radiation quality employed. See table below.

TABLE 3: TABULATED VALUES OF THE SNR_{in}^2 GIVEN BY THE IEC STANDARDS 62220-1 AND 62220-1-2.

Radiation Quality No.	$SNR_{in}^2 [1/(\mu\text{Gy} \times \text{mm}^2)]$
RQA5	30174
RQAM	5975

1. Select one of the 3 exposure levels used in the calculation of the NNPS.
2. Apply the formula keeping that exposure value. Use the averaged MTF and NNPS values.
3. Repeat steps 1 to 3 for the remaining exposure levels.
4. Plot DQE vs. Spatial Frequency for the three exposure steps.

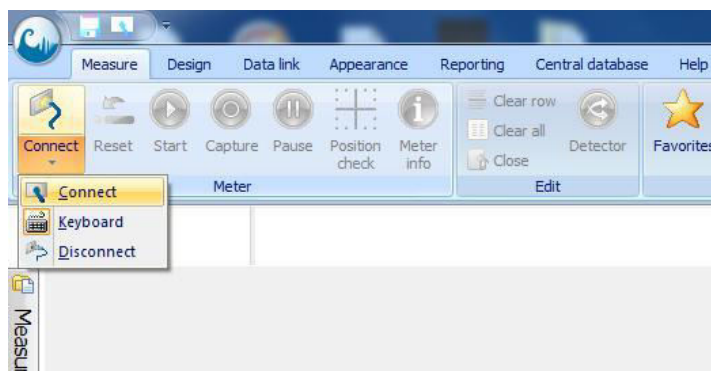
Document Title	Document Number	Revision
Conversion Function, Modulation Transfer Function and Detective Quantum Efficiency Measurements and Analysis	DX-001538	B
This document is confidential and proprietary to PerkinElmer		

10.0 APPENDICES

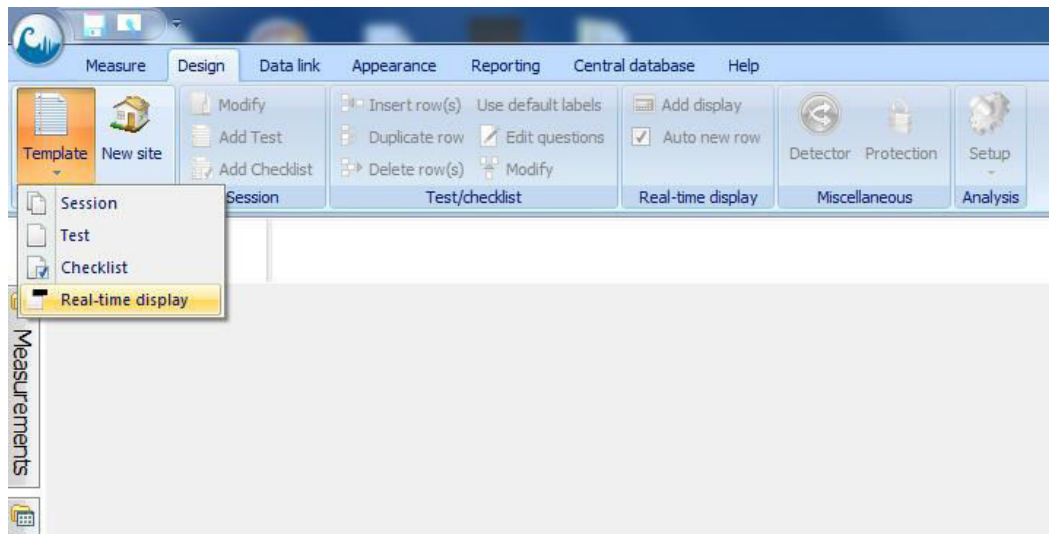
Appendix 1 – Software instructions for Dose Measurements

These set of instructions explain how to use the Ocean Software with the RTI Piranha radiation meter for dose exposure readings related with CF, MTF and NNPS measurements. Follow these instructions after the radiation meter is appropriately placed under the X-ray beam.

1. Open the Ocean software from RTI and connect to the radiation meter.

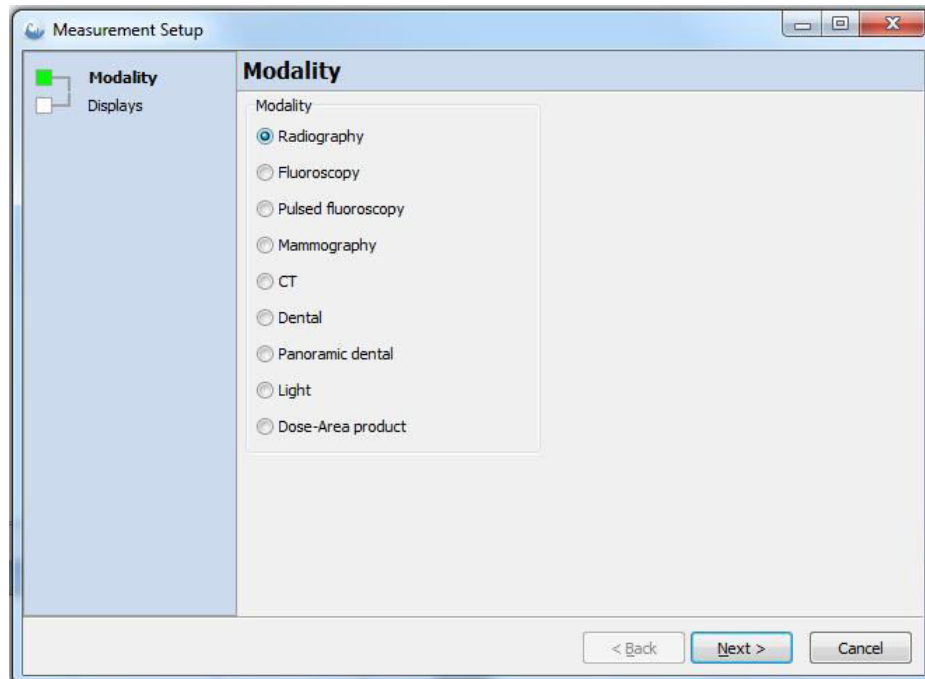


2. Check that the meter is connected, click in the 'Design' section and select Template – Real-time display.

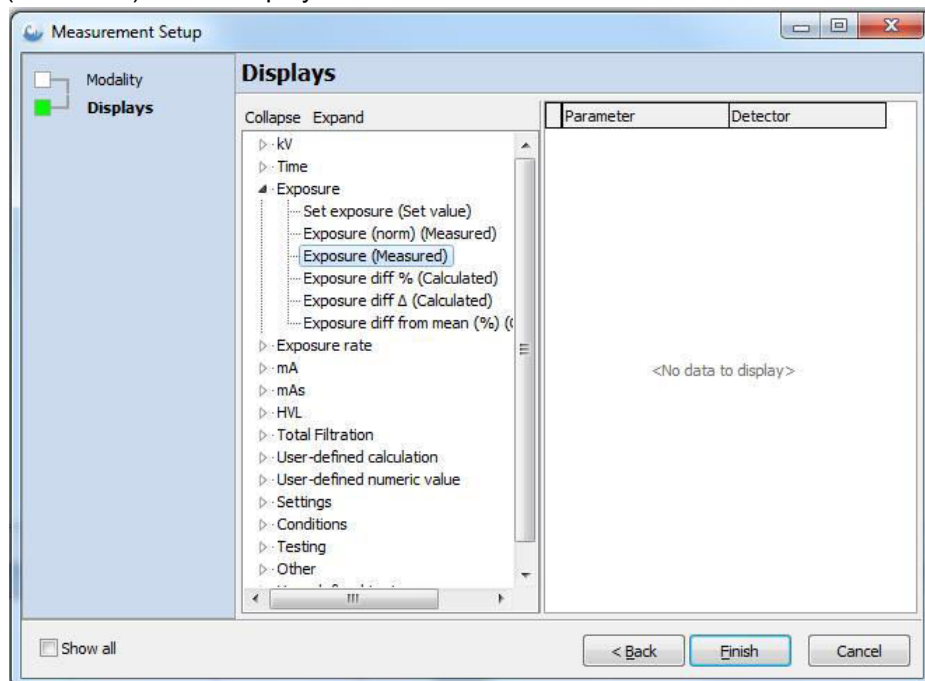


3. A window called "Measurements Setup - Modality" will be opened. Select Radiography for RQA5 and Mammography for RQAM and click in "Next".

Document Title	Document Number	Revision
Conversion Function, Modulation Transfer Function and Detective Quantum Efficiency Measurements and Analysis	DX-001538	B
This document is confidential and proprietary to PerkinElmer		

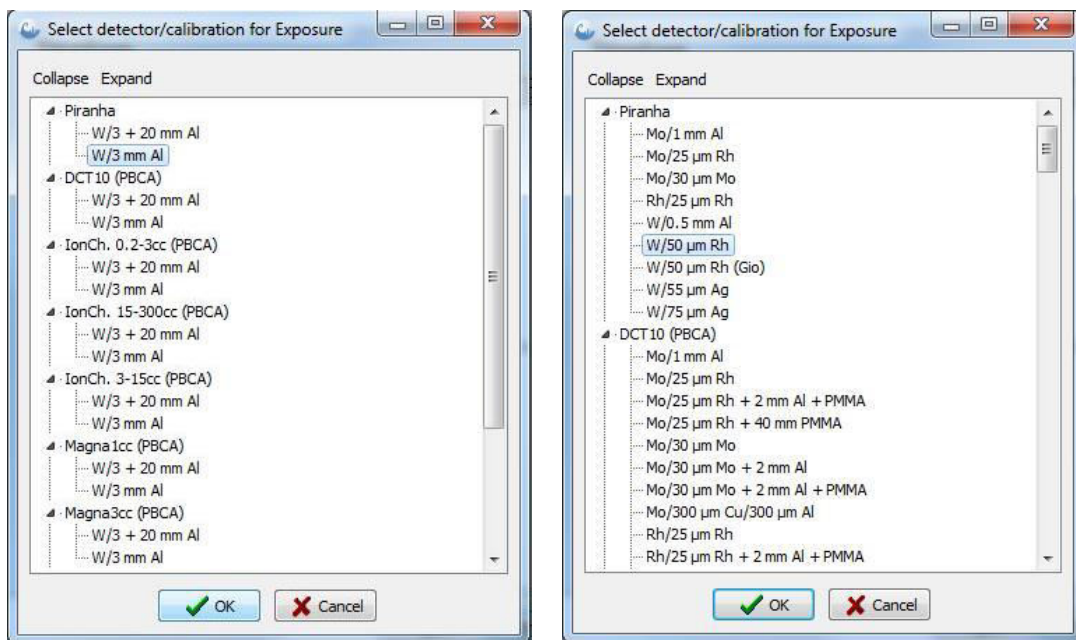


4. The “Display” windows will be opened, select “Exposure” and add “Exposure (Measured)” to the display list.



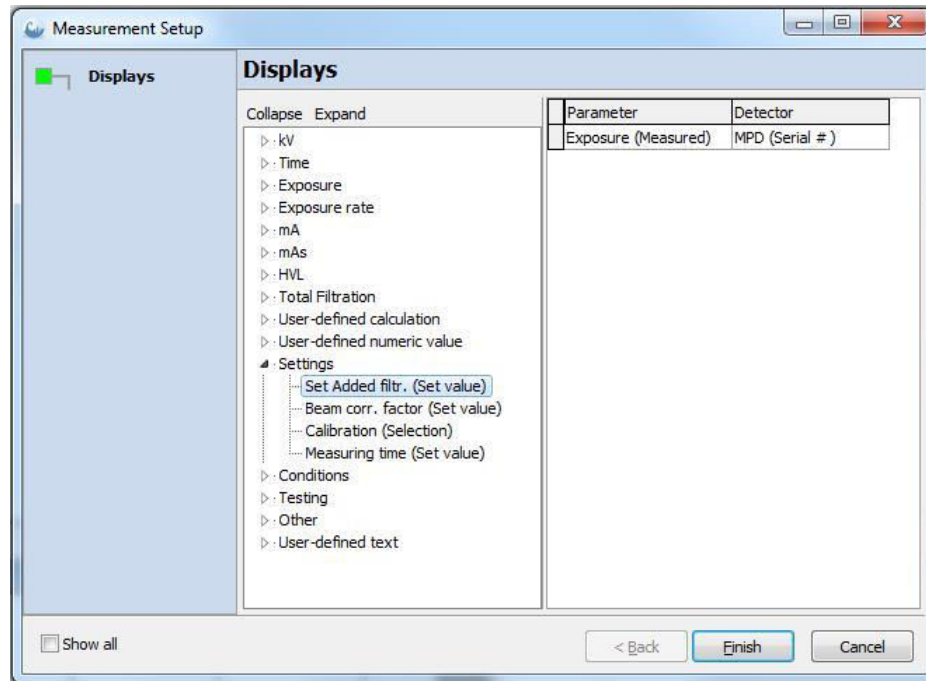
5. A window named “Select detector/calibration for Exposure” will be opened. Select “Piranha – W/3mmAl” for RQA5 (Left figure) or “Piranha – W/50µm Rh” for RQAM (Right figure) and click “OK”.

Document Title	Document Number	Revision
Conversion Function, Modulation Transfer Function and Detective Quantum Efficiency Measurements and Analysis	DX-001538	B
This document is confidential and proprietary to PerkinElmer		

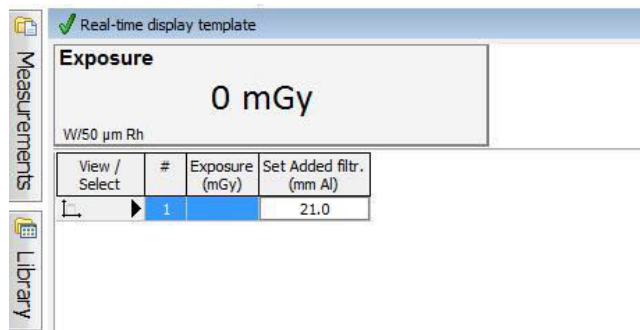


6. In the "Display" windows select now "Settings" and add "Set Added filtr. (Set value)" to the display list. Click "Finish"

Document Title	Document Number	Revision
Conversion Function, Modulation Transfer Function and Detective Quantum Efficiency Measurements and Analysis	DX-001538	B
This document is confidential and proprietary to PerkinElmer		



7. Back to the main window, specify the amount of mmAl added as additional filtration in the "Set Added filtr. (mmAl)" column.



8. Irradiate the radiation meter; the readings will be shown in the "Exposure (mGy)" column.

Appendix 2 – Current steps

RQAM: 5, 6, 8, 10, 12, 16, 20, 25, 32, 40, 50, 63, 80, 100, 125 mA

RQA5: 10, 12, 16, 20, 25, 32, 40, 50, 63, 80, 100, 125 mA

Document Title	Document Number	Revision
Conversion Function, Modulation Transfer Function and Detective Quantum Efficiency Measurements and Analysis	DX-001538	B
This document is confidential and proprietary to PerkinElmer		

11.0 REVISION HISTORY

Revision	Sections Changed	Originator	ECO No.	ECO Date
A	Initial Release	Elena Marimón Muñoz	100318	25/09/2013
B	Updated version	Elena Marimón Muñoz		30/06/2014